

## **Distribution Agreement**

In presenting this dissertation as a partial fulfillment of the requirements for an advanced degree from Emory University, I agree that the Library of the University shall make it available for inspection and circulation in accordance with its regulations governing materials of this type. I agree that permission to copy from, or to publish, this dissertation may be granted by Professor Craig L. Hill, or, in his absence, by the Dean of the Graduate School when such copying or publication is solely for scholarly purposes and does not involve potential financial gain. It is understood that any copying from, or publication of, this dissertation that involves potential financial gain will not be allowed without written permission.

---

(Zhen Luo)

The Polyoxometalate / NO<sub>x</sub> / Br<sub>x</sub> Catalysts for  
Aerobic Sulfoxidations

By

Zhen Luo  
Doctor of Philosophy

Chemistry

---

Craig L. Hill  
Advisor

---

Dale E. Edmondson  
Committee Member

---

Karl S. Hagen  
Committee Member

Accepted:

---

Lisa A. Tedesco, Ph.D.  
Dean of the Graduate School

---

Date

The Polyoxometalate / NO<sub>x</sub> / Br<sub>x</sub> Catalysts for  
Aerobic Sulfoxidations

By

Zhen Luo

B.S.; Jilin University, 2000

M.S.; Institute of Chemistry, Chinese Academy of Science, 2003

Advisor: Professor Craig L. Hill

An Abstract of

A dissertation submitted to the Faculty of the  
Graduate School of Emory University in partial fulfillment of  
the requirements for the degree of  
Doctor of Philosophy

in Chemistry

2009

## Abstract

### The Polyoxometalate / NO<sub>x</sub> / Br<sub>x</sub> Catalysts for Aerobic Sulfoxidations

By Zhen Luo

In attempts to make a nitrate and bromide containing transition-metal-substituted-polyoxometalate (POM) catalyst developed in our group practically applicable, an *in situ* layer-by-layer self-assembly procedure has been developed to immobilize this POM onto solid supports. The solid-supported POMs efficiently catalyze aerobic sulfoxidation under ambient conditions. The addition of protic acids to the system significantly enhances the catalytic activities while water elongates the induction period and inhibits the reaction.

To obtain disorder-free X-ray crystal structures which provide insightful albeit indirect evidence regarding the mechanism of the POM-catalyzed sulfoxidation, divacant [ $\gamma$ -SiW<sub>10</sub>O<sub>36</sub>]<sup>8-</sup> and trivacant [ $\alpha$ -P<sub>2</sub>W<sub>15</sub>O<sub>56</sub>]<sup>12-</sup> POMs have been used as synthetic precursors of the catalysts. Two multi-copper-substituted polytungstosilicates, K<sub>9</sub>Na<sub>2</sub>Cu<sub>0.5</sub>[ $\gamma$ -Cu<sub>2</sub>(H<sub>2</sub>O)SiW<sub>8</sub>O<sub>31</sub>]<sub>2</sub>·38H<sub>2</sub>O and K<sub>3</sub>H<sub>4</sub>Cu<sub>0.5</sub>{Cu[Cu<sub>7.5</sub>Si<sub>2</sub>W<sub>16</sub>O<sub>60</sub>(H<sub>2</sub>O)<sub>4</sub>(OH)<sub>4</sub>]<sub>2</sub>}·9H<sub>2</sub>O, and a series TBA salts of Well-Dawson sandwich POMs have been prepared and characterized by X-ray crystallography, IR and elemental analysis. The complex [(*n*-C<sub>4</sub>H<sub>9</sub>)<sub>4</sub>N]<sub>11</sub>H<sub>5</sub>[Cu<sub>4</sub>(P<sub>2</sub>W<sub>15</sub>O<sub>56</sub>)<sub>2</sub>], proved to be inactive in the absence of NO<sub>3</sub><sup>-</sup> and Br<sup>-</sup>; however, a system containing NO<sub>3</sub><sup>-</sup>, Br<sup>-</sup> and copper-substituted POM is the most effective (rapid and selective) catalytic system for aerobic sulfoxidation to date.

In order to probe the mechanism of the catalytic reaction, the kinetics of sulfoxidation catalyzed by simplified systems that contain only nitrate and bromide from different sources were investigated. The yellow active specie of the  $\text{NO}_x/\text{Br}$  system previously documented in our research group has been unequivocally identified to be  $\text{TBABr}_3$ . A mechanism based on the bromine sulfoxidation and aerobic bromine regeneration catalyzed by  $\text{NO}_x$  is proposed and the kinetic data fit the equations associated with the mechanism.

# The Polyoxometalate / NO<sub>x</sub> / Br<sub>x</sub> Catalysts for Aerobic Sulfoxidations

By

Zhen Luo

B.S.; Jilin University, Beijing, 2000

M.S.; Institute of Chemistry, Chinese Academy of Science, 2003

Advisor: Professor Craig L. Hill

A dissertation submitted to the Faculty of the  
Graduate School of Emory University in partial fulfillment of  
the requirements for the degree of  
Doctor of Philosophy

in Chemistry

2009

## **Acknowledgement**

I would like to thank everyone who helped me reach this milestone in my life. I am grateful to the professors and instructors at Institute of Chemistry, CAS and Emory University who have guided me throughout my education. I would especially like to thank my advisor, Dr. Craig. L Hill, for his guide, support and encouragement during my staying at Emory.

Finally, I want to express my deepest gratitude to my wife, Hailun Wang and my parents for their love, patience and encouragement.

## Table of Contents

|  |            |
|--|------------|
| <b>Abstract</b>  | <b>iv</b>  |
| <b>Acknowledgement</b>   | <b>vii</b> |
| <b>List of Figures</b>   | <b>ix</b>  |
| <b>List of Tables</b>  | <b>xv</b>  |
| <br>   |            |
| <b>Chapter One:</b> Introduction of Transition-metal-substituted Polyoxometalates (TMSPs) and TMSPs Catalyzed Sulfoxidation  | <b>1</b>   |
| <b>Chapter Two:</b> Synthesis and Characterization of Solid- Support Catalytic TMSP Materials for Aerobic Sulfoxidation  | <b>20</b>  |
| <b>Chapter Three:</b> Kinetics and Mechanistic Studies of the NO <sub>x</sub> /Br Systems for Catalytic Aerobic Sulfoxidation  | <b>60</b>  |
| <b>Chapter Four:</b> Multi-Copper Polyoxoanions. 1. Synthesis, Characterization, X-ray Crystal Structures, and magnetism of a new dimeric silicotungstate  | <b>92</b>  |
| <b>Chapter Five:</b> Multi-Copper Polyoxoanions. 2. Synthesis, Characterization, X-ray Crystal Structure and Magnetism of a One-dimensional Silicotungstate Array                                    | <b>114</b> |
| <b>Chapter Six:</b> Multi-Copper Polyoxoanions. 3. Synthesis, structure, magnetism and catalytic properties of a polyoxometalate with coordinatively unsaturated d-electron-transition metal centers | <b>139</b> |

## List of Figures

### Chapter One

- Figure 1-1. Polyhedral representation of isopolyanions, A and B, and heteropolyanions, C and D. A),  $[W_6O_{19}]^{2-}$ ; B),  $[V_{10}O_{28}]^{6-}$ ; C),  $[\alpha\text{-SiW}_{12}O_{40}]^{4-}$ ; D),  $[\alpha\text{-P}_2W_{18}O_{62}]^{6-}$ . 3
- Figure 1-2. a) Bond representation of a  $WO_6$  octahedron unit; b) Resonance representation of a  $VO_6$  octahedron unit. 5
- Figure 1-3. The five Baker-Figgis isomers of the Keggin structure:  $\alpha$ ,  $\beta$ ,  $\gamma$ ,  $\delta$ ,  $\epsilon$ . The rotated  $M_3O_{13}$  group(s) are show in light crosshatch. 6
- Figure 1-4. IUPAC numbering scheme of  $[\alpha\text{-M}_2W_{18}O_{62}]^{n-}$  (the Wells-Dawson structure) 7
- Figure 1-5. General route for synthesis of dodecatungstosilicate isomers and related mono-, bi- and tri-vacant polysilicotungstates. 8
- Figure 1-6. Relationships between the different polytungstodiphosphate species. 10
- Figure 1-7. Polyhedral representations of TMSPs: a).  $[(\gamma\text{-Cu}_2(\text{H}_2\text{O})\text{SiW}_8\text{O}_{31})_2]^{12-}$ , b)  $[\text{Mn}_4(\text{H}_2\text{O})_2(\text{PW}_9\text{O}_{34})_2]^{10-}$ , c)  $[(\gamma\text{-Cr}_2(\text{H}_2\text{O})_2\text{SiW}_{10}\text{O}_{36})]^{2-}$ , d)  $[\{\text{Fe}_2(\text{OH})_3(\text{H}_2\text{O})_2\}_3(\gamma\text{-SiW}_{10}\text{O}_{36})_3]^{15-}$ , e)  $[\text{Mn}_4(\text{H}_2\text{O})(\text{P}_2\text{W}_{15}\text{O}_{56})_2]^{16-}$ , f)  $[\alpha_2\text{-Co}(\text{H}_2\text{O})\text{P}_2\text{W}_{17}\text{O}_{61}]^{10-}$ , g)  $[\alpha_1\text{-Co}(\text{H}_2\text{O})\text{PW}_{17}\text{O}_{61}]^{10-}$ . 12
- Figure 1-8. Some typical chemical warfare agents. 13
- Figure 1-9. TMSP catalyzed sulfoxidation under ambient conditions. 15

### Chapter Two

- Figure 2-1. The catalytic cycle of  $\text{NO}_2$ -catalyzed  $\text{O}_2$ -based sulfoxidation. 29
- Figure 2-2. Conversion of CEES oxidation after 1.0 hour in the presence of 5 mM d-electron-transition-metal-substituted POM and 34 mM  $\text{TBAFeBr}_4$ . Other conditions:  $25^\circ\text{C}$ , 1.0 atm  $\text{O}_2$ , 2.5 mL  $\text{CH}_3\text{CN}$ ,  $[\text{CEES}] = 360 \text{ mM}$ ; \*

5mM of pure  $\text{TBA}_7\text{PW}_{11}\text{O}_{39}$  were used in place of the d-electron-transition-metal-substituted POM. 32

Figure 2-3. Time profile of aerobic CEES (0.35 mol/L) oxidation catalyzed by  $\text{Fe}/\text{Cu}/\text{PW}_{11}/\text{Br}/\text{NO}_3$  (0.05 g, 0.005 mmol based on POM) at 25°C (ambient conditions) in 2.5 mL acetonitrile. Consumption of CEES (◆) and production of CEESO (■) are shown. 33

Figure 2-4. The GC traces showing effective 100% selective oxidation of CEES to CEESO. a), b), c) are traces taken at 1 min, 2 h and 30 h, respectively. 35

Figure 2-5. Illustration of the environment for the catalyst in homogenous (a) and the solid-supported catalysts in heterogeneous (b) reactions; solid dots represent the target molecules (CEES) and empty dot represented the metal-POM complexes. 42

Figure 2-6. Catalytic activity of POM immobilized on the following supports:  $\text{TiO}_2$  (▲),  $\text{Al}_2\text{O}_3$  (■) and cationic silica (◆) (0.13 g, 0.01 mmol of POM) for air-based sulfoxidation of CEES (0.35 mol/L) at 25°C (ambient conditions) in 2.5 mL acetonitrile. Conversion of CEES to CEESO and the fitted curves are shown. 44

Figure 2-7. The surface charge density of  $\text{TiO}_2$  nanoparticles as a function of pH. Conditions: 25 °C; 1 atm of Ar;  $\text{TiO}_2$  nanoparticles (0.05 g) were suspended in 8 mL of 0.1 M NaCl. The point of zero charge (pzc), as determined, by titration is 9.80. 47

Figure 2-8. The surface charge density of  $\text{Al}_2\text{O}_3$  as a function of pH. Conditions: 25 °C; 1 atm of Ar;  $\text{Al}_2\text{O}_3$  nanoparticles (0.05 g) were suspended in 8 mL of 0.1 M NaCl. The point of zero charge (pzc), as determined by titration, is 7.91. 48

Figure 2-9. The surface charge density of  $(\text{Si}/\text{AlO}_2)^+$  nanoparticles as a function of pH. Conditions: 25 °C; 1 atm of Ar;  $\text{Al}_2\text{O}_3$  nanoparticles (0.05 g) were suspended in 8 mL of 0.1 M NaCl. The pzc of  $(\text{Si}/\text{AlO}_2)^+$  is 6.60. 49

Figure 2-10. Profiles of aerobic CEES sulfoxidation catalyzed by  $\text{Fe}/\text{Cu}/\text{PW}_{11}/\text{Br}/\text{NO}_3/\text{TiO}_2$  in the presence (■) or absence (◆) of TsOH. Conditions: 0.13 g (0.01 mmol) of POM, 0.35 mol/L of CEES, air at 25°C

(ambient conditions) in 2.5 mL acetonitrile, and 20mg of TsOH in the acidified reaction. 52

Figure 2-11. The effect of different amounts of H<sub>2</sub>O (from 1 μL to 100 μL) added to the typical catalytic sulfoxidation system: a) conversions after 3 hrs; b) conversions after 20 hrs. 53

Figure 2-12. Profiles of aerobic CEES sulfoxidation catalyzed by Fe/Cu/PW<sub>11</sub>/Br/NO<sub>3</sub>/TiO<sub>2</sub> that is freshly prepared (■), exposed to water-saturated air or 100% relative humidity “RH” (◆), and initially exposed to water vapor and then partially dried at 50°C in an oven for 2 hours (▲). Conditions: 0.13 g (0.01 mmol) of POM, 0.35 mol/L CEES under air at 25°C (ambient conditions) in 2.5 mL acetonitrile. 56

### Chapter Three

Figure 3-1. The absorption spectra of different NO<sub>x</sub>/Br systems in acetonitrile. From up to down at peak 269 nm: red — TBABr<sub>3</sub>; green — TBABr/NOBF<sub>6</sub>; purple —, Br<sub>2</sub>; blue — TBABr/TBANO<sub>2</sub>. 68

Figure 3-2. Time profile of catalytic CEES consumption in a freshly prepared TBABr/TBANO<sub>3</sub> system. Conditions: [CEES]<sub>0</sub> = 0.32 M, [TBANO<sub>3</sub>] = 0.016 M, [TBABr] = 0.016 M, CH<sub>3</sub>CN=2.3 mL, T = 70 °C. Solid square, ■: experimental data. Red line, —: exponential fit from 200 to 1600 min. 70

Figure 3-3. Kinetics of CEES oxidation by air catalyzed by bromide-free TBA<sub>3</sub>H<sub>2</sub>[Fe(NO<sub>3</sub>)PW<sub>11</sub>O<sub>39</sub>] (TBA{FePW<sub>11</sub>}) (□), TBA{FePW<sub>11</sub>} + TBABr (◇) and TBA{FePW<sub>11</sub>} + TBABr +TBANO<sub>3</sub> (△) at 25°C (ambient conditions) in acetonitrile. Conditions: [CEES]<sub>0</sub> = 0.35 M (105 μL), TBA{FePW<sub>11</sub>} = 0.016 M, [TBABr] = 0.016 M, [TBANO<sub>3</sub>] = 0.016 M, CH<sub>3</sub>CN=2.3 mL. 71

Figure 3-4. Proposed mechanism for the selective aerobic oxidation of sulfide to sulfoxide catalyzed by the NO<sub>x</sub>/Br systems. 73

Figure 3-5. Kinetics of CEES consumption in an aged TBANO<sub>3</sub>/TBABr system catalyzed sulfoxidation (■); red curve (—): first order fit; (●): time profile of the absorbance at 269 nm of the reaction system (200 times

diluted). Conditions:  $[\text{CEES}] = 0.35 \text{ M}$ ,  $[\text{TBANO}_3] = 0.018 \text{ M}$ ,  $[\text{TBABr}] = 0.110 \text{ M}$ ,  $[\text{TsOH}] = 0.018 \text{ M}$ ,  $[\text{1,3-dichlorobenzene}] = 0.018 \text{ M}$ ,  $\text{CH}_3\text{CN} = 2.3 \text{ mL}$ ,  $T = 70 \text{ }^\circ\text{C}$ . 79

Figure 3-6. (■): time profile of the absorbance at 269 nm of the regeneration of  $\text{Br}_3^-$ . Red curve (—): fit with eq. 18. Conditions: a portion of 10  $\mu\text{L}$  solution from an ongoing catalytic sulfoxidation reaction was diluted 50-fold; conditions of the sulfoxidation reaction:  $[\text{CEES}]_0 = 108 \text{ mM}$ ,  $[\text{TBANO}_3] = 25 \text{ mM}$ ,  $[\text{TBABr}] = 25 \text{ mM}$ ,  $[\text{HClO}_4] = 5 \text{ mM}$ ,  $\text{CH}_3\text{CN} = 2.0 \text{ mL}$ ,  $T = 70 \text{ }^\circ\text{C}$ . 81

Figure 3-7. Kinetics of CEES oxidation by air in water-free (□) and water containing (◇)  $\text{NO}_x/\text{Br}$  systems at 70  $^\circ\text{C}$  in acetonitrile. Conditions for the water-free system:  $[\text{CEES}]_0 = 108 \text{ mM}$  (25  $\mu\text{L}$ ),  $[\text{TBANO}_3] = 25 \text{ mM}$ ,  $[\text{TBABr}] = 25 \text{ mM}$ ,  $[\text{H}_2\text{SO}_4] = 2.5 \text{ mM}$ ,  $\text{CH}_3\text{CN} = 2.0 \text{ mL}$ ,  $T = 70^\circ\text{C}$ ; conditions for the water-containing system:  $[\text{CEES}]_0 = 108 \text{ mM}$  (25  $\mu\text{L}$ ),  $[\text{TBANO}_3] = 25 \text{ mM}$ ,  $[\text{TBABr}] = 25 \text{ mM}$ ,  $[\text{HClO}_4] = 5 \text{ mM}$ ,  $[\text{H}_2\text{O}] = 277 \text{ mM}$  (10  $\mu\text{L}$ ),  $\text{CH}_3\text{CN} = 2.0 \text{ mL}$ ,  $T = 70^\circ\text{C}$  85

Figure 3-8. Kinetics of CEES consumption catalyzed by aged  $\text{NO}_x/\text{Br}$  system containing 10  $\mu\text{L}$  (277 mM) (◇), 50  $\mu\text{L}$  (1.38 M) (□) and 100  $\mu\text{L}$  (2.77 M) (○) of water under air at 70 $^\circ\text{C}$  in acetonitrile. Conditions:  $[\text{CEES}]_0 = 108 \text{ mM}$  (25  $\mu\text{L}$ ),  $[\text{TBANO}_3] = 25 \text{ mM}$ ,  $[\text{TBABr}] = 25 \text{ mM}$ ,  $[\text{HClO}_4] = 5 \text{ mM}$ ,  $\text{CH}_3\text{CN} = 2.0 \text{ mL}$ ,  $T = 70^\circ\text{C}$ . Color curves: least-squares fit based on eq. 29. 88

## Chapter Four

Figure 4-1. Ball and stick representation of  $[\gamma\text{-Cu}_2(\text{H}_2\text{O})\text{SiW}_8\text{O}_{31}]_2^{12-}$  (1a, the polyanion of 1) showing 50% probability ellipsoids and selected atomic labels. 102

Figure 4-2. A combination polyhedral/ball-and-stick representation of the  $[\gamma\text{-Cu}_2(\text{H}_2\text{O})\text{SiW}_8\text{O}_{31}]^{6-}$  subunit of 1. 103

Figure 4-3. Temperature dependence of  $\chi T$  at 0.1 Tesla for 1 featuring a maximum at approx. 10 K due to competing FM/AFM exchange coupling.

Black squares: experimental data; Solid line: best fit to model Hamiltonian (see text). 106

Figure 4-4. The central fragment of the  $\{\text{Cu}_4\text{W}_{16}\}$  cluster anion emphasizing the superexchange pathways between the  $s = 1/2$  Cu(II) centers (Cu: dark gray spheres, O: small gray spheres, Si: white spheres, W: light grey spheres). FM  $J_1$  exchange (represented by short dashed lines) is mediated by  $\mu$ -O bridges with Cu-O bond distances of 1.93 – 2.04 Å (dark grey bonds) and Cu-O-Cu bond angles of 93.9° and 99.6°. Weak AFM coupling ( $J_2$ , long dashed lines) between the FM coupled  $\text{Cu}_2$  dimers proceeds through O-Si-O and O-W-O groups (light grey bonds) that, in all cases, involves one Jahn-Teller elongated Cu-O bond (thin black). 107

## Chapter Five

Figure 5-1. Ball and stick representation of  $[\text{Cu}\{\text{Cu}_{7.5}\text{Si}_2\text{W}_{16}\text{O}_{60}(\text{H}_2\text{O})_4(\text{OH})_4\}_2]^{8-}$  (2a, the polyanion of 2) showing 50% probability ellipsoids and selected atomic labels. Cu: blue; O: red; Si: orange; W: green. 125

Figure 5-2. A combination polyhedral/ball-and-stick representation of the  $\{\text{Cu}_9\text{Si}_2\text{W}_{16}\text{O}_{60}(\text{H}_2\text{O})_4(\text{OH})_4\}$  subunit of 2. 126

Figure 5-3. Structural view of the one-dimensional array of 2 from the  $c$  axis direction. 127

Figure 5-4. X-band ESR spectrum of compound 2, measured as a microcrystalline powder at 290 K. 130

Figure 5-5. Temperature dependence of  $\chi T$  of 2 at 0.1 Tesla (black squares) and at 5.0 Tesla (red carets, the data follows the 0.1 Tesla curve for higher temperatures). 131

Figure 5-6. Field dependence of the magnetization,  $M$ , of 2 at 1.8 132

## Chapter Six

Figure 6-1. Thermogravimetric analysis (TGA) of fresh crystallized 3. 145

Figure 6-2. Potentiometric titration of the 3 by using TBAOH (1 M in methanol) 146

Figure 6-3. Ball-and-stick representation of  $[\text{Cu}_4(\text{P}_2\text{W}_{15}\text{O}_{56})_2]^{16-}$  (polyanion 3a of compound 3) showing 50% probability ellipsoids and selected atomic labels. 155

Figure 6-4. Coordination environments of the central  $\text{Cu}(\text{II})_4$  group in 3 with atom numbers of positions primarily involved in magnetic exchange (Cu: large grey circles, O: small black circles). Bonds to equatorial ligand positions are highlighted in dark grey. Dotted bond lines indicate bonds to the two proximal P centers of the  $\{\text{P}_2\text{W}_{15}\}$  groups. 163

Figure 6-5. Temperature dependence of  $\chi_m T$  for 3 at 0.1 Tesla ( $2.0 \text{ K} < T < 300 \text{ K}$ ). Inset:  $\chi_m$  of 3 as a function of the applied field  $B_0$  at 2.0 K, illustrating saturation effects. Experimental data: open circles, least squares fit to the employed model (see text): blue line. 164

## List of Tables

### Chapter Two

|   |    |
|---|----|
| Table 2-1. Aerobic oxidation of 2-chloroethyl ethyl sulfide (CEES) in acetonitrile by nitrate and bromide-containing polyoxometalate (POM)-based catalysts. | 30 |
| Table 2-2. Catalytic activity of different solid-supported POM catalysts  | 43 |
| Table 2-3. BET Surface area of different supports and one supported catalyst  | 50 |

### Chapter Three

|   |     |
|---|-----|
| Table 3-1. The constants and the associated <i>K</i> values obtained by least-squares fit of aerobic CEES oxidation catalyzed by the NO <sub>x</sub> /Br systems shown in Figure 3-8. | 89  |
| Table 4-1. Crystallographic Data and Structure Refinement for 1   | 98  |
| Table 4-2. Select bond distance (Å) and bond angles (°) for 1   | 105 |

### Chapter Five

|   |     |
|---|-----|
| Table 5-1. Crystallographic Data and Structure Refinement for 2 | 119 |
| Table 5-2. Select bond distances (Å) and bond angles (°) for 2  | 133 |

### Chapter Six

|   |     |
|---|-----|
| Table 6-1. Crystal data for 3·2CH <sub>2</sub> ClCH <sub>2</sub> Cl·2CHCl <sub>3</sub>  | 150 |
| Table 6-2. Bond valence sum of selected bridge atom of 3  | 158 |
| Table 6-3. Select bond distance (Å) and bond angles (°) for 3   | 158 |
| Table 6-4. Aerobic oxidation of 2-chloroethyl ethyl sulfide (CEES) in acetonitrile catalyzed by analogues or components of the “hot catalyst” . | 162 |

## List of Abbreviations

|                  |   |
|------------------|---|
| Å                | Angstrom  |
| <i>a, b, c</i>   | unit cell axial lengths   |
| <i>n</i> -Bu     | <i>n</i> -butyl   |
| Br               | bromine   |
| °C               | degrees Celsius   |
| calcd.           | Calculated  |
| CEES             | 2-chloroethyl ethyl sulfide   |
| CIF              | crystallographic information file   |
| cm <sup>-1</sup> | reciprocal centimeter   |
| DMS              | dimethyl sulfide  |
| DMSO             | dimethyl sulfoxide  |
| DSC              | differential scanning calorimetry   |
| equiv.           | equivalent  |
| EXAFS            | extended X-ray absorption fine structure method   |
| Fe               | iron  |
| F.W.             | formula weight  |
| <i>F</i> (000)   | structure factor for the unit cell; it is equal to the total number of electrons in the unit cell |
| FT-IR            | Fourier transform infrared spectroscopy   |
| g                | grams(s)  |
| h                | hour(s)   |
| IS               | internal standard   |
| Hz               | Hertz   |
| K                | kelvin  |
| L                | ligand  |
| m                | medium (FT-IR)  |
| M                | molarity  |
| Me               | methyl  |
| mg               | milligram(s)  |
| MHz              | megahertz   |
| min              | minutes(s)  |
| mL               | milliliters(s)  |
| Mn               | manganese   |
| mmol             | millimole   |
| mol              | mole  |
| nm               | nanometer   |
| NMR              | nuclear magnetic resonance spectroscopy   |
| OAc              | acetate   |
| pH solution      | potential of hydrogen, a measure of the acidity or alkalinity of a solution                       |
| Ph               | phenyl  |
| POM              | polyoxometalate   |
| ppm              | part per million  |
| Pt               | platinum  |

|                         |   |
|-------------------------|---|
| <i>R</i>                | discrepancy index for crystal structure refinement  |
| <i>s</i>                | strong (FT-IR)  |
| sec                     | second(s)   |
| sh                      | shoulder (FT-IR)  |
| TBA                     | tetrabutylammonium  |
| THpA                    | tetraheptylammonium   |
| TMSP                    | transition-metal-substituted polyoxometalate  |
| TGA                     | thermogravimetric analysis  |
| UV                      | ultraviolet   |
| <i>V</i>                | volume of the unit cell   |
| vs                      | very strong (FT-IR)   |
| w                       | weak (FT-IR)  |
| <i>Z</i>                | number of molecules per unit cell   |
| $\alpha, \beta, \gamma$ | interaxial angles between unit cell vector <b>b</b> and <b>c</b> , <b>a</b> and <b>c</b> , and <b>a</b> and <b>b</b> , respectively |
| $\delta$                | chemical shift (expressed in ppm for NMR)   |
| $\epsilon$              | molar extinction (or absorption) coefficient  |
| $\theta$                | the glancing angle of the X-ray beam to the “reflecting plane”  |
| $\lambda$               | wavelength  |
| $\mu$                   | the total linear absorption coefficient (with unit of $\text{cm}^{-1}$ )  |

# *Chapter 1*

Introduction to Transition-metal-  
substituted Polyoxometalates (TMSPs)  
and TMSP-Catalyzed Sulfoxidation

## General Information

Polyoxometalates (POMs) are class of highly tunable inorganic compounds formed by the linkage of early transition metals in their highest oxidation state ( $d^0$ ) with oxygen atoms.<sup>1-3</sup> The early transition metals which form POMs are referred to as *addenda* atoms. POMs formed exclusively from addenda and oxygen atoms are named *isopolyanions*. POMs formed by adding to the addenda-based structures one or more other elements are named *heteropolyanions* (Figure 1-1). The elements that can function as addenda atoms in POMs appear to be limited to those with a favorable combination of both size (cationic radius), charge, and the accessibility of empty d orbitals for metal-oxygen bonding.<sup>1-3</sup> Transition metals in group VB and VIB are the only elements known have the proper charge-radius ratio and appropriate strength of the M-O bonds to act as addenda to form POMs. However, the heteroatoms, other than addenda, in heteropolyanions have no such limitations and can be virtually any element in the periodic table. A combination of the extensive acid-base and oxidation-reduction chemistry of polyoxometalates make these complexes highly diverse<sup>4</sup> with applications in medicine<sup>5</sup> and more importantly, catalysis.<sup>6-10</sup>

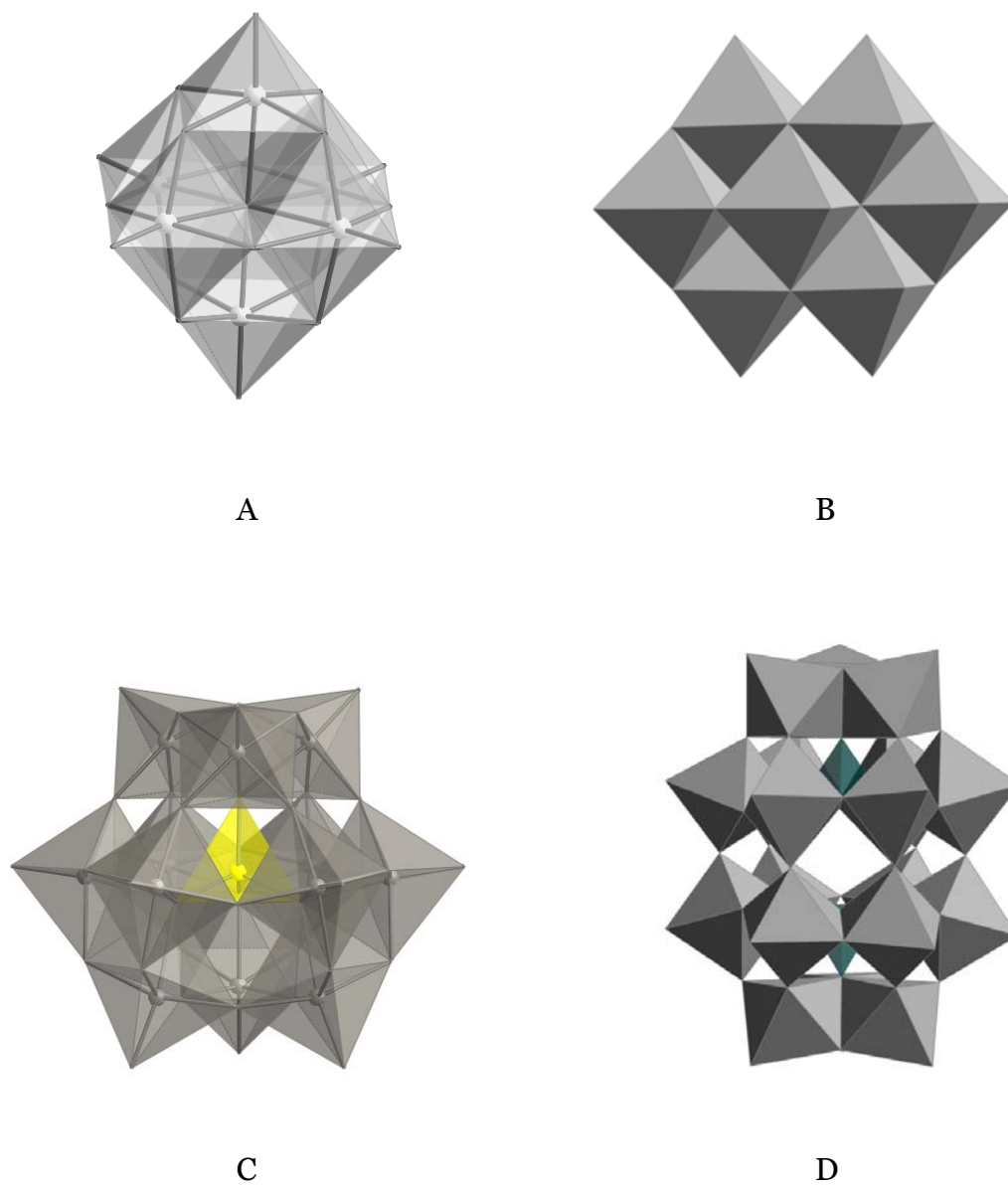


**Figure 1-1.** Polyhedral representation of isopolyanions, A and B, and heteropolyanions, C and D. A),  $[\text{W}_6\text{O}_{19}]^{2-}$ ; B),  $[\text{V}_{10}\text{O}_{28}]^{6-}$ ; C),  $[\alpha\text{-SiW}_{12}\text{O}_{40}]^{4-}$ ; D),  $[\alpha\text{-P}_2\text{W}_{18}\text{O}_{62}]^{6-}$ .

Polyoxometalates are often formed by corner-, edge- and face-sharing of the basic  $\text{MO}_6$  octahedral units. Corner- and edge-sharing linkages are the most common linkages found in POMs. Face-sharing linkages are also found but these linkages are rare because of the large electrostatic repulsion caused by the close packing of the two highly charged metal atoms. It has been noticed that  $\text{MO}_6$  octahedra containing three or more terminal oxo-groups are not observed. This restriction, named “Lipscomb principle,”<sup>1</sup> has been explained in terms of the strong trans-influence of terminal M-O bonds facilitating dissociation of the cluster. For each  $\text{MO}_6$  octahedron, there are three different types of metal-oxygen bonds (Figure 1-2). Each metal center forms one short bond to a terminal oxygen, which corresponds to a double bond. Four longer bonds formed between metal center and bridging oxygens are corresponding to single bonds, and the bond between the core oxygen and center metal is a very long and weak bond. The terminal oxygens,  $\text{O}_t$ , formed the outmost layer of POMs are usually the least basic and help prevent further polymerization which allows for the formation of discrete complexes. The inner core oxygens,  $\text{O}_i$ , are the most basic oxygens POMs, but they are sterically inaccessible and thus usually chemically inert. The bridging oxygens,  $\text{O}_b$ , became most active according to their greater basicity and accessibility.

The physically and chemically different environments of these oxygen atoms provide facilitate characterization of POMs. With the weakest W-O bond, the  $\text{O}_i$  locates upfield in the  $^{17}\text{O}$  NMR, while the deshielding effect associated with the terminal  $\text{WO}_t$  bond makes the  $\text{O}_t$  oxygens exhibit the most downfield peaks.<sup>3</sup>

In IR spectrum, the three different W-O bond strengths reflect peaks with different and usually discrete absorption frequencies.<sup>1</sup>

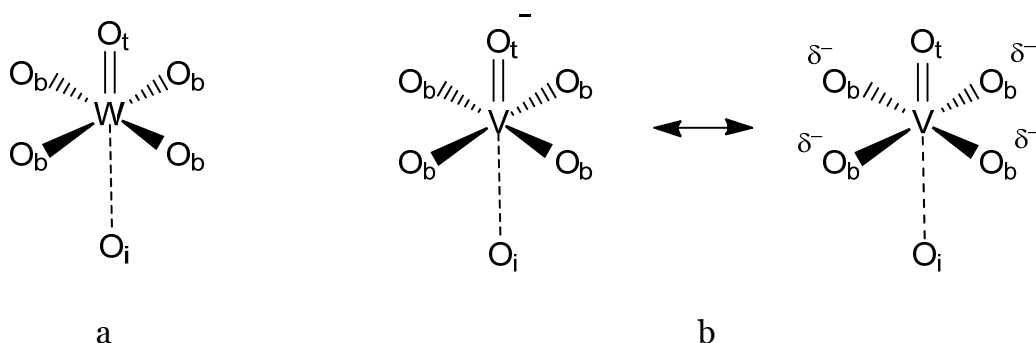


**Figure 1-2.** a) Bond representation of a  $\text{WO}_6$  octahedron unit; b) Resonance representation of a  $\text{VO}_6$  octahedron unit.

## Heteropolyanion Structures

Of the several hundred discrete POM structures known, two of the most common are the Keggin and the Wells-Dawson polyanions. The Keggin structure is formed by a single  $\text{XO}_4$  tetrahedron surrounded by four  $\text{M}_3\text{O}_{13}$  triad at each of its vertices. These triads are linked by corner-sharing with each other and the central tetrahedron. Geometrically, five isomers can be formed by successive  $60^\circ$  rotation of the  $\text{M}_3\text{O}_{13}$  groups (Figure 1-3). Among all the five isomers, the  $\alpha$ -Keggin structure, which has the overall  $T_d$  symmetry, is the most thermodynamic stable.

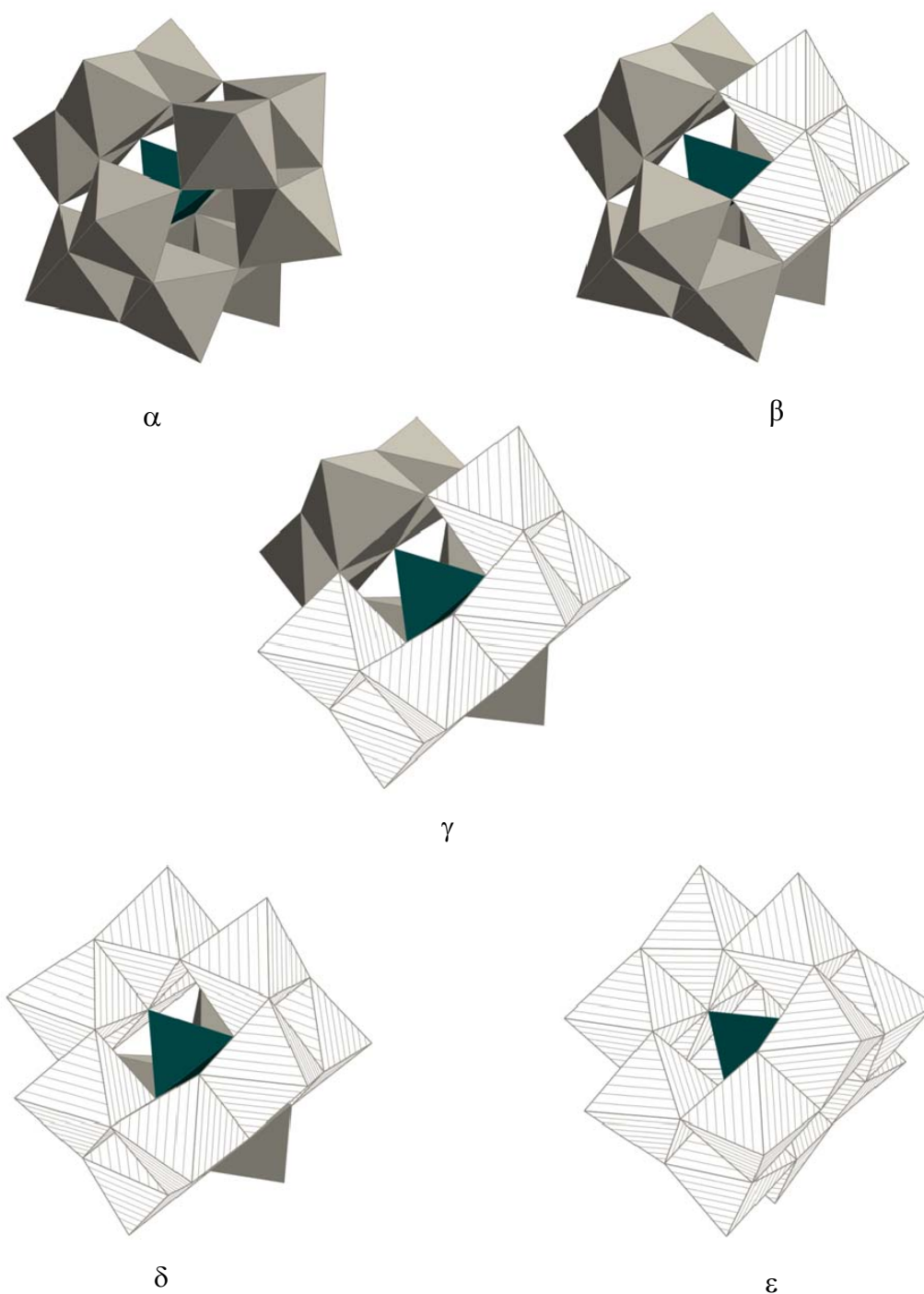


**Figure 1-3.** The five Baker-Figgis isomers of the Keggin structure:  $\alpha$ ,  $\beta$ ,  $\gamma$ ,  $\delta$ ,  $\epsilon$ . The rotated  $M_3O_{13}$  group(s) are show in light crosshatch.

The Wells-Dawson structure has general formula  $[X_2M_{18}O_{62}]^{n-}$ . It is formed by two  $XO_4$  tetrahedra each coordinating one  $M_3O_{13}$  triad cap and one  $M_6O_{14}$  belt which links to the other  $M_6O_{14}$  belt by sharing corner oxygen atoms (Figure 1-4). Although Baker and Figgis<sup>11</sup> proposed six isomers of the Dawson structures, only four of them have been observed to date<sup>12</sup> and the  $\alpha$  and  $\beta$  isomers are the most common ones.

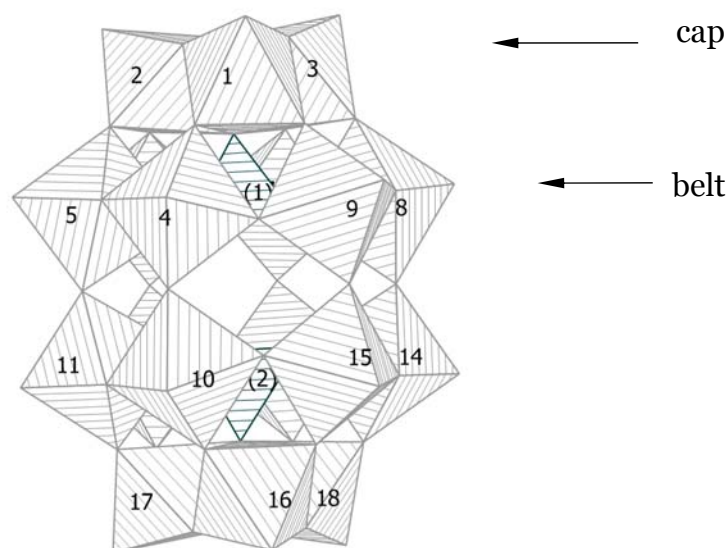


**Figure 1-4.** IUPAC numbering scheme of  $[\alpha-M_2W_{18}O_{62}]^{n-}$  (the Wells-Dawson structure)

The structurally saturated parent (or “plenary”) Keggin and Wells-Dawson POMs are usually stable at low pH environment. At a higher pH, a complex series of hydrolysis reactions occur. With the removal of one or more  $MO_x$  unit from the parent structure, defect or “lacunary” POMs are formed.

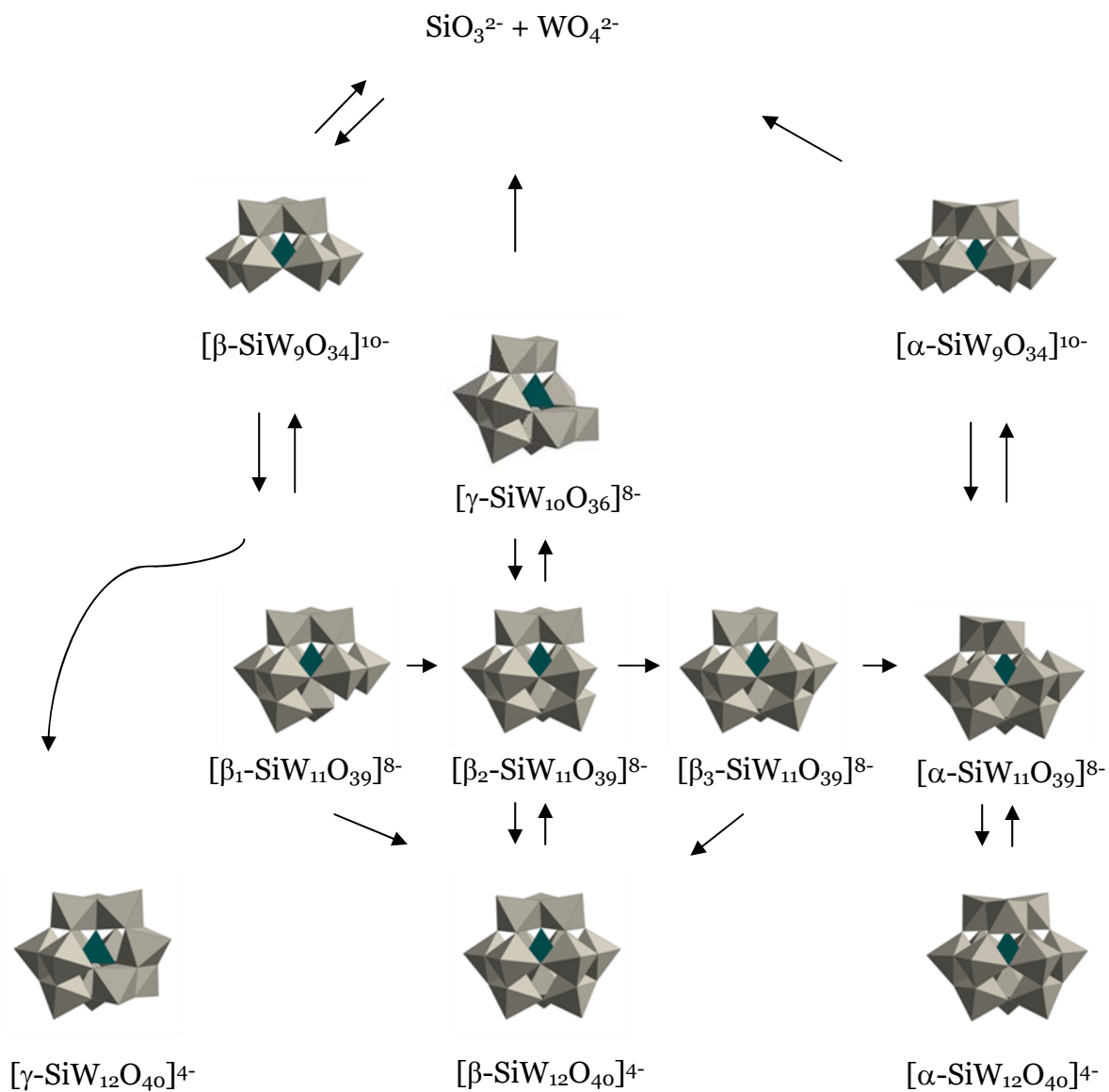


**Figure 1-5.** General route for synthesis of dodecatungstosilicate isomers and related mono-, bi- and tri-vacant polysilicotungstates.

For the Keggin type POMs, mono-, bi- and tri-lacunary species can be formed under different hydrolysis conditions. Four monolacunary Keggin polytungstosilicate isomers are known as shown in Figure 1-5.<sup>13</sup> All the  $\beta$  isomers are unstable in solution and slowly convert to the  $\alpha$  isomer. For the Keggin type polytungstophosphates only the  $\alpha$  isomer is observed. According to the “Lipscomb Principle”, no stable  $\{XW_{10}\}$  species can be prepared by removing a  $WO_6$  octahedra from the  $\alpha$ -,  $\beta_1$ - and  $\beta_3$ - $[XW_{10}O_{39}]^n$ . Indeed, from the hydrolysis of  $[\beta_2\text{-SiW}_{11}\text{O}_{39}]^{8-}$ , a  $\{\text{SiW}_{10}\}$  species has been prepared and identified to be  $[\gamma\text{-SiW}_{10}\text{O}_{36}]^{8-}$ . There are two types of trivacant lacunary POMs species which are designated A and B. The A type is formed by removing three corner-sharing  $WO_6$  octahedron from three neighboring  $W_3O_{13}$  triads in the POM. The B type is formed by removing an edge-sharing  $W_3O_6$  cap.

Multi-lacunary Wells-Dawson structures can also be prepared by controlled hydrolysis. There are two monovacant isomers derived from the  $\alpha$ -Well-Dawson structure. The  $\alpha_2$  isomer,  $[\alpha_2\text{-P}_2\text{W}_{17}\text{O}_{61}]^{10-}$ , is obtained by removing a  $WO_x$  octahedra from one of the cap  $W_3O_{13}$  triads of the  $[\alpha\text{-P}_2\text{W}_{18}\text{O}_{62}]^{6-}$ . The  $\alpha_1$  isomer has the lacunary site in the belt position and can only be prepared by adding  $WO_x$  octahedra to a hexavacant Well-Dawson structure  $[\text{P}_2\text{W}_{12}\text{O}_{48}]^{14-}$ . The hexavacant POM is formed by removing six  $WO_x$  units along the  $C_3$  axis of the  $[\alpha\text{-P}_2\text{W}_{18}\text{O}_{62}]^{6-}$ . The common trivacant  $[\text{P}_2\text{W}_{15}\text{O}_{56}]^{12-}$  is formed by the removal of one of the cap  $M_3O_{13}$  triads from the parent structure. The formation and conversion of these species is shown in Figure 1-6.

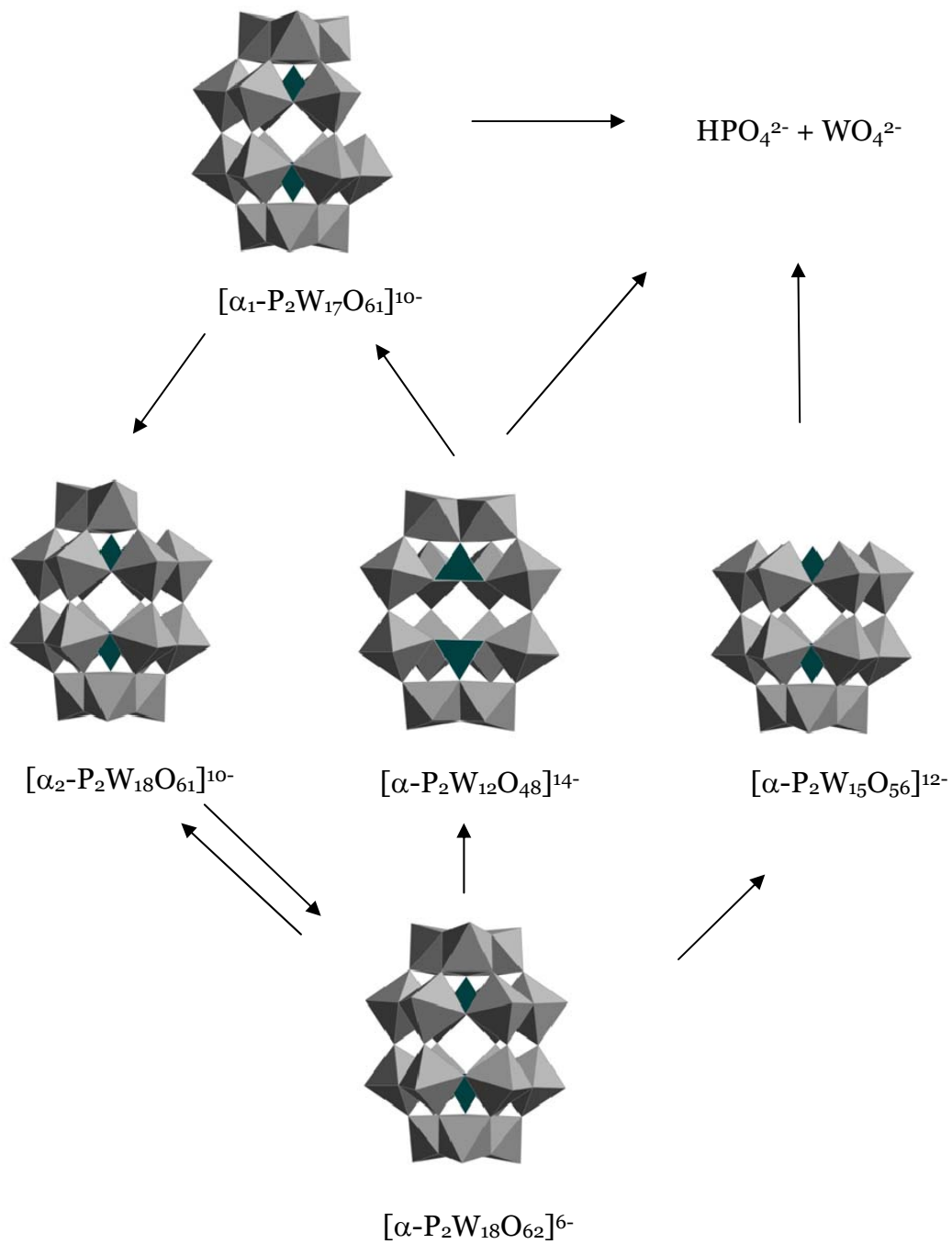


**Figure 1-6.** Relationships between the different polytungstodiphosphate species.

The lacunary POMs can react with d-electron transition metals and afford transition-metal substituted POMs (TMSPs) with the d-electron centers coordinated in the lacunary sites. The reaction between monovacant POMs and transition metals usually results in saturated monosubstituted TMSPs. The monovacant POM functions as a pentadentate ligand and usually the metal coordinated in the lacunary site has a sixth ligand. As a consequence of the high  $T_d$  symmetry, the transition metal in the monosubstituted  $\alpha$ -Keggin always disorders in the twelve symmetric positions which prevents the X-ray diffraction from obtaining disorder-free structures.<sup>14</sup> As for the monosubstituted Keggin POM, the six belt positions in the  $\alpha_1$ -monosubstituted Well-Dawson POM and the three cap positions in the  $\alpha_2$  isomers of this polyanion are also frequently disordered in crystals.<sup>15</sup> The coordination between trivacant POMs and low-valent d-electron transition metals leads to more complex TMSP compounds than the mono-substituted Keggin and Wells-Dawson derivatives. The most common POMs derived from the use of tri-vacant polyanions are two types of sandwich-like structures<sup>9, 16</sup>: the A-type sandwich POMs that contain three corner-sharing transition metal  $MO_6$  octahedra between two  $[A-\alpha-XW_9O_{34}]^{n-}$  units, and the B-type sandwich POMs that contain four edge-sharing metal octahedra between two B- $\alpha$ -trivacant units. These trivacant units can be derived from either the Keggin or Wells-Dawson structural families. The divacant POM,  $[\gamma-SiW_{10}O_{36}]^{8-}$ , slowly isomerizes to  $[\alpha-SiW_{12}O_{40}]^{4-}$  in aqueous solution. The coordination between the divacant POM and transition metals under different conditions can lead to saturated disubstituted POMs,<sup>17, 18</sup> disubstituted dimers,<sup>19</sup>

and many other complexes.<sup>20-23</sup> Structures of some well-documented TMSPs are illustrated in Figure 1-7.

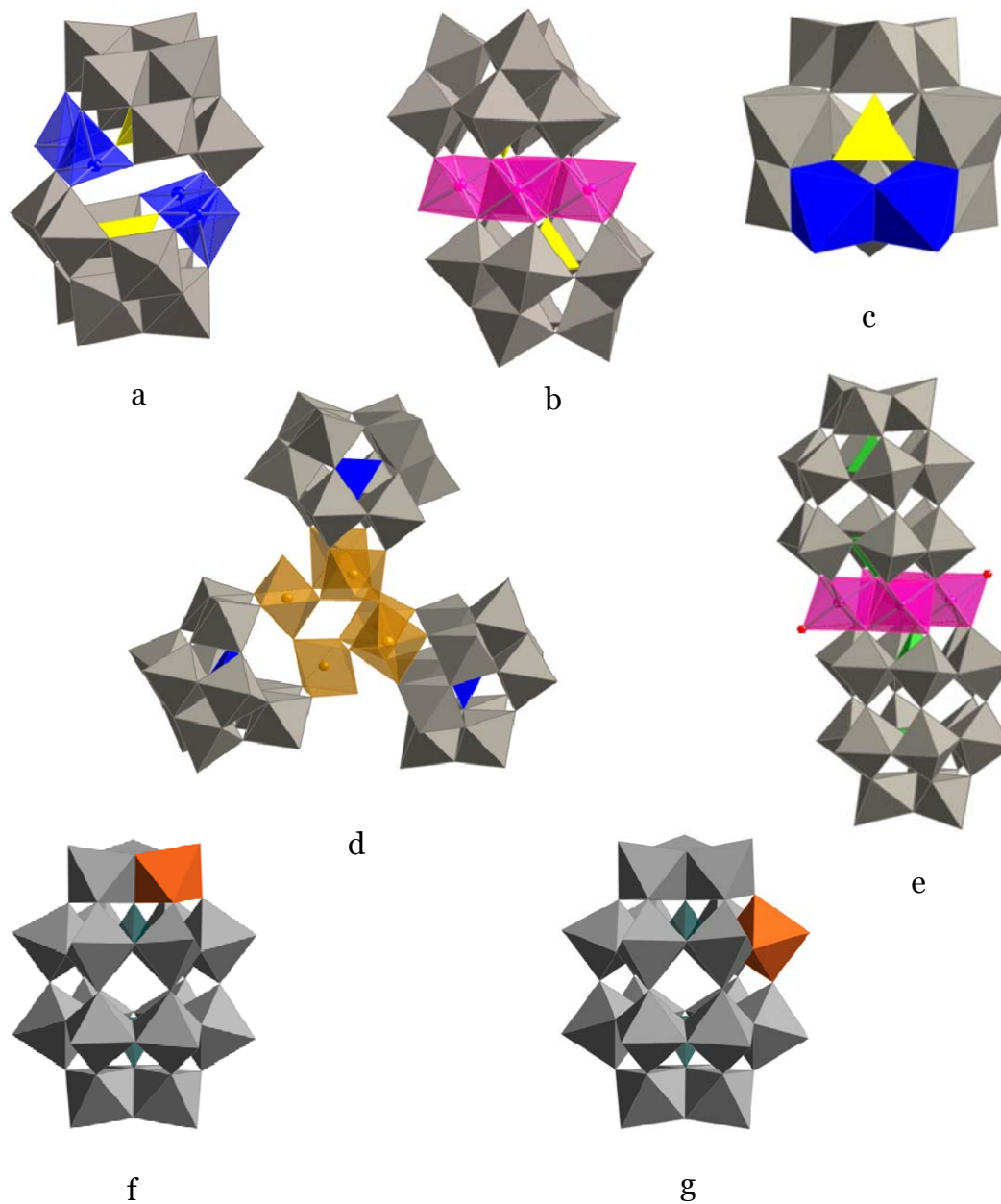


**Figure 1-7.** Polyhedral representations of TMSPs: a).  $[(\gamma\text{-Cu}_2(\text{H}_2\text{O})\text{SiW}_8\text{O}_{31})_2]^{12-}$ , b)  $[\text{Mn}_4(\text{H}_2\text{O})_2(\text{PW}_9\text{O}_{34})_2]^{10-}$ , c)  $[\gamma\text{-Cr}_2(\text{H}_2\text{O})_2\text{SiW}_{10}\text{O}_{36}]^{2-}$ , d)  $[\{\text{Fe}_2(\text{OH})_3(\text{H}_2\text{O})_2\}_3(\gamma\text{-SiW}_{10}\text{O}_{36})_3]^{15-}$ , e)  $[\text{Mn}_4(\text{H}_2\text{O})(\text{P}_2\text{W}_{15}\text{O}_{56})_2]^{16-}$ , f)  $[\alpha_2\text{-Co}(\text{H}_2\text{O})\text{P}_2\text{W}_{17}\text{O}_{61}]^{10-}$ , g)  $[\alpha_1\text{-Co}(\text{H}_2\text{O})\text{PW}_{17}\text{O}_{61}]^{10-}$ .

### Decontamination: Sulfoxidation catalyzed by TMSPs

Chemical warfare agents (CWAs) have been developed in laboratories around the world. CWAs are cheap, relatively accessible, and easy to transport making them some of the most feared and unpredictable agents of mass destruction in the hands of terrorists. On March 1995, the releasing of sarin (see Figure 1-8) into the Tokyo subway system killed 12 people and injured over 5,000. Decontamination, aimed at eliminating these hazardous CWAs, is required in battlefield as well as in public places which are vulnerable to terrorist attacks.

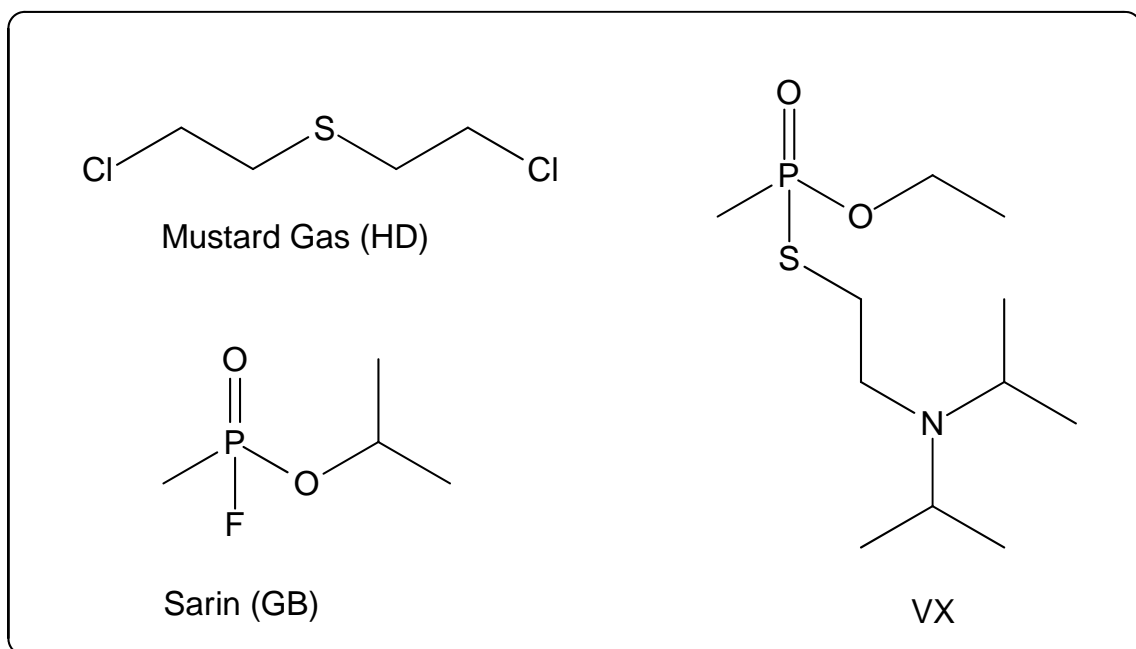


**Figure 1-8.** Some typical chemical warfare agents.

According to the intrinsic chemical structures of these CWAs, oxidation and hydrolysis are the most common methods used for decontamination.<sup>24</sup> The nerve agents (principally VX, GB and GD) are a class of organic phosphorus compounds and can be decontaminated by hydrolysis.<sup>25</sup> Mustard gas (HD) and

VX contain a reduced sulfur group making them both susceptible to potential oxidative decontamination.<sup>24, 26</sup> Most of the decontamination systems currently used by U.S. Army contain reagents that oxidize HD stoichiometrically although rapidly. Popular stoichiometric decontaminants range from the old STB (Tropical Standard Bleach, a concentrated basic solution of NaOCl) and DS2 (hydroxide in glyme type solvents) to the newer green and effective bicarbonate/peroxide systems.<sup>24</sup> All these reagents contain large amounts of oxidant and are corrosive to most surfaces and deleterious to the skin. In addition, these decontamination systems aren't amenable to use as solids and they must be stored in special containers. As a consequence, they aren't viable as components for self-decontaminating coatings, fabrics and filter materials which are widely needed for preventive defense and protection.

TMSPs have long been investigated as oxidation catalysts because they combine attractive physical and chemical properties with highly tunable redox chemistry. Early studies by Hill and coworkers demonstrated that TMSPs can act as efficient oxygenation (oxo transfer oxidation) catalysts for various hydrocarbons.<sup>27-32</sup> Recently Okun and Hill laboratory co-workers<sup>9, 14, 33-36</sup> reported that several TMSPs can catalyze the selective conversion of 2-chloroethyl ethyl sulfide (CEES), a mustard (HD) simulant, to CEESO in organic solvents under ambient conditions (Figure 1-9). Investigations revealed that NO<sub>x</sub> species may be involved in sulfoxidation catalyzed by iron-substituted Keggin POMs.<sup>14</sup> Previously, Bosch and Kochi<sup>37</sup> found that nitrogen dioxide can catalyze selective sulfoxidation under ambient conditions by air via a nitrosonium complex intermediate. By combining the knowledge of nitrosonium

intermediates in catalytic sulfoxidation with the data on transition-metal-substituted-POM catalyzed oxidation, the Hill group developed a highly active multicomponent oxidation catalyst that the group has termed the “hot catalyst” because of its unprecedented reactivity (not because it is thermally activated).<sup>38</sup> The hot catalyst comprises the tetrabutylammonium (TBA) salt of tetrabrominoferrate and the TBA salt of a d-electron-metal-substituted POM to which nitrate is likely terminally bonded. Further investigation showed that the hot catalyst is not only highly effective in catalyzing the sulfoxidation but also efficiently removing many amines, aldehydes and mercaptans that constitute nearly all odors in human environments.<sup>39</sup> However, the mechanism of these TMSP-catalyzed sulfoxidation and other oxidations remained uncertain in these earlier studies.

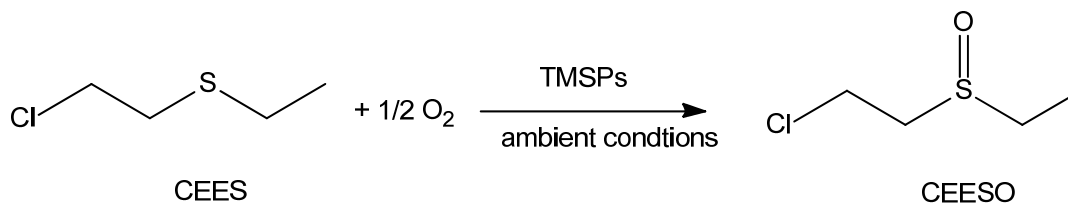


**Figure 1-9.** TMSP catalyzed sulfoxidation under ambient conditions.

### Goal of This Work

Recent studies have clearly shown that transition-metal-substituted POMs developed in our group have considerable potential in commercial applications in industrial oxidation catalysis, chemical warfare agent decontamination and household deodorization. Significantly, the development of practically useful TMSP-based catalysts requires the development of methods to immobilize POMs

on various solid supports surfaces. Parts of thesis address optimization of catalyst components, reproducible preparation of the hot catalyst, and development of an *in-situ* self-assemble method for loading (immobilizing) catalysts on different supports in order to enhance their activity and stability for applications.

Understanding the mechanism of TMSP-catalyzed sulfoxidation is both scientifically and practically significant. Elucidation of such mechanisms can help us design and improve the catalytic activity of the current TMSP-based catalysts. However, two factors have hindered mechanistic investigation to date: these catalysts are a mixture of TMSPs and other inorganic salts, and as noted above, these structurally and compositionally complicated systems aren't amenable to characterization by X-ray crystallography, due to disordered crystals, and NMR because of paramagnetism. In this thesis, the divacant  $\gamma$ -Keggin and trivacant Well-Dawson POMs are used as precursors. Two novel multi-copper-substituted polysilicotungstates and a series Well-Dawson sandwich-type POMs are described. More importantly, a simplification of the catalytic system has lead to the proposal of a bromine/tri-bromide based mechanism for the very fast catalytic aerobic (air-based) sulfoxidation reactions, and considerable kinetics and other data are consistent with this proposal.

## References

- (1) Pope, M. T., *Heteropoly and Isopoly Oxometalates*. Springer-Verlag: Berlin, 1983; p 180.

- (2) Pope, M. T., Isopolyanions and Heteropolyanions. In *Comprehensive Coordination Chemistry*, Wilkinson, G.; Gillard, R. D.; McCleverty, J. A., Eds. Pergamon Press: New York, 1987; Vol. 3, p Chapter 38.
- (3) Day, V. W.; Klemperer, W. G., *Science* **1985**, *228*, 533-541
- (4) Pope, M. T., Molybdenum Oxygen Chemistry: Oxides, Oxo Complexes, and Polyoxoanions. In *Progress in Inorganic Chemistry*, Lippard, S. J., Ed. John Wiley & Sons, Inc.: New York, 1991; Vol. 39, pp 181-257.
- (5) Rhule, J. T.; Hill, C. L.; Judd, D. A.; Schinazi, R. F., *Chem. Rev.* **1998**, *98*, 327-357
- (6) Hill, C. L.; Prosser-McCartha, C. M., *Coord. Chem. Rev.* **1995**, *143*, 407-455
- (7) Okuhara, T.; Mizuno, N.; Misono, M., *Advances in Catalysis* **1996**, *41*, 113-252
- (8) Mizuno, N.; Misono, M., *Chem. Rev.* **1998**, *98*, 199-218
- (9) Okun, N. M.; Anderson, T. M.; Hill, C. L., *J. Am. Chem. Soc.* **2003**, *125*, 3194-3195
- (10) Hill, C. L., *Chem. Rev.* **1998**, *98*, 1-2
- (11) Baker, L. C. W.; Figgis, J. S., *J. Am. Chem. Soc.* **1970**, *92*, 3794-3797
- (12) Contant, R.; Thouvenot, R., *Inorganica Chimica Acta* **1993**, *212*, 41-50
- (13) Tézé, A.; Hervé, G.,  $\alpha$ -,  $\beta$ -, and  $\gamma$ -Dodecatungstosilicic Acids: Isomers and related Lacunary Compounds. In *Inorg. Syn.*, Ginsberg, A. P., Ed. John Wiley and Sons: New York, 1990; Vol. 27, pp 85-96.
- (14) Okun, N. M.; Tarr, J. C.; Hillesheim, D. A.; Zhang, L.; Hardcastle, K. I.; Hill, C. L., *J. Mol. Catal. A. Chem.* **2006**, *246*, 11-17

- (15) Bartis, J.; Kunina, Y.; Blumenstein, M.; Francesconi, L. C., *Inorg. Chem.* **1996**, *35*, 1497-1501
- (16) Randall, W. J.; Droege, M. W.; Mizuno, N.; Nomiya, K.; Weakley, T. J. R.; Finke, R. G., Metal Complexes of the Lacunary Heteropolytungstates [B-alpha-PW<sub>9</sub>O<sub>34</sub>]<sup>9-</sup> and [alpha-P<sub>2</sub>W<sub>15</sub>O<sub>56</sub>]<sup>12-</sup>. In *Inorg. Syn.*, Cowley, A. H., Ed. John Wiley & Sons, Inc.: New York, 1997; Vol. 31, pp 167-185.
- (17) Xin, F.; Pope, M. T., *Inorg. Chem.* **1996**, *35*, 5693-5695
- (18) Nozaki, C.; Kiyoto, I.; Minai, Y.; Misono, M.; Mizuno, N., *Inorg. Chem.* **1999**, *38*, 5724-5729
- (19) Geletii, Y. V.; Botar, B.; Kögerler, P.; Hillesheim, D. A.; Musaev, D. G.; Hill, C. L., *Angew. Chem. Int. Ed.* **2008**, *47*, 3896-3899. Selected as the VIP Article by the reviewers and editor. Published online 3/20/08 DOI: 10.1002/anie.200705652
- (20) Luo, Z.; Kögerler, P.; Cao, R.; Hill, C. L., *Polyhedron* **2009**, *28*, 215-220
- (21) Luo, Z.; Kögerler, P.; Cao, R.; Hakim, I.; Hill, C. L., *Dalton Trans.* **2008**, 54-58
- (22) Bassil, B. S.; Nellutla, S.; Kortz, U.; Stowe, A. C.; Tol, J. v.; Dalal, N. S.; Keita, B.; Nadjo, L., *Inorg. Chem.* **2005**, *44*, 2659-2665
- (23) Bassil, B. S.; Kortz, U.; Tigan, A. S.; Clemente-Juan, J. M.; Keita, B.; Oliveira, P. d.; Nadjo, L., *Inorg. Chem.* **2005**, *44*, 9360-9368
- (24) Yang, Y. C.; Baker, J. A.; Ward, J. R., *Chem. Rev.* **1992**, *92*, 1729-1743
- (25) Yang, Y.-C., *Acc. Chem. Res.* **1999**, *32*, 109-115
- (26) Smith, B. M., *Chem. Soc. Rev.* **2008**, 470 - 478
- (27) Hill, C. L.; Bouchard, D. A., *J. Am. Chem. Soc.* **1985**, *107*, 5148-5157

- (28) Schmidt, J. A.; Hilinski, E. F.; Bouchard, D. A.; Hill, C. L., *Chem. Phys. Lett.* **1987**, *138*, 346-51
- (29) Hill, C. L., Catalytic Oxygenation of Unactivated C-H Bonds. Superior Oxo Transfer Catalysts and the 'Inorganic Porphyrin'. In *Activation and Functionalization of Alkanes*, Hill, C. L., Ed. Wiley: New York, 1989; pp 243-279.
- (30) Chambers, R. C.; Hill, C. L., *J. Am. Chem. Soc.* **1990**, *112*, 8427-33
- (31) Hill, C. L., *Catal. Met. Complexes* **1992**, *9*, 253-80
- (32) Hill, C. L.; Kozik, M.; Winkler, J.; Hou, Y.; Prosser-McCartha, C. M., *Adv. Chem. Ser.* **1993**, *238*, 243-59
- (33) Okun, N. M.; Anderson, T. M.; Hardcastle, K. I.; Hill, C. L., *Inorg. Chem.* **2003**, *42*, 6610-6612
- (34) Okun, N. M.; Anderson, T. M.; Hill, C. L., *J. Mol. Catal. A: Chem.* **2003**, *197*, 283-290
- (35) Okun, N. M.; Ritorto, M. D.; Anderson, T. M.; Apkarian, R. P.; Hill, C. L., *Chem Mater.* **2004**, *16*, 2551-2558
- (36) Hill, C. L.; Okun, N. M.; Hillesheim, D. A.; Geletii, Y. V., Catalysts for Aerobic Decontamination of Chemical Warfare Agents Under Ambient Conditions. In *ACS Symposium Series*, Reynolds, J. G.; Lawson, G. E.; Koester, C. J., Eds. American Chemical Society: Washington, D.C., 2007; Vol. 980, pp 198-209.
- (37) Bosch, E.; Kochi, J. K., *J. Org. Chem.* **1995**, *60*, 3172-3183
- (38) Okun, N. M.; Luo, Z.; Hill, C. L. *P&G Research Report*; Emory University: Atlanta, 2006.
- (39) Luo, Z.; Okun, N. M.; Hill, C. L. *P&G Research Report*; Emory University: Atlanta, 2007-2008.

## *Chapter 2*

# Synthesis and Characterization of Solid-Supported Catalytic TMSP Materials for Aerobic Sulfoxidation

with Nelya M. Okun, and Craig L. Hill

(partially submitted to PCT Int. Appl. (2008), 44pp, PCT/US2007/007590, and the research reports of Gentex Co., TDA Research Inc. and P&G Co.)

## Abstract

A nitrate and bromide-containing transition-metal-substituted POM (TMSP)-based catalyst has been developed. This material catalyzes fast and selective sulfoxidation using ambient air as the oxidant. To make this catalyst practically applicable, several different solid supports were evaluated including  $\text{TiO}_2$ ,  $\text{SiO}_2$ , carbon and cationic silica ( $(\text{Si}/\text{AlO}_2)^+$ ). The active catalysts were obtained by using an *in situ* layer-by-layer self-assembly procedure involving the catalyst components and each support material. The subsequent work shows that addition of proton to the final catalytic systems significantly enhances sulfoxidation while water inhibits them.

## Introduction

The development of new materials to catalyze the selective aerobic oxidation of sulfur-containing compounds under ambient conditions (1 atm air/ $\text{O}_2$  and  $25^\circ\text{C}$ ) is of both intellectual and practical interest.<sup>1-7</sup> The sulfoxidation of sulfides (thioethers) is important in both the organic synthesis and the decontamination of chemical warfare agents, especially for the decontamination of sulfur mustard (HD). The selected mono-sulfoxidated product of HD, mustard sulfoxide<sup>8</sup>, is much less toxic than the overoxidized (di-oxo) product, mustard sulfone.<sup>9</sup> When the decontamination research is performed in laboratory, 2-chloroethyl ethyl sulfide (CEES), a HD analogue, is always used. The net catalytic air ( $\text{O}_2$ )-based oxidative decontamination of CEES is illustrated in Scheme 2-1.



enhancing its activity and stability for future commercial applications by using different supports, POMs and additives. Trivalent  $\text{Na}_9[\text{A-PW}_9\text{O}_{34}]$  and its derivatives are used as parent POMs, and  $\text{TiO}_2$ ,  $\text{Al}_2\text{O}_3$  and  $\text{SiO}_2$  are used as supports in our investigation. The final catalysts are self-assembled on the surface of the supports. The catalytic activities of these products are measured by the sulfoxidation of CEES to CEESO in liquid phase. Different methods are used to modify the catalyst. The catalyst is stable in the temperature range from 0 to  $80^\circ\text{C}$ . Experiment results indicate an induction period exists in the catalytic oxidation. The addition of protic acids significantly reduces the induction period and enhances catalytic ability. In contrast, a low concentration of water (>4% weight) remarkably increases the induction period and inhibits the activity of catalyst. Interestingly, a subsequent drying process (specifically water removal) can lead to complete recovery of activity of the previously wet catalyst.

## **Experiments**

### *General methods and materials*

$\text{Na}_9[\text{A-PW}_9\text{O}_{34}]$  was prepared by the literature methods,<sup>21</sup> and its purities were checked by FT-IR. Carbon beads,  $\text{Al}_2\text{O}_3$  and  $\text{TiO}_2$  nanoparticles were obtained from Gentex Corporation;  $\text{SiO}_2$  was obtained from TDA Corporation, and all the materials were used as received.  $\text{Cr}(\text{NO}_3)_3 \cdot 9\text{H}_2\text{O}$ ,  $\text{Mn}(\text{NO}_3)_2$ ,  $\text{Fe}(\text{NO}_3)_3 \cdot 9\text{H}_2\text{O}$ ,  $\text{Co}(\text{NO}_3)_2$ ,  $\text{Ni}(\text{NO}_3)_2 \cdot 6\text{H}_2\text{O}$ ,  $\text{Cu}(\text{NO}_3)_2 \cdot 2.5\text{H}_2\text{O}$ , acetonitrile, 1,3-dichlorobenzene and 2-chlorethyl ethyl sulfide (CEES) were purchased from Aldrich and used without further purification. The infrared spectra were

recorded on a Nicolet 510 FT-IR spectrometer. Oxidation products were identified by gas chromatography-mass spectrometry (GC/MS; Hewlett Packard 5890 series II gas chromatograph connected to a Hewlett Packard 5971 mass selective detector) and quantified by gas chromatography (GC; Hewlett Packard 5890 series gas chromatograph equipped with a flame ionization detector, 5% phenyl methyl silicone capillary column, N<sub>2</sub> carrier gas, and a Hewlett Packard 3390A series integrator). The BET surface areas of carbon and catalysts were determined by Quantachrome model NOVA 2000 surface area analyzer. The surface charge density and point of zero charge were obtained through potentiometric titration.

*1. Preparation of the "hot catalyst", a mixture complex contained nitrate, bromide and transition-metal-substituted POMs ("Fe/Cu/PW<sub>11</sub>/Br/NO<sub>3</sub>")*

*Step 1.*

The overall preparation starts with the preparation of TBA<sub>9-x</sub>Na<sub>x</sub>PW<sub>11</sub>O<sub>39</sub>. Solid Na<sub>9</sub>[A-PW<sub>9</sub>O<sub>34</sub>]•7H<sub>2</sub>O (10 g, ca. 3.7 mmol) is dissolved in 100 mL of deionized water. To this solution TBABr (80 g, ca. 248 mmol) dissolved in 160 mL of deionized water is added. The mixture is stirred for 30 min at room temperature. The slightly acidic conditions convert [PW<sub>9</sub>O<sub>34</sub>]<sup>9-</sup> to [PW<sub>11</sub>O<sub>39</sub>]<sup>7-</sup> *in situ*. The resulting precipitate TBA<sub>7-x</sub>Na<sub>x</sub>PW<sub>11</sub>O<sub>39</sub> (ca. 15.8 g) is separated by filtration over a fine frit, washed with 2-3 portions of 100 mL of water and vacuum dried overnight.

*Step 2.*

Solid  $\text{Cu}(\text{NO}_3)_2$  (0.52 g, 2.8 mmol) is dissolved in 20 mL of acetonitrile to which solid  $\text{TBA}_{7-x}\text{Na}_x\text{PW}_9\text{O}_{11}$  (4.0 g,  $\sim 1.4$  mmol) dissolved in 20 mL of acetonitrile is added with vigorous stirring. A greenish-blue solution is formed. The solution is placed in a beaker for several days until all the solvent evaporates. The resulting white-blue product (4.5 g) henceforth is referred to as “TBA/Cu/PW<sub>11</sub>/NO<sub>3</sub>”

### *Step 3.*

An arbitrary amount of “TBA/Cu/PW<sub>11</sub>/NO<sub>3</sub>” is weighed and mixed with  $\text{TBAFeBr}_4$  (1:1 weight %) using a mortar and pestle. The final product is dark brown and stored in a 100 ml brown vial. This product is referred to henceforth as “Fe/Cu/PW<sub>11</sub>/Br/NO<sub>3</sub>”.

## *2. Modifying the hot catalysts by using different transition metals*

The effect of different first-row transition metals on the activity of the catalytic materials was studied. The preparation of the hot catalysts with different added transition metal complexes is similar to preparation of the parent hot catalyst given above..

Step 1 is the same as described in hot catalyst preparation. In step 2 solid  $\text{Cr}(\text{NO}_3)_3 \cdot 9\text{H}_2\text{O}$ ,  $\text{Mn}(\text{NO}_3)_2$ ,  $\text{Co}(\text{NO}_3)_2$  or  $\text{Ni}(\text{NO}_3)_2 \cdot 6\text{H}_2\text{O}$  is used instead of  $\text{Cu}(\text{NO}_3)_2$ . The resulting metal-substituted TBA POM salts are henceforth referred to as  $\text{TBA/Cr/PW}_{11}/\text{NO}_3$ ,  $\text{TBA/Mn/PW}_{11}/\text{NO}_3$ ,  $\text{TBA/Co/PW}_{11}/\text{NO}_3$  and  $\text{TBA/Ni/PW}_{11}/\text{NO}_3$ . The final products are obtained by mixing an arbitrary amount of “TBA/M/PW<sub>11</sub>/NO<sub>3</sub>” (M = Cr, Mn, Co and Ni) with  $\text{TBAFeBr}_4$  (1:1

weight %) using a mortar and pestle and these subsequent products are henceforth referred to as “Fe/Cr/PW<sub>11</sub>/Br/NO<sub>3</sub>, Fe/Mn/PW<sub>11</sub>/Br/NO<sub>3</sub>, Fe/Co/PW<sub>11</sub>/Br/NO<sub>3</sub>, and Fe/Ni/PW<sub>11</sub>/Br/NO<sub>3</sub>”.

### *3. Preparation of solid supported POM catalysts*

#### *Step 1.*

To a solution of Na<sub>9</sub>PW<sub>9</sub>O<sub>34</sub>•7H<sub>2</sub>O (3.5 g; 1.2 mmol) in water (350 mL) carbon beads (31.5 g) are added at once while stirring. The mixture is stirred overnight at ambient temperature, washed with water on the filter and dried in air. The amount of POM bound to the surface is determined by subtracting the amount of POM (mmol) precipitated by addition of TBABr to a supernatant combined with the water collected after washing the beads, from the initial amount of POM used in the reaction. The resulting product (henceforth referred to as “PW<sub>11</sub>/C”) contains 0.099 g or 0.034 mmol of bound POM per 1 g of carbon.

#### *Step 2.*

To PW<sub>11</sub>/C (1.0 g; 0.034 mmol POM) suspended in 10 mL of acetonitrile is added FeBr<sub>3</sub> (0.030 g; 0.10 mmol) dissolved in 1.0 mL of acetonitrile. The mixture is stirred until all the solvent is evaporated, washed with acetonitrile on the filter and air dried. The resulting product is henceforth referred to as “Fe/PW<sub>11</sub>/Br/C”.

#### *Step 3.*

To Fe/PW<sub>11</sub>/Br/C (1 g; 0.034 mmol of PW<sub>11</sub>) suspended in 10 mL of acetonitrile is added solid Cu(NO<sub>3</sub>)<sub>2</sub> (0.019 g 0.10 mmol). The mixture is stirred

until all the solvent is evaporated, washed with acetonitrile on the filter and air dried resulting in final product henceforth referred to as “Fe/PW<sub>11</sub>/Br/Cu/NO<sub>3</sub>/C”. Analogous procedures are used for preparation of all other catalysts on Al<sub>2</sub>O<sub>3</sub>, TiO<sub>2</sub> and aluminum modified cationic silica ((Si/AlO<sub>2</sub>)<sup>+</sup>).

#### *4. BET surface area measurements*

The specific surface area of the samples is obtained by the standard method of Brunauer-Emmet-Teller (BET) adsorption isotherms applied in a relative pressure range from 0.06 to 0.35. Prior to determination of the isotherm the samples (~0.3 - 0.5 g) are outgassed overnight at 150 °C under vacuum to remove the moisture and other contaminants. The nitrogen adsorption-desorption isotherms of the samples are recorded at 77 K and analyzed with Enhanced Data Reduction Program, version 2.13. The pore size distribution is calculated on the basis of desorption data by employing the Barret-Joyner-Halenda (BJH) method.

#### *5. Catalytic oxidation of the HD analogue 2-chloroethyl ethyl sulfide (CEES) in acetonitrile solution*

In a typical CEES oxidation reaction, 0.01 mmol of “Fe/Cu/PW<sub>11</sub>/Br/NO<sub>3</sub>” (~ 32 mg) or 130 mg solid-supported POM is weighed out into 20-mL vial and dissolved / suspended in 2.3 mL of acetonitrile. 1,3-Dichlorobenzene (0.095 mL) (GC internal standard) is added to the vials, and they are sealed. After stirring for 5-10 min, 0.105 mL CEES is added via syringe to a vial fitted with a PTFE septum. Air access during the experiment is provided through a needle in the

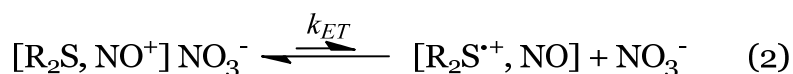
cap. The reaction is monitored for 20 h. Aliquots are analyzed by GC analysis every 20 min.

## Results and Discussion

### *Preparation and catalytic activity of Fe/Cu/PW<sub>11</sub>/Br/NO<sub>3</sub> complex*

Sulfoxidation is an important reaction in organic synthesis and many studies in this field have been conducted in the past decades.<sup>1, 22, 23</sup> Early in 1865, Macker<sup>24</sup> had reported the use of nitric acid to selectively oxidize dibenzyl sulfide to dibenzyl sulfoxide. However, the application of nitric acid for sulfoxidation in organic synthesis has been largely ignored. More recent studies by Bosch and Kochi<sup>1</sup> found that nitrogen dioxide can catalyze selective sulfoxidation under ambient conditions by air via a nitrosonium complex intermediate.

Their proposed mechanism is as follows:



The catalytic cycle is illustrated as in Figure 2-1. In the proposed mechanism, the formation of the nitrosonium complex and thioether radical cation plays an important role in the sulfoxidation, and the charge/electron transfer in the nitrosonium-thioether complex (which forms the thioether radical cation complex) is the rate-determining step.

Previously, Okun and coworkers<sup>12-16</sup> in our group discovered that several iron and copper substituted POMs catalyze O<sub>2</sub>/air-based selective sulfoxidation. The data implicating the potential importance of nitrosonium intermediates in catalytic sulfoxidation combined with the data on transition-metal-substituted POM-catalyzed oxidation suggested to us that a metal-substituted POM containing a terminally bound nitrate or related group might also function as a selective catalyst for thioether oxidation. In order to find a highly active nitrate containing POM complex, Fe(NO<sub>3</sub>)<sub>3</sub>, FeBr<sub>3</sub>, Cu(NO<sub>3</sub>)<sub>2</sub> and TBA<sub>x</sub>H<sub>7-x</sub>PW<sub>11</sub>O<sub>39</sub> were used and the liquid phase catalytic activities of CEES oxidation of different combinations are recorded as in Table 2-1.<sup>17</sup>

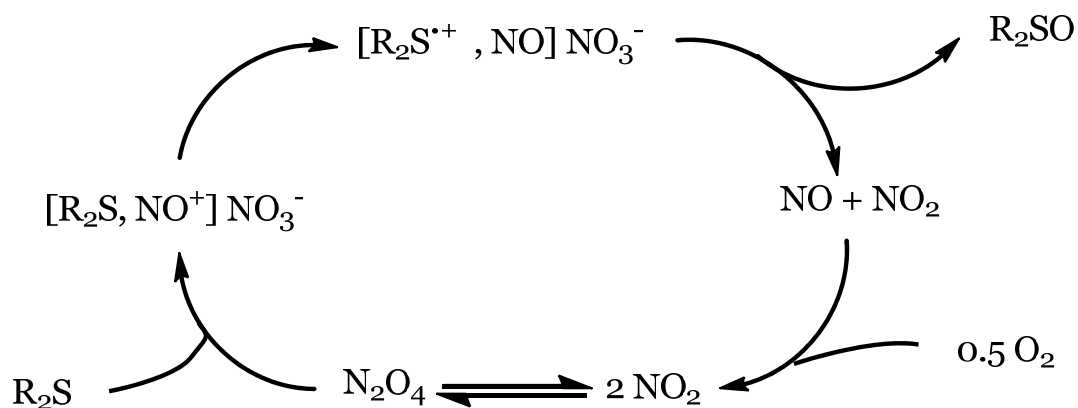


**Figure 2-1.** The catalytic cycle of NO<sub>2</sub>-catalyzed O<sub>2</sub>-based sulfoxidation.

**Table 2-1.** Aerobic oxidation of 2-chloroethyl ethyl sulfide (CEES) in acetonitrile by nitrate and bromide-containing polyoxometalate (POM)-based catalysts.

| Catalyst combinations  | [catalyst]<br>(g) | [POM]<br>(mmol) | % conv. | TON <sup>a</sup> |
|--|-------------------|-----------------|---------|------------------|
| TBA <sub>5-x</sub> H <sub>x</sub> [Fe(NO <sub>3</sub> )]/(A-PW <sub>11</sub> O <sub>39</sub> ) (referred as “TBA <sub>5-x</sub> Fe/N”) | 0.020             | 0.005           | 56      | 98               |
| TBA <sub>5-x</sub> H <sub>x</sub> [FeBr]/(A-PW <sub>11</sub> O <sub>39</sub> ) (referred as “TBA <sub>5-x</sub> Fe/Br”)                | 0.014             | 0.003           | 0       | 0                |
| TBA <sub>6-x</sub> H <sub>x</sub> [Cu(NO <sub>3</sub> )]/(A-PW <sub>11</sub> O <sub>39</sub> ) (referred as “TBA <sub>6-x</sub> Cu/N”) | 0.024             | 0.005           | 32      | 56               |
| TBA <sub>5-x</sub> Fe/N + TBA <sub>5-x</sub> Fe/Br   | 0.034             | 0.005           | 60      | 105              |
| TBA <sub>6-x</sub> Cu/N + TBA <sub>5-x</sub> Fe/Br   | 0.038             | 0.005           | 75      | 131              |

General conditions: 0.875 mmol (0.35 M) of CEES, catalyst (quantity given in column 2, estimated amount of bound POM given in column 3), 1 atm of air, 0.876 mmol (0.35 M) of 1,3-dichlorobenzene (internal standard) were stirred in 2.5 mL of acetonitrile at 25 °C for 20 h in the 20-mL vial; <sup>a</sup> turnovers = moles of converted CEES/ mol of catalyst.

The catalytic data show that without the presence of the nitrate group in the catalyst, there is no observable CEES oxidation after 20 hours. When iron or copper nitrate are used, the POM complexes show considerable catalytic activity for CEES oxidation and one of the complex combinations ( $\text{TBA}_{6-x}\text{Cu}/\text{N} + \text{TBA}_{5-x}\text{Fe}/\text{Br}$ ) converts 75% CEES to CEESO in 20 hours, which translates to 131 turnovers.

To investigate this complicated catalytic system further, the effects of different first-row transition metals (*e.g.*,  $\text{Fe}/\text{M}/\text{PW}_{11}/\text{Br}/\text{NO}_3$ ) on turnover were assessed.  $\text{Cr}(\text{NO}_3)_3 \cdot 9\text{H}_2\text{O}$ ,  $\text{Mn}(\text{NO}_3)_2$ ,  $\text{Co}(\text{NO}_3)_2$  and  $\text{Ni}(\text{NO}_3)_2 \cdot 6\text{H}_2\text{O}$  were used in the preparation of  $\text{Fe}/\text{M}/\text{PW}_{11}/\text{Br}/\text{NO}_3$  materials and the effects of these different transition metals on the catalytic activities were recorded (see Figure 2-2).

The data show that without the transition metal, the material is totally inactive. Among these metals, the Cu-containing catalyst has the best catalytic activity.

Based on these data, preparation for nitrate and bromide-containing POMs ( $\text{Fe}/\text{Cu}/\text{PW}_{11}/\text{Br}/\text{NO}_3$ ) have been developed. The catalytic activities in oxidizing CEES to CEESO by a typical  $\text{Fe}/\text{Cu}/\text{PW}_{11}/\text{Br}/\text{NO}_3$  mixture complex (the hot catalyst) are shown in Figure 2-3.

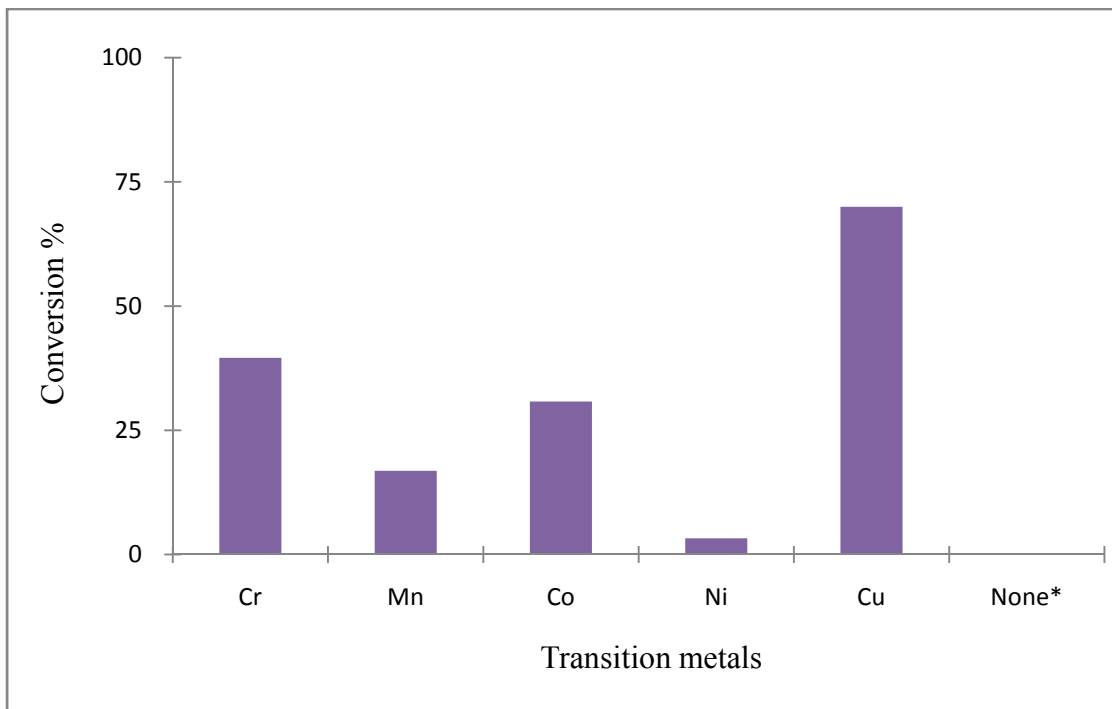


**Figure 2-2.** Conversion of CEES oxidation after 1.0 hour in the presence of 5 mM d-electron-transition-metal-substituted POM and 34 mM TBAFeBr<sub>4</sub>. Other conditions: 25°C, 1.0 atm O<sub>2</sub>, 2.5 mL CH<sub>3</sub>CN, [CEES]= 360 mM; \* 5mM of pure TBA<sub>7</sub>PW<sub>11</sub>O<sub>39</sub> were used in place of the d-electron-transition-metal-substituted POM.

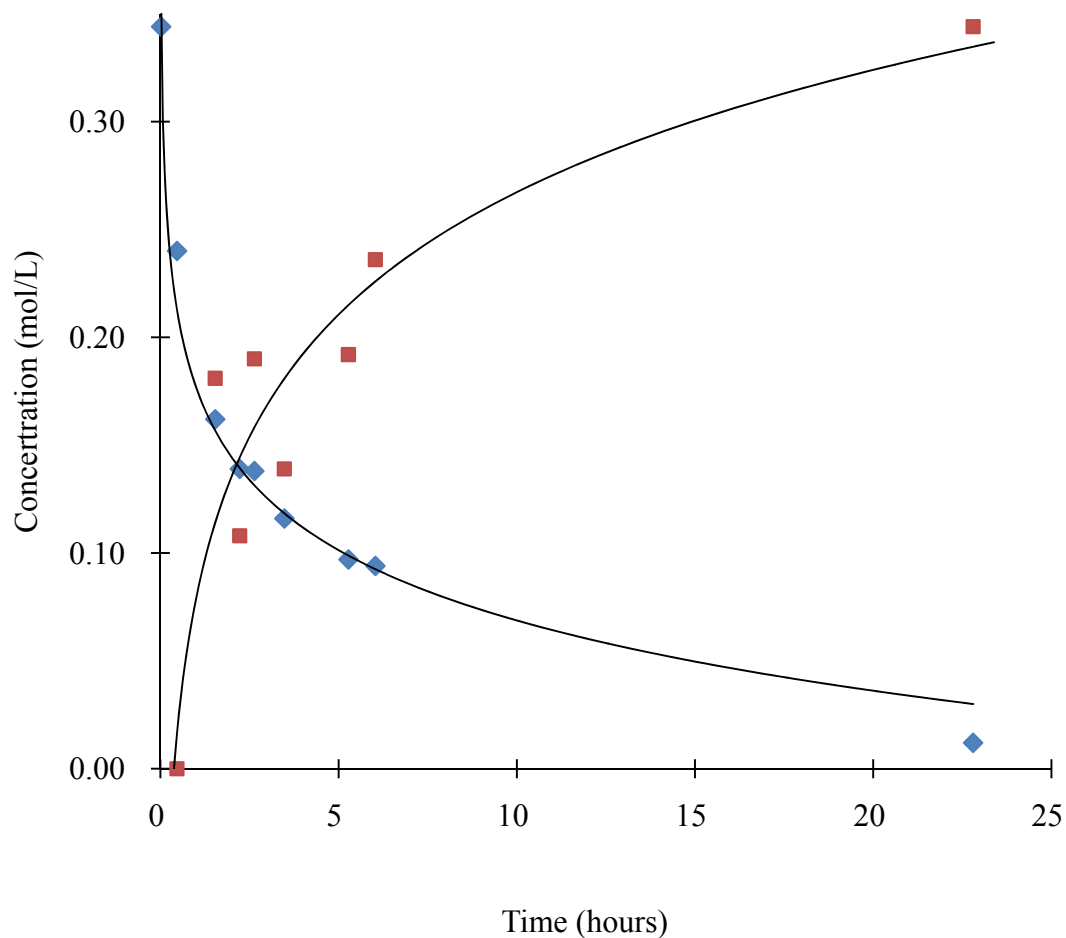


**Figure 2-3.** Time profile of aerobic CEES (0.35 mol/L) oxidation catalyzed by Fe/Cu/PW<sub>11</sub>/Br/NO<sub>3</sub> (0.05 g, 0.005 mmol based on POM) at 25°C (ambient conditions) in 2.5 mL acetonitrile. Consumption of CEES (◆) and production of CEESO (■) are shown.

The kinetic data show that the catalytic sulfoxidation is a pseudo-first-order reaction. The exponential equations used for fitting both the CEES consumption and CEESO generation curves as follows:

$$\text{CEES:} \quad \ln[\text{CEES}]_t = -1.6 - 0.231t \quad (4)$$

$$\text{CEESO:} \quad \ln(0.35 - [\text{CEESO}]_t) = -1.5 - 0.205t \quad (5)$$

The associated rate constant ( $k$ ) for the reaction is  $0.231 \text{ h}^{-1}$  and  $0.205 \text{ h}^{-1}$  based on the fitting. The exponential fitted data for the consumption of CEES and production of CEESO do not match well. This mis-match in the data could be a result of the lower sensitivity and larger error in the gas chromatography (GC) measurement of CEESO compared to CEES. With the highly polar sulfoxo group CEESO has a higher boiling point than CEES ( $279^\circ\text{C}$  versus  $156\sim 157^\circ\text{C}$ ), and it is more soluble in water than in less polar organic solutions. Also, some unknown small peaks appeared in the beginning of reaction, which indicate possible intermediate formed in the reaction (see Figure 2-4). All these properties result in a less intense peak and a longer retention time in the GC trace for CEESO versus CEES. The curve fitting calculations (by Microsoft Excel) of kinetic data for catalytic consumption of CEES always produces a curve that is smoother than that for CEESO production ( $R^2 = 0.9818$  versus  $0.9681$ ). In order to reduce the systematic error in the GC measurement, a conversion curve is always used. Thus CEES consumption is used for precise kinetic measurements (see Chapter 3). The conversion is defined as:

$$\text{Conversion}_t = \frac{[\text{CEESO}]_t}{[\text{CEES}]_t + [\text{CEESO}]_t} \times 100\% \quad (6)$$

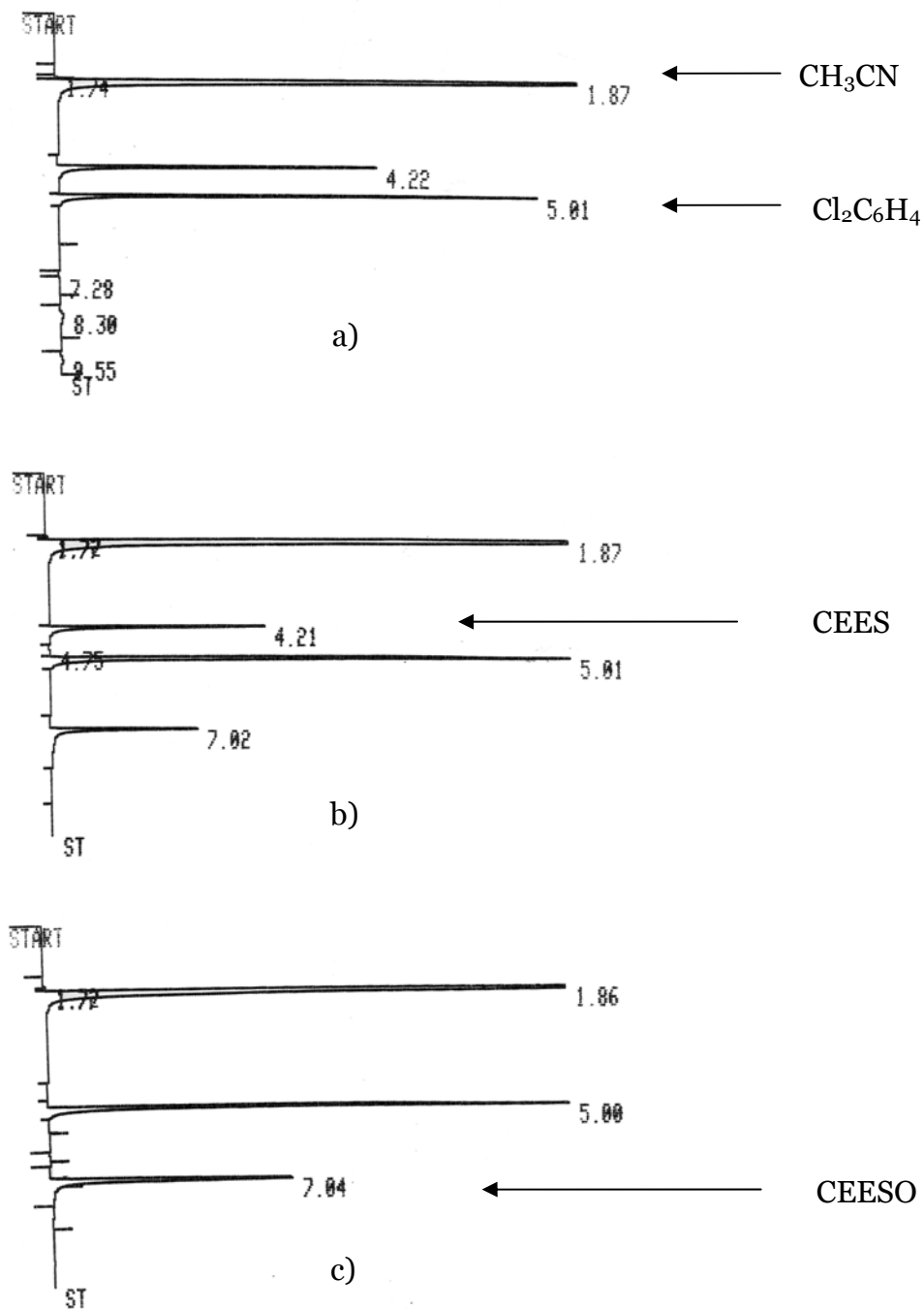


**Figure 2-4.** The GC traces showing effective 100% selective oxidation of CEES to CEESO. a), b), c) are traces taken at 1 min, 2 h and 30 h, respectively.

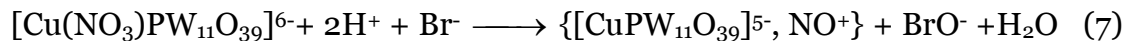
The conversion data show that CEES consumption is very fast at the beginning; however, no CEESO appears in the first 30 minutes. After 130 minutes nearly 60% CEES in the system is converted to CEESO. The reaction speed decreases after an hour and the 100% conversion requires about 20 hours. No sulfone (CEESO<sub>2</sub>) peak appears in the GC trace which means the sulfoxidation is highly selective (Figure 2-4). All the catalytic data reveal a very powerful catalyst that has potential applicability for the decontamination of sulfides such as mustard, thiols (ubiquitous odorants in human environments), H<sub>2</sub>S (a toxic industrial chemical or “TIC”) and other sulfur-based functional groups under ambient conditions. Also, the data show that the exponential curves do not fit the data well especially at the end of the reaction, which indicates that the sulfoxidation may have a complicated mechanism.

*A mechanism involving nitrosonium cation? The first assumption*

In order to develop practically applicable catalysts, many factors, such as humidity and temperature changes, which typically do not exist under laboratory conditions, must be considered. Clearly, understanding the mechanism of the catalytic reaction will be very helpful in assessing and understanding the impact of such factors.

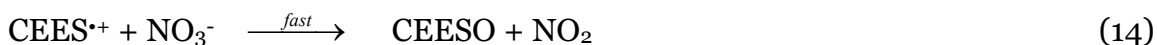
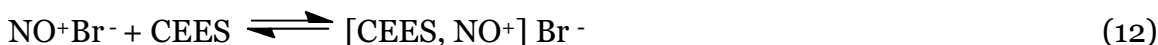
Because catalytic data in Table 2-1 show that in the absence of nitrate the metal-substituted POM is totally inactive, the possibility of a nitrosonium POM salt as a catalytic intermediate should be considered. Accordingly, two possible ways the POMs might be involved in the catalysis are as follows:

A. Nitrosonium-POM intermediate process:



The completed cycle is somewhat analogous to that in Figure 2-1.

B. Nitrosonium Bromide intermediate process:



The completed catalytic cycle is similar to that in Figure 2-1.

In proposed mechanism A, formation of a nitrosonium-POM complex in the first step is assumed. CEES should quickly coordinate to the Cu center on the POM in this complex. Following by a slow electron transfer process, the radical cation,  $\text{CEES}^{\bullet+}$  formed will be quickly oxidized to CEESO. Alternatively, mechanism B involves the formation of nitrosonium bromide catalyzed by POM, and the nitrosonium bromide helps catalyzing the CEES sulfoxidation. In both mechanisms, bromate is involved in the formation of nitrosonium. Further investigation found that the “ $\text{TBA}_{5-x}\text{Fe}/\text{N}$ ” used in Table 2-1 also contains

considerable amount of Br<sup>-</sup> which is introduced from TBA<sub>x</sub>H<sub>7-x</sub>PW<sub>11</sub>O<sub>39</sub> where a large amount of excess TBABr was used in preparation of monovacant precursor.

Recent research performed by Hillesheim, Young and Gueletii<sup>25</sup> in our group suggests that the proposed mechanism B is less likely. In their research they used a simplified system: a mixture containing only NOPF<sub>6</sub> and TBABr. The obvious inference is that this mixture forms the NO<sup>+</sup>Br<sup>-</sup> directly. The mixture has also been found to be active in catalyzing the aerobic oxidation of CEES. However, numerous observations are inconsistent with the suggestion that NOBr is the major product. NOBr is a known volatile compound (b.p. ~24°C) and yellow in color, but the UV-Vis spectrum of the NOPF<sub>6</sub> and TBABr mixture displays no peaks around 225 nm and 425 nm which are characteristic of BrNO and NOBr, respectively.<sup>26</sup> Also, the material they isolated after a completed catalytic reaction is a solid and retains its catalytic activity after heating to ~80 °C. The isolated material cannot be NOBr because NOBr is unstable and known to irreversibly dissociate to NO and Br radicals at such temperatures.<sup>27</sup> Isolation of the stable and catalytic active compound not only directly excludes proposed mechanism B above but also questions the formation of nitrosonium because all the methods they used to characterize the compound (IR, UV-Vis, NMR and mass spectrometry) showed no evidence for the existence of nitrosonium. Unfortunately, they also failed to indentify the compound by these characterization methods, thus they stated both the compound and its mechanism of its sulfoxidation remain unclear. In order to understand the “mysterious” compound obtained by Gueletii and Hillesheim, similar systems were investigated. One key compound has now been indentified and a Br<sub>2</sub>/Br<sub>3</sub><sup>-</sup>

based mechanism is proposed and confirmed by kinetic studies. These studies are summarized in Chapter 3.

### *Solid-supported POM catalysts*

The POM-based “hot catalyst” exhibits highly selective and efficient activity for sulfoxidation under ambient conditions. This highly unusual property makes it a promising candidate for potential commercial applications including chemical-weapon-decontaminating coating layers in army uniforms, air filters and household deodorizers. However, most commercially useful catalysts must work under heterogeneous conditions. This makes commercial catalysts easy to apply and reuse/recycle.

In our current work, commercially available  $\text{TiO}_2$ ,  $\text{Al}_2\text{O}_3$  from Gentex Corporation,  $\text{SiO}_2$  from TDA Corporation, PET fibers from Proctor and Gamble (P&G) and self-made cationic silica ( $\text{Si}/(\text{AlO}_2)^+$ ) have been used as solid supports for the hot catalyst. The catalytic activities have been measured and some factors which hinder/enhance the catalytic activities are being studied.

Previous work in our group lead to a simple and easy method to load the POM catalysts on solid supports.<sup>4</sup> Generally the solid support is added to an acetonitrile solution of the hot catalyst. After the mixture is stirred for several hours the resulting catalyst-supported solid is collected by filtration and dried overnight. The solid-supported catalyst prepared by this method retains its catalytic activity in gas phase sulfoxidation. Unfortunately, the liquid phase catalysis experiments demonstrated that the supported catalyst can be easily washed off the supports by organic solvents resulting in completely inactive

residual solid. Therefore, this simple established method might only be suitable for preparing supported hot catalyst materials which are used in gas phase catalysis. In order to attach the catalyst firmly on the surface of the supports, alternative methods have been developed.

Since POMs are a very large (and rapidly increasing) family of metal clusters with high negative charges, they should display strong electrostatic interactions with a positively charged surfaces.<sup>15, 28, 29</sup> Inspired by this suggestion, several different methods have been tested and an *in-situ* layer-by-layer (step-by-step) self-assembly catalyst preparation has been developed. In this preparation, a solid support is first suspended in water or acetonitrile solution, then the sodium or TBA salt of the parent POM (normally  $[\text{A-PW}_9\text{O}_{34}]^{9-}$  or its derivatives) is added and stirred overnight. The POM-supported solid is collected by filtration and dried. The POM not bound to the support is measured by weighting the remains of evaporated filtrate. The calculated amount of loaded POM varies from 5 to 15 weight percent for different supports. The dried POM-loaded solid is resuspended in acetonitrile solution and  $\text{FeBr}_3$  is added. The solution is continually stirred until all the solvent is evaporated. After washing the remaining solid with acetonitrile, the same procedure is repeated and  $\text{Cu}(\text{NO}_3)_2$  is added instead of  $\text{FeBr}_3$ . The final product is obtained again by washing the solid with acetonitrile and then drying under air. The resulting product is stable in acetonitrile and can be used as a heterogeneous catalyst for liquid phase reactions. During preparation, the sequence of adding  $\text{FeBr}_3$  and  $\text{Cu}(\text{NO}_3)_2$  is exacting. The solid supported POM catalyst exhibits little catalytic activity when it is prepared by adding  $\text{Cu}(\text{NO}_3)_2$  first and  $\text{FeBr}_3$  subsequently.

The solid-supported POM catalyst prepared by adding  $\text{FeBr}_3$  first and then  $\text{Cu}(\text{NO}_3)_2$  gives a much higher activity. This phenomenon may be partially attributed to the fast ligand exchange at the  $\text{Cu}(\text{II})$  center of the POM. The six coordinated  $\text{Cu}(\text{II})$  with a  $d^9$  electron configuration has a strong Jahn-Teller distortion in the ground state which makes axial bonds longer than equatorial ones. This leads to a rapid ligand exchange. In contrast, ligand change for  $\text{Fe}(\text{III})$  is considerably slower, in part because of its charge ( $3+$  versus  $2+$ ; the water-exchange rate constant for  $\text{Cu}^{2+}$  is about  $10^7$  times higher than that of  $\text{Fe}^{3+}$ ,  $10^9$  versus  $10^2$ ). Therefore, the catalytic activity is poor for the catalyst prepared by adding  $\text{Cu}(\text{NO}_3)_2$  before  $\text{FeBr}_3$  since most of the nitrate group is lost in the following resuspending and washing processes. When  $\text{Cu}(\text{NO}_3)_2$  is added in the last step, less nitrate group is lost in the washing process resulting in high catalytic activity of the final product.

$\text{Al}_2\text{O}_3$ ,  $\text{TiO}_2$ ,  $\text{SiO}_2$  and cationic silica supported catalysts have been obtained by using the similar *in-situ* layer-by-layer self-assembly preparation. Their catalytic activity data are listed in Table 2-2. This data shows that all the bulk supports are inactive in catalyzing aerobic sulfoxidation. Also the catalysts supported on the silica (both the commercial available "Davisil" provided by TDA and MCM-41 made in our laboratory) are inactive. The  $\text{TiO}_2$ ,  $\text{Al}_2\text{O}_3$ , and cationic silica supported catalysts all demonstrate considerable activity while the  $\text{TiO}_2$  supported catalyst,  $\text{TBA}/\text{Fe}/\text{PW}_{11}/\text{Br}/\text{Cu}/\text{NO}_3/\text{TiO}_2$ , converts 20% percent of CEES to CEESO in 20 hours (which translates 17.5 turnovers). The turnover rates of the solid-supported catalysts are much lower than those for the catalysts

in solution. This declining of activity is attributed to two factors: First, in a heterogeneous system, the number of effective sites of the catalyst is much less than that for the same amount catalyst in solution (homogeneous catalytic conditions). Some supported catalyst molecules are always covered or residing in crevices that renders them inaccessible or less accessible to the substrates in solution (e.g. CEES and  $O_2$  in this case). Steric constraints and other factors that can lower the effective local concentration of the substrate at the active site of supported catalysts, such as electrostatic repulsion, can also be operative (Figure 5). Secondly, the amount of loaded catalyst is calculated based on the amount of unloaded POM measured at the end of the preparation of step 1; however, the loss of POM in the subsequent stirring and washing processes is inevitable.

Figure 2-6 shows the kinetic data for air based sulfoxidation catalyzed by  $TiO_2$ ,  $Al_2O_3$  and cationic silica supported POMs. Unlike the immediate start of catalysis after the addition of hot catalyst, an induction period appears for all the sulfoxidation reactions catalyzed by solid supported POMs.

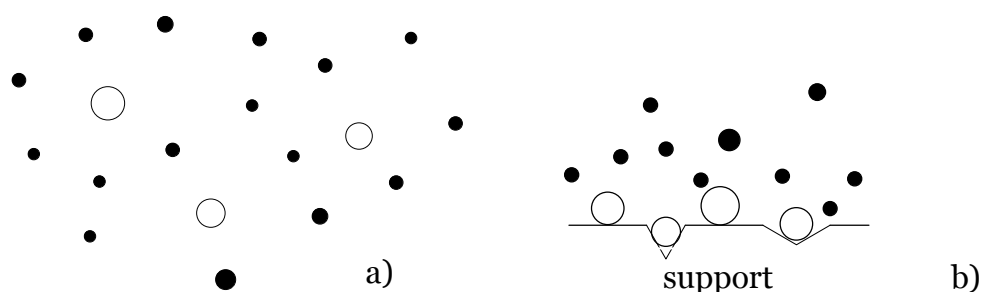


**Figure 2-5.** Illustration of the environment for the catalyst in homogenous (a) and the solid-supported catalysts in heterogeneous (b) reactions; solid dots represent the target molecules (CEES) and empty dot represented the metal-POM complexes.

**Table 2-2.** Catalytic activity of different solid-supported POM catalysts

| Catalyst  | [POM]<br>(mmol) | % conv. | TON  |
|---|-----------------|---------|------|
| Al <sub>2</sub> O <sub>3</sub>  | 0               | 0       | 0    |
| TiO <sub>2</sub>  | 0               | 0       | 0    |
| Silica (Davisil Si 1600)  | 0               | 0       | 0    |
| Silica (MCM 41)   | 0               | 0       | 0    |
| (Si/AlO <sub>2</sub> ) <sup>+</sup> (cationic silica)                               | 0               | 0       | 0    |
| TBA/Fe/PW <sub>11</sub> /Br/Cu/NO <sub>3</sub> /Al <sub>2</sub> O <sub>3</sub>      | 0.01*           | 7       | 6.1  |
| TBA/Fe/PW <sub>11</sub> /Br/Cu/NO <sub>3</sub> /TiO <sub>2</sub>                    | 0.01*           | 20      | 17.5 |
| TBA/Fe/PW <sub>11</sub> /Br/Cu/NO <sub>3</sub> /(Si/AlO <sub>2</sub> ) <sup>+</sup> | 0.01*           | 5       | 4.4  |
| TBA/Fe/PW <sub>11</sub> /Br/Cu/NO <sub>3</sub> /SiO <sub>2</sub><br>(Davisil)       | 0.01*           | 0       | 0    |
| TBA/Fe/PW <sub>11</sub> /Br/Cu/NO <sub>3</sub> /SiO <sub>2</sub><br>(MCM 41)        | 0.01*           | 0       | 0    |

General conditions: 0.875 mmol (0.35 M) of CEES, 1.0 atm of air, 0.876 mmol (0.35 M) of 1,3-dichlorobenzene (internal standard) were stirred in 2.5 mL of acetonitrile at 25 °C for 20 h in the 20-mL vial. \*Estimated amounts of bound POM were calculated based on the amount of POM in the preparation procedure (see text).

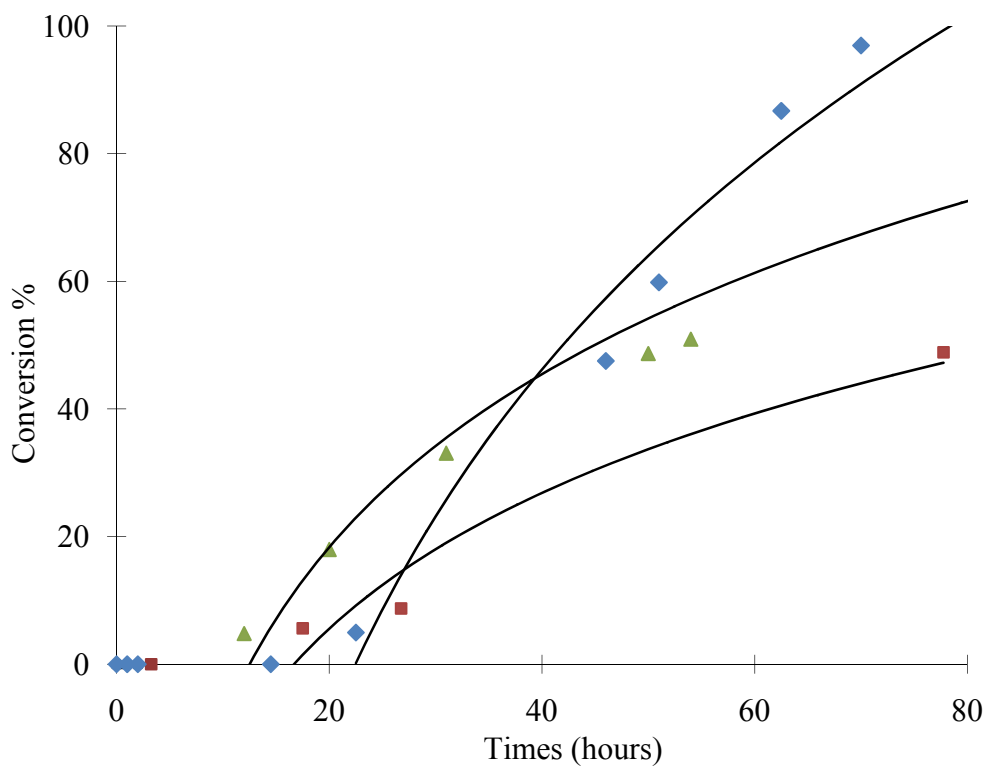
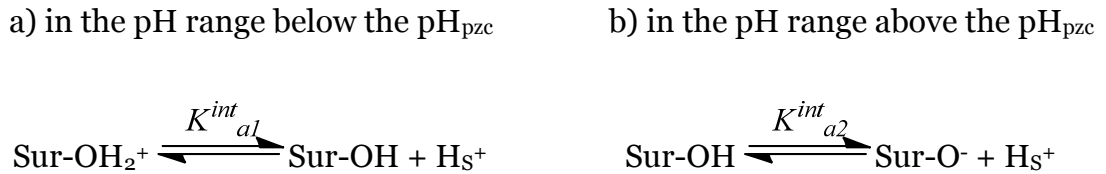


**Figure 2-6.** Catalytic activity of POM immobilized on the following supports: TiO<sub>2</sub> (▲), Al<sub>2</sub>O<sub>3</sub> (■) and cationic silica (◆) (0.13 g, 0.01 mmol of POM) for air-based sulfoxidation of CEES (0.35 mol/L) at 25°C (ambient conditions) in 2.5 mL acetonitrile. Conversion of CEES to CEESO and the fitted curves are shown.

Among these catalysts, the TiO<sub>2</sub>-supported POM has the shortest induction period and the POM supported on cationic silica has the fastest reaction speed. The cationic-silica-supported POM converts 100% CEES to CEESO in 80 hours and other two catalysts convert 100% CEES to CEESO in 150 hours. Several features of the supports may affect the POM loading and this results in different activities of the final catalysts. Two of these properties, surface charge and specific surface area are discussed below.

The *in-situ* layer-by-layer preparation principally involves electrostatic attraction between the POM and the solid support surface. Therefore, the surface charge of the supports will greatly affect the POM loading during catalyst preparation. The point of zero charge (pzc) is an important property of materials. A bulk material exhibits a positively charged surface when its pH value is lower than its pzc. The pzc of a bulk material can be determined as following



where the “Sur” represents the solid surface, the subscript s denotes the surface phase. The intrinsic surface ionization constants,  $K_{a1}^{\text{int}}$  and  $K_{a2}^{\text{int}}$  can be calculated from

$$\text{p}K_{a1}^{\text{int}} = \text{pH} + \log[\alpha^+ / (1 - \alpha^+)] + e\psi_0 / 2.3kT \quad (15)$$

$$\text{p}K_{a2}^{\text{int}} = \text{pH} - \log[\alpha^- / (1 - \alpha^-)] + e\psi_0 / 2.3kT \quad (16)$$

$$\text{pH}_{\text{pzc}} = 0.5 (\text{p}K_{a1}^{\text{int}} + \text{p}K_{a2}^{\text{int}}) \quad (17)$$

where  $\alpha^+$  and  $\alpha^-$  denotes the fraction of charged sites, which can be calculated as a ratio of the surface charge densities.  $\psi_0$  represents the mean potential of the surface charge plane, which depends on the potential-determining ionic reactions.

In practice, the point of zero charge can also be obtained by potentiometric titration or mass titration. The surface charge density and pzc of  $\text{TiO}_2$ ,  $\text{Al}_2\text{O}_3$ ,  $(\text{Si}/\text{AlO}_2)^+$  measured by potentiometric titration are recorded (see Figure 2-7, Figure 2-8, and Figure 2-9).

The titration results afford a pzc of  $\text{TiO}_2$ ,  $\text{Al}_2\text{O}_3$  and cationic silica 9.80, 7.91 and 6.60 respectively. The pzc of commercially supplied  $\text{SiO}_2$  (Davisil SI 1600) is 2.0 according to its MSDC (material safety data sheet). Clearly, in a neutral pH condition the surface of  $\text{TiO}_2$ ,  $\text{Al}_2\text{O}_3$  and cationic silica are positively or near neutrally charged. The surface of  $\text{SiO}_2$  is highly negatively charged. This charge difference can partially explain why  $\text{TiO}_2$ ,  $\text{Al}_2\text{O}_3$  and cationic silica supported catalysts are active in sulfoxidation catalysis, but  $\text{SiO}_2$  supported catalyst is totally inactive.

Specific surface area is another important feature for a catalytic support system. It is obvious that a support with a larger specific surface area should absorb/load more catalyst and have more “effective sites” for catalytic reaction. The BET surface areas of different supports and one  $\text{TiO}_2$  supported catalyst measured by nitrogen adsorption are given in Table 2-3.

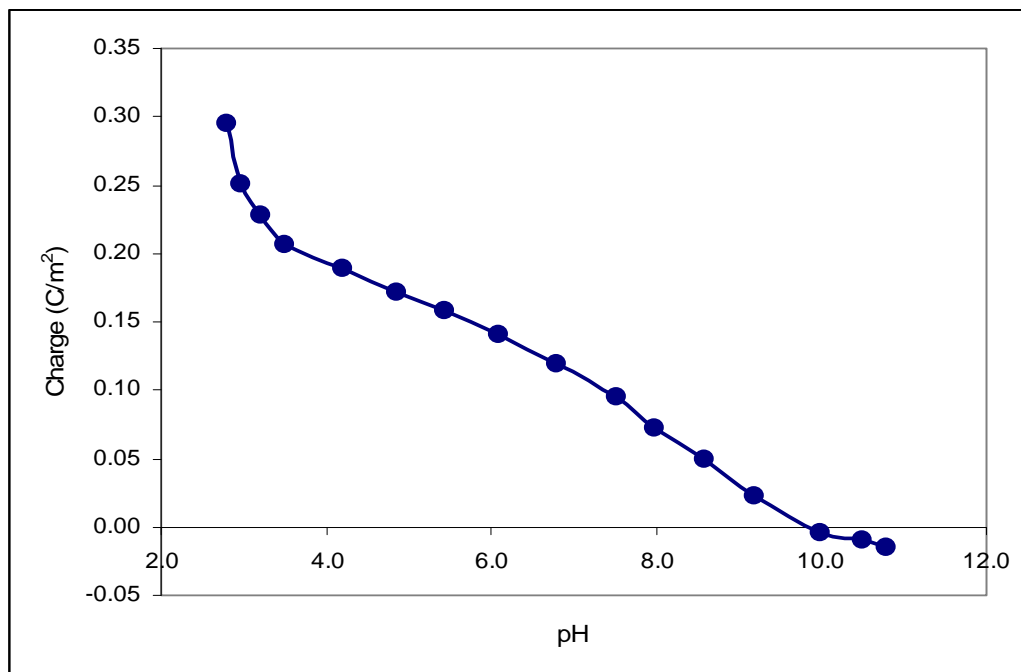


**Figure 2-7.** The surface charge density of TiO<sub>2</sub> nanoparticles as a function of pH. Conditions: 25 °C; 1 atm of Ar; TiO<sub>2</sub> nanoparticles (0.05 g) were suspended in 8 mL of 0.1 M NaCl. The point of zero charge (pzc), as determined, by titration is 9.80.

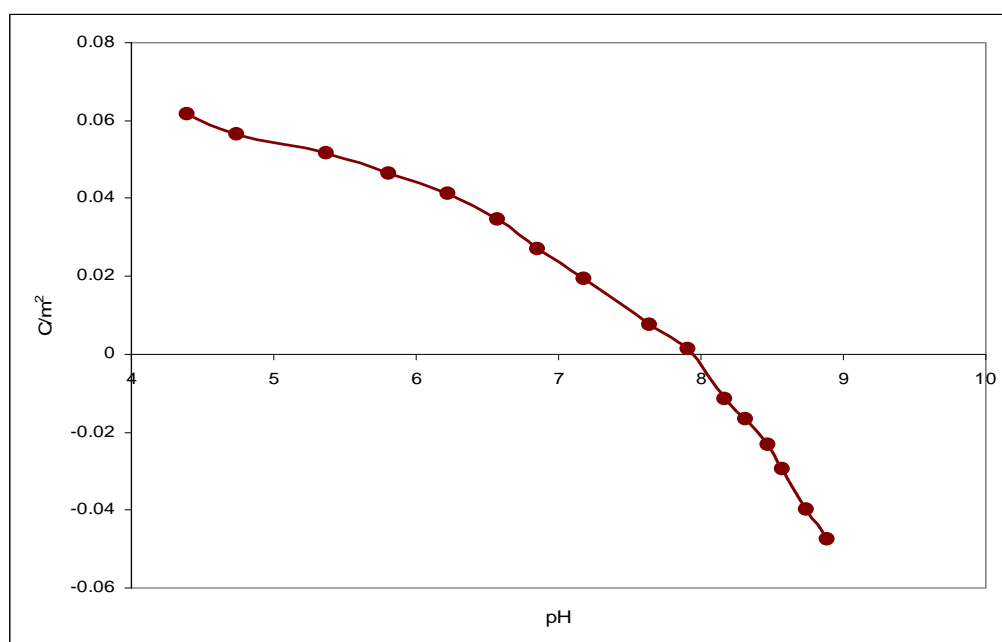


**Figure 2-8.** The surface charge density of  $\text{Al}_2\text{O}_3$  as a function of pH. Conditions: 25 °C; 1 atm of Ar;  $\text{Al}_2\text{O}_3$  nanoparticles (0.05 g) were suspended in 8 mL of 0.1 M NaCl. The point of zero charge (pzc), as determined by titration, is 7.91.

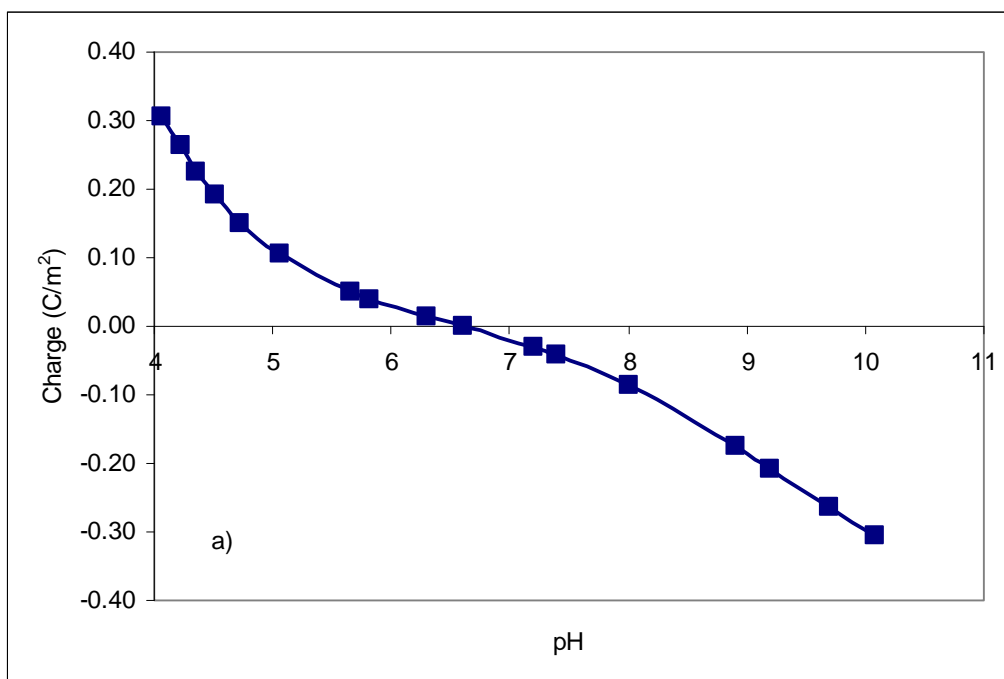


**Figure 2-9.** The surface charge density of (Si/AlO<sub>2</sub>)<sup>+</sup> nanoparticles as a function of pH. Conditions: 25 °C; 1 atm of Ar; Al<sub>2</sub>O<sub>3</sub> nanoparticles (0.05 g) were suspended in 8 mL of 0.1 M NaCl. The pzc of (Si/AlO<sub>2</sub>)<sup>+</sup> is 6.60.

The BET data prove that all the supports we tested have a high surface area ( $> 100 \text{ m}^2/\text{g}$ ). After POM is loaded, the surface area of the POM-loaded support decreases correspondingly. The higher catalytic activity of the  $\text{TiO}_2$ -supported catalyst compared to the  $\text{Al}_2\text{O}_3$ -supported may partially be attributed to the larger surface area of  $\text{TiO}_2$ . The catalyst supported on cationic silica, despite the relatively low surface area of this support, gives the highest catalytic activity of these supported catalysts. The solid-supported POM catalysts are rather complicated systems and their catalytic activity may not be easily predicted by analysis of a few simple factors. However, the study of surface charge and surface area is still the most insightful way to understand the nature of POM loading on the surface of supports and they facilitate systematic searches for better solid supports. Based on the study,  $\text{TiO}_2$ , which has a large specific surface area and a highly positively charged surface under neutral conditions, was selected as the support for the following experiments.

**Table 2-3.** BET Surface area of different supports and one supported catalyst

| Material   | $\text{TiO}_2$ | $\text{Al}_2\text{O}_3$ | $(\text{Si}/\text{Al}_2\text{O})^+$ | $\text{Fe}/\text{PW}_{11}/\text{Br}/\text{Cu}/\text{NO}_3/\text{TiO}_2$ |
|--|----------------|-------------------------|-------------------------------------|---|
| BET surface area<br>( $\text{m}^2/\text{g}$ ) <sup>a</sup> | 550            | 480                     | 210                                 | 314   |

General conditions:  $\text{N}_2$ , 77 K, relative pressure range 0.06 – 0.45; samples are outgassed overnight at 150 °C under vacuum; <sup>a</sup> standard BET equation is applied.

### *Effect of protons on the solid-supported POM catalyst*

The kinetic data in Figure 2-6 show an induction period for the air-based sulfoxidation catalyzed by the solid-supported POM materials. In the supported catalyst, a positively charged surface not only helps bind the negatively charged POM, but also the anions  $\text{Br}^-$  and  $\text{NO}_3^-$ . Furthermore, because of the electrostatic repulsion between the positively charge surface and protons, fewer protons are associated with the immobilized POMs. Protonation phenomenons are likely involved in the catalytic induction period. To activate the solid-supported POM catalyst and reduce the induction period, *p*-toluenesulfonic acid (TsOH), a good proton donor in organic phase, was selected and used as an additive in some sulfoxidation reactions. Figure 2-10 shows kinetic data for sulfoxidation catalyzed by the  $\text{Fe/Cu/PW}_{11}/\text{Br}/\text{NO}_3/\text{TiO}_2$  system with and without addition of TsOH.

The kinetic data show that with the addition of 20 mg of TsOH into the system, the sulfoxidation speed increases dramatically, and the induction period for this catalysis reaction is effectively eliminated. With TsOH added  $\text{Fe/Cu/PW}_{11}/\text{Br}/\text{NO}_3/\text{TiO}_2$  converts 100% CEES to CEESO in no more than 30 hours; while without TsOH this reaction takes more than 120 hours. These results confirm that the proton plays an important role in sulfoxidation catalyzed by the nitrate-group-containing transition-metal-substituted POMs. Protons are general co-catalysts in sulfoxidations catalyzed by these supported catalysts. .

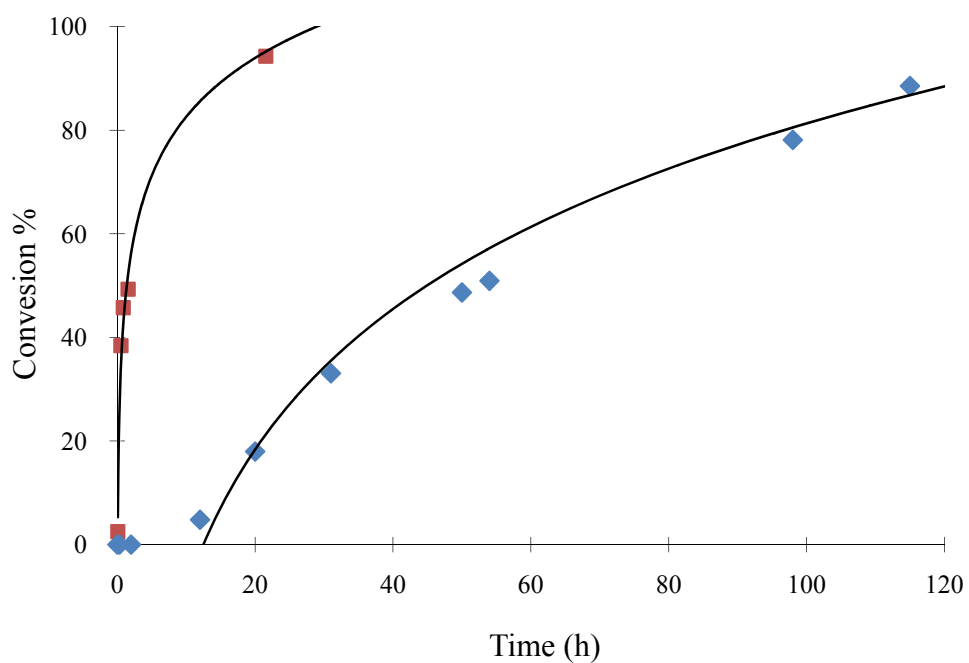


**Figure 2-10.** Profiles of aerobic CEES sulfoxidation catalyzed by Fe/Cu/PW<sub>11</sub>/Br/NO<sub>3</sub>/TiO<sub>2</sub> in the presence (■) or absence (◆) of TsOH. Conditions: 0.13 g (0.01 mmol) of POM, 0.35 mol/L of CEES, air at 25°C (ambient conditions) in 2.5 mL acetonitrile, and 20mg of TsOH in the acidified reaction.

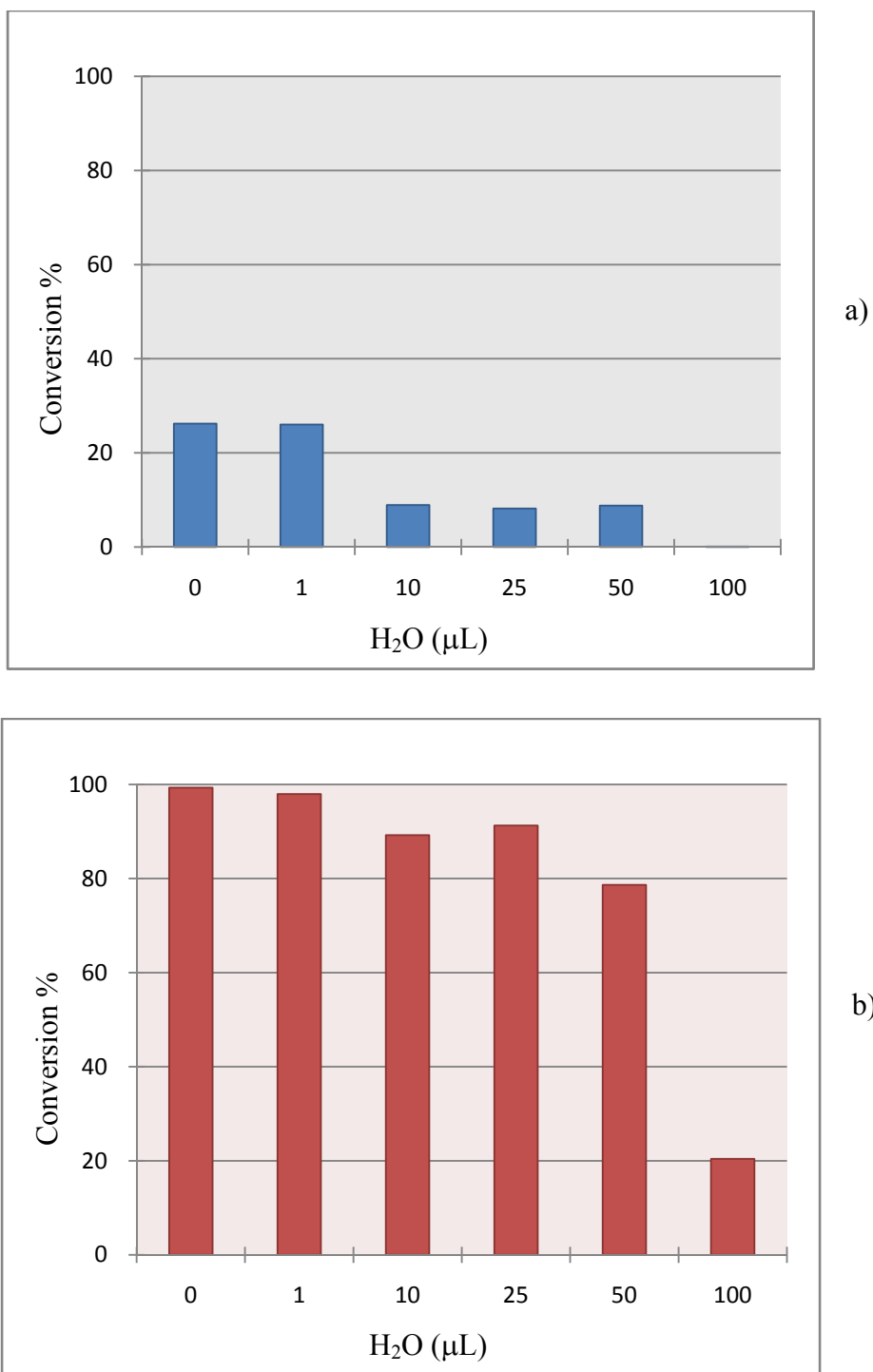


**Figure 2-11.** The effect of different amounts of H<sub>2</sub>O (from 1 μL to 100 μL) added to the typical catalytic sulfoxidation system: a) conversions after 3 hrs; b) conversions after 20 hrs.

### *The effect of water on the solid-supported POM catalysts*

In an open environment, humidity and temperature are two of the most common variables. To study how the catalysts work in such an environment, the effects of these two variables were evaluated. The changes in sulfoxidation activity catalyzed by the solid-supported POMs have been recorded as a function of added water (Figure 2-11). The charts clearly indicate that addition of trace water has little to no effect on the catalysis. This is understandable given that under ambient conditions, trace amounts of water are present, even on days with low humidity. When considerable amounts of water have been introduced into the catalytic system, the reaction is greatly inhibited in the first few hours. When 100  $\mu\text{l}$  of water are added ( $\sim 4\%$  in weight), no CEESO peak can be detected after 3 hours, and the reaction conversion is much lower than in the other reactions after 100 hours (20% versus 78%~99%). It is evident that large amount of water increases the induction period and inhibits the sulfoxidation catalysis. Significantly however, the catalyst still shows some activity even after 100  $\mu\text{l}$  water was added. This phenomenon indicates that although inhibited by water, the active components of the catalyst are not likely damaged (irreversibly altered) by water.

The following experiments have also been conducted to further investigate the water effect on the  $\text{TiO}_2$ -supported catalyst. The  $\text{Fe}/\text{PW}_{11}/\text{Br}/\text{Cu}/\text{NO}_3/\text{TiO}_2$  catalyst was treated in a vapor-saturated container for two days and then dried in an oven at  $50^\circ\text{C}$  for 2 h. The activities of this catalyst before and after the vapor treatment and after the subsequent drying are given in Figure 2-12).

The data also confirm that the addition or existence of water/vapor significantly inhibits the sulfoxidation catalysis. Importantly, if the water-containing supported POM catalyst is dried most if not all its catalytic activity returns. The data also indicate that the catalyst is stable in both high humidity and high temperature. Catalytic time courses (reactions) for the fresh, dry catalyst is fit well with exponential functions; these are fit less well for the water-treated catalyst. The latter case suggests that the sulfoxidation exhibits much more complicated kinetics than the first-order processes seen with the fresh, dry catalyst. The wet and subsequently dried catalyst behaves kinetically like the original dry catalyst and not like the wet catalyst. Furthermore, evaluation of catalysts placed in a dark and dry drawer for 3 months and longer showed little decrease in catalytic activity.

## **Conclusions**

Based on former work in Hill laboratory, a highly active catalyst for sulfoxidation using ambient air ( $O_2$ ) has been developed. More than 90 turnovers in 90 minutes are observed. Binding (immobilizing) the catalyst on different traditional supports has been systematically investigated and an effective way to prepare active solid-supported POM catalysts has been developed. Liquid-phase catalytic aerobic sulfoxidation studies indicate that the presence of a Brønsted acid greatly enhances the catalytic activity while water remarkably inhibits the catalytic activity of the solid-supported catalysts.

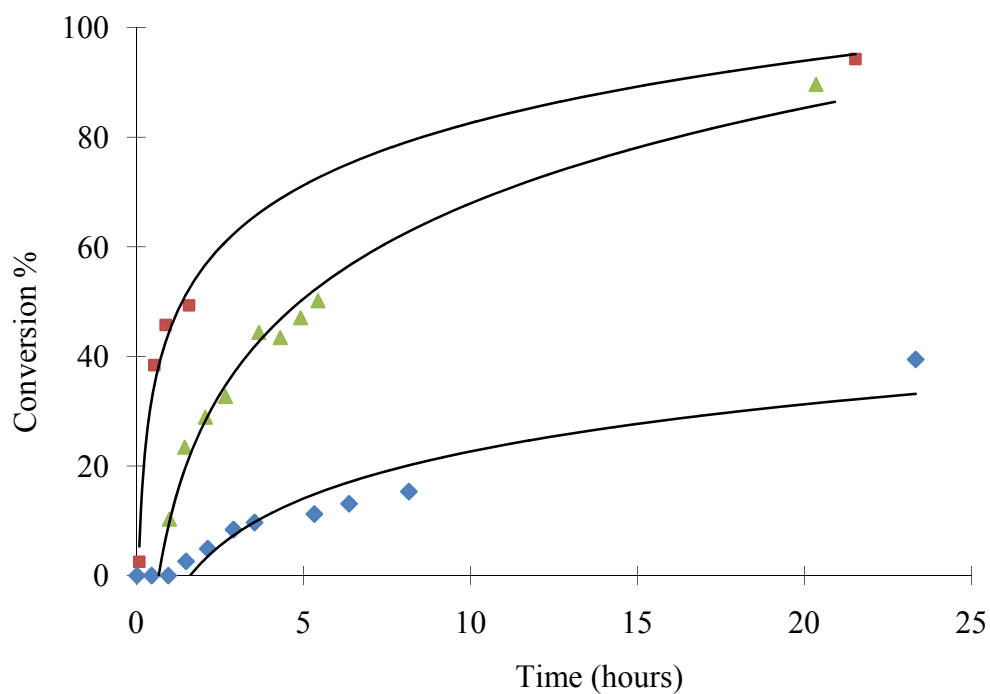


**Figure 2-12.** Profiles of aerobic CEES sulfoxidation catalyzed by Fe/Cu/PW<sub>11</sub>/Br/NO<sub>3</sub>/TiO<sub>2</sub> that is freshly prepared (■), exposed to water-saturated air or 100% relative humidity “RH” (◆), and initially exposed to water vapor and then partially dried at 50°C in an oven for 2 hours (▲). Conditions: 0.13 g (0.01 mmol) of POM, 0.35 mol/L CEES under air at 25°C (ambient conditions) in 2.5 mL acetonitrile.

**References**

- (1) Bosch, E.; Kochi, J. K., *J. Org. Chem.* **1995**, *60*, 3172-3183.
- (2) Srivastava, R. S.; Milani, B.; Alessio, E.; Mestroni, G., *Inorg. Chimica Acta* **1992**, *191*, 15-17.
- (3) Haruta, M., *Catal. Surv. Jpn.* **1997**, *1*, 61-73.
- (4) Xu, L.; Boring, E.; Hill, C., *J. Catal.* **2000**, *195*, 394-405.
- (5) Boring, E.; Geletii, Y. V.; Hill, C. L., *J. Am. Chem. Soc.* **2001**, *123*, 1625-1635.
- (6) Martín, S. E.; Rossi, L. I., *Tetrahedron Letters* **2001**, *42*, 7147-7151.
- (7) Rossi, L. I.; Martin, S. E., *Appl. Catal. A* **2003**, *250*, 271-278.
- (8) Munro, N. B.; Talmage, S. S.; Griffin, G. D.; Waters, L. C.; Watson, A. P.; King, J. F.; Hauschild, V., *Environ. Health Perspectives* **1999**, *107*, 933-974.
- (9) Yang, Y. C.; Baker, J. A.; Ward, J. R., *Chem. Rev.* **1992**, *92*, 1729-1743.
- (10) Kamata, K.; Yonehara, K.; Sumida, Y.; Yamaguchi, K.; Hikichi, S.; Mizuno, N., *Science* **2003**, *300*, 964-966.
- (11) Groves, J. T.; Quinn, R., *J. Am. Chem. Soc.* **1985**, *107*, 5790-5792.
- (12) Okun, N. M.; Anderson, T. M.; Hardcastle, K. I.; Hill, C. L., *Inorg. Chem.* **2003**, *42*, 6610-6612.
- (13) Okun, N. M.; Anderson, T. M.; Hill, C. L., *J. Am. Chem. Soc.* **2003**, *125*, 3194-3195.
- (14) Okun, N. M.; Anderson, T. M.; Hill, C. L., *J. Mol. Catal. A: Chem.* **2003**, *197*, 283-290.
- (15) Okun, N. M.; Ritorto, M. D.; Anderson, T. M.; Apkarian, R. P.; Hill, C. L., *Chem Mater.* **2004**, *16*, 2551-2558.

- (16) Okun, N. M.; Tarr, J. C.; Hillesheim, D. A.; Zhang, L.; Hardcastle, K. I.; Hill, C. L., *J. Mol. Catal. A. Chem.* **2006**, *246*, 11-17.
- (17) Okun, N. M.; Luo, Z.; Hill, C. L. *Gentex Research Report*; Emory University: Atlanta, 2005.
- (18) Luo, Z.; Okun, N. M.; Hillesheim, D. A.; Geletii, Y. V.; Hill, C. L. *TDA Research Report*; Emory University: Atlanta, 2005-2006.
- (19) Okun, N. M.; Luo, Z.; Hill, C. L. *P&G Research Report*; Emory University: Atlanta, 2006.
- (20) Luo, Z.; Okun, N. M.; Hill, C. L. *P&G Research Report*; Emory University: Atlanta, 2007-2008.
- (21) Domaille, P. J., Vanadium (V) Substituted Dodecatungstophosphates. In *Inorganic Syntheses*, Ginsberg, A. P., Ed. John Wiley and Sons: New York, 1990; Vol. 27, pp 96-104.
- (22) Drabowicz, J.; Kielbasinski, P.; Mikolajczyk, M., Synthesis of sulphoxides. In *Syntheses of Sulphones, Sulphoxides and Cyclic Sulphides*, Patai, S.; Rappoport, Z., Eds. John Wiley & Sons: Chichester, 1994; pp 529-648.
- (23) Ballistreri, F. P.; Tomaselli, G. A.; Toscano, R. M., *J. Mol. Catal.* **1991**, *68*, 269-275.
- (24) Macker, C., *Liebigs Ann. Chem.* **1865**, *136*, 75.
- (25) Hillesheim, D. A.; Young, P.; Gueletii, Y. V., Unpublished Work.
- (26) Maier, G.; Reisenauer, H. P.; Marco, M. D., *Chem. Eur. J.* **2000**, *6*, 800-808.
- (27) Retcliffe, C. T.; Shreeve, J. M., Nitrosyl Halides. In *Inorg. Syn.*, Jolly, W. L., Ed. McGraw-Hill Book Company, Inc: 1968; Vol. XI, pp 194-200.

(28) Cheng, L.; Cox, J. A., *Chem. Mater.* **2002**, *14*, 6-8.

(29) Kuhn, A.; Anson, F. C., *Langmuir* **1996**, *12*, 5481-5488.

# *Chapter 3*

Kinetics and Mechanistic Studies  
of the NO<sub>x</sub>/Br Systems for Catalytic  
Aerobic Sulfoxidation

## Abstract

The kinetics of aerobic sulfoxidation catalyzed by the  $\text{NO}_x/\text{Br}$  systems have been investigated by UV-Vis and GC techniques. The yellow-colored active solid which can be isolated from different sources of  $\text{NO}_x$  and Br has been indentified to be the TBA salt of  $\text{Br}_3^-$ . Without the presence of bromine and its derivatives the system is not catalytically active in aerobic sulfoxidation. Based on bromine sulfoxidation and aerobic regeneration of bromine catalyzed by nitrate, a mechanism of the  $\text{NO}_x/\text{Br}$ -catalyzed sulfoxidation has been proposed. The differential equations and their solutions deduced from the mechanism match the observed kinetic data well and strongly support the postulated mechanism.

## Introduction

The “hot catalyst”, containing a complex mixture of a nitrate, bromide and a transition-metal-substituted polyoxometalate (a TMSP), developed in Hill group can not only efficiently catalyze the aerobic sulfoxidation but also absorb and decontaminate many household odors.<sup>1, 2</sup> To probe the mechanism of this catalytic sulfoxidation and the nature of the hot catalyst, Hillesheim and coworkers<sup>3</sup> had investigated a related simplified catalytic system that contained only nitrate and bromide or their derivatives from different sources. They claimed that the presence of nitrate and bromide anions is critical to the catalysis. Unfortunately, they failed to identify the actual formula of the active catalyst and thus referred to the simplified system as “ $\text{NO}_x/\text{Br}$ ”.

In the investigation of TMSP-containing more complex systems, we found that if the  $\text{TBAFeBr}_4$  was mixed with the freshly-prepared TBA salt of the TMSP, the resulted brown product was very active in catalyzing the sulfoxidation of CEES, but when recrystallized TMSPs were used, the  $\text{TBAFeBr}_4$ /TBA-TMSP mixtures were no longer active (see Chapter 6). Under the preparation conditions an excess of nitrate was present in the freshly prepared TMSPs and this excess was removed during the recrystallization. This phenomenon confirmed the importance of nitrate group in the hot catalyst and led us paid too much attention to the nitrate component of the catalytic systems in our earlier investigations.

In the previous studies performed by Hillesheim and coworkers,<sup>3</sup> it was found that a light yellow complex was formed in all active systems containing  $\text{NO}_3^-$  and  $\text{Br}^-$ ; also, the yellow complex can be obtained using other sources of  $\text{NO}_x$  and  $\text{Br}^-$ . Furthermore, they found that the yellow complex can form a solid after removal of solvent. The yellow complex is quite thermally stable, which rules out volatile  $\text{NOBr}$  and  $\text{BrNO}_2$  as the active species. In their investigation, they used  $\text{NOPF}_6$  and  $\text{TBABr}$  as typical sources for  $\text{NO}_x$  and  $\text{Br}^-$  and found the best ratio of  $\text{Br}^-$ :  $\text{NO}^+$  for preparing the highest active catalyst was about 2:1. They tried to identify the active species by FT-IR, UV-vis and electrospray ionization mass spectrometry. The FT-IR exhibited no discernable nitrogen oxide stretches. A peak near 270 nm was found in the UV-Vis spectrum but this peak did not match any  $\text{NO}_x\text{Br}$  compounds in the literature. The mass spectrum only revealed the presence of only  $\text{PF}_6^+$  and  $\text{Br}^-$ . They also studied the kinetics of aerobic CEES oxidation catalyzed by the yellow complex but obtained very complicated data.

Although these studies did not reveal the true nature of the  $\text{NO}_x/\text{Br}$  system it provided useful information.

In the work of Hillesheim and coworkers most of the characterization methods used were aimed at trying to identify nitrosonium ion and its derivatives. The other crucial component of the system, “ $\text{Br}^-$ ”, was neglected. The absorption maximum in the UV-Vis spectrum of the isolated yellow complex at 270 nm does not match any documented  $\text{NO}_x$  compounds, but it is near the absorbance of  $\text{Br}_3^-$  in acetonitrile. Furthermore, the  $\text{TBABr}_3$  salt is known to be a yellow solid, stable under below  $80^\circ\text{C}$  and is commercially available. According to these facts, I surmised that the mysterious  $\text{NO}_x/\text{Br}$  system is likely a mixture containing  $\text{TBA}^+$ ,  $\text{NO}_3^-$  and  $\text{Br}_3^-$ . Therefore, a mechanism for sulfoxidation catalyzed by the  $\text{NO}_x/\text{Br}$  system is postulated as follows: first,  $\text{Br}_2$  forms from oxidation of  $\text{Br}^-$  by  $\text{NO}_3^-/\text{NO}_x$ . The excess of  $\text{Br}^-$  associates with  $\text{Br}_2$  to form  $\text{Br}_3^-$ , which gives the characteristic peak around 270 nm. After formation,  $\text{Br}_2/\text{Br}_3^-$  oxidizes CEES to CEESO in the system while  $\text{NO}_x$  functions as the catalyst to regenerate  $\text{Br}_2$  aerobically. To prove this hypothesis, several catalytic systems containing  $\text{NO}_x$  and  $\text{Br}$  from different sources were designed and evaluated. The kinetics of the aerobic sulfoxidation catalyzed by optimized systems is measured by UV-vis and GC techniques. All the resulting data are consistent with the proposed mechanism.

## Experiments

### *General methods and materials*

$\text{Na}_9[\text{A-PW}_9\text{O}_{34}]$  was prepared by the literature methods,<sup>4</sup> and its purity was checked by FT-IR.  $\text{TBANO}_3$ ,  $\text{TBANO}_2$ ,  $\text{NOBF}_4$ ,  $\text{Br}_2$ ,  $\text{TBABr}$ ,  $(\text{CH}_2)_6\text{N}_4\text{HBr}_3$ ,  $\text{HClO}_4$ , acetonitrile, 1,3-dichlorobenzene, bromocyclohexane and 2-chlorethyl ethyl sulfide (CEES) were purchased from Aldrich and used without further purification. The infrared spectra were recorded on a Nicolet 510 FT-IR spectrometer. The electronic absorption spectra were taken on an Agilent 8453 UV-vis spectrometer. Oxidation products were identified by gas chromatography-mass spectrometry (GC/MS; Hewlett Packard 5890 series II gas chromatograph connected to a Hewlett Packard 5971 mass selective detector) and quantified by gas chromatography (GC; Hewlett Packard 5890 series gas chromatograph equipped with a flame ionization detector, 5% phenyl methyl silicone capillary column,  $\text{N}_2$  carrier gas, and a Hewlett Packard 3390A series integrator).

### *Preparation of the catalytic systems*

#### 1. Preparation of the fresh $\text{NO}_x/\text{Br}$ catalyst

To 5 mL of  $\text{CH}_3\text{CN}$  are added 161 mg (0.5 mmol) of  $\text{TBABr}$  and 152 mg (0.5 mmol) of  $\text{TBANO}_3$ . The solution is stirring until all TBA salts are dissolved. The mixture solution is then carefully transferred to a 10 mL volumetric flask and diluted by  $\text{CH}_3\text{CN}$  to mark. To observe the induction period in kinetics of the sulfoxidation, the freshly prepared catalyst must be used immediately.

## 2. Preparation of aged NO<sub>x</sub>/Br catalyst

To 8 mL of CH<sub>3</sub>CN is added 20.5 μL (0.8 mmol) of Br<sub>2</sub>. To 5 ml of CH<sub>3</sub>CN are added 161 mg (0.5 mmol) of TBABr and 145 mg (0.45 mmol) of TBANO<sub>3</sub>. The solution is stirred until all TBA salts are dissolved. To this solution is added 0.01 mmol of Br<sub>2</sub> (100 μL Br<sub>2</sub> solution prepared in the first step) and 14 mg (0.05 mmol) of TBANO<sub>2</sub>. The solution is transferred to a volumetric flask. To the flask is added 25 μL of 4M HClO<sub>4</sub> (0.1 mmol) and the solution turns to yellow immediately. The solution is finally diluted by CH<sub>3</sub>CN to mark.

## 3. Modified Preparation of TBA<sub>3</sub>H<sub>2</sub>[Fe(NO<sub>3</sub>)PW<sub>11</sub>O<sub>39</sub>]

The preparation of TBA<sub>3</sub>H<sub>2</sub>[Fe(NO<sub>3</sub>)PW<sub>11</sub>O<sub>39</sub>] is similar to the method used by Okun and coworkers<sup>5</sup> except that TBANO<sub>3</sub> was used instead of TBABr to obtain the precursor. Solid Na<sub>7</sub>[α-PW<sub>11</sub>O<sub>39</sub>]·74H<sub>2</sub>O (1 g, ca. 0.34 mmol) is dissolved in 10 mL of deionized water. To this solution, TBANO<sub>3</sub> (3.8 g, ca. 12.4 mmol) dissolved in 8 mL of deionized water is added. The mixture is stirred for 30 min at room temperature. The resulting precipitate is separated by filtration, redissolved in 15 mL of acetonitrile, to which a solid Fe(NO<sub>3</sub>)<sub>3</sub> · 9H<sub>2</sub>O (0.16 g, 0.4 mmol) is added under vigorous stirring. A dark reddish-brown solution and a small amount of oily precipitate are formed. The solution is separated from the oily product, filtered through the fine filter paper (Fisher brand P2) to remove the suspended precipitate, stirred for 1.5 h at ambient temperature and re-filtered through the P2 paper. The filtrate is left in air and light green crystals (0.5 g; 39% yield) are produced.

### *Catalytic oxidation of CEES, the HD analogue, in acetonitrile solution*

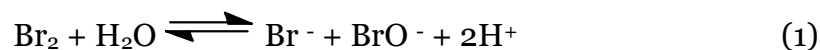
In a typical CEES oxidation reaction, 1 mL of  $\text{NO}_x/\text{Br}$  solution, which contains 0.05 mmol  $\text{NO}_3^-$  and 0.05 mmol  $\text{Br}^-$ , is mixed with 1 mL of acetonitrile in a 5 mL vial. To this mixture, 25  $\mu\text{L}$  of 1,3-dichlorobenzene or bromocyclohexane (GC internal standard) is added, and the vial is then sealed. After stirring for 1 min, 25  $\mu\text{L}$  of CEES is injected by a syringe to a vial fitted with a PTFE septum. Air access during the experiment is provided through a needle in the septum on the cap. In order to accelerate the reaction, the temperature is elevated to 70°C. Aliquots are analyzed by GC analysis every 15 - 30 min and the reaction is monitored for 10 - 20 hrs.

## **Result and discussion**

### *TBABr<sub>3</sub>: the active yellow species*

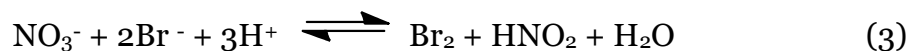
When both TBA nitrate and bromide salts were dissolved in acetonitrile solution no significant changes were observed in the first few hours. However, the addition of a drop of acid turns the colorless solution yellow. If  $\text{TBANO}_2$  or  $\text{NOBF}_4$  is used instead of  $\text{TBANO}_3$ , the color change is rapid even without acid. UV-Vis spectra of the acetonitrile solution of these  $\text{NO}_x/\text{Br}$  system show that the yellow color is due to a strong absorption peak near 269 nm which tails to  $\lambda > 400$  nm. The absorption maximum at 269 nm exactly matches the absorption of  $\text{Br}_3^-$  in acetonitrile. Figure 3-1 shows the spectra of  $\text{TBABr}_3$  standard and other  $\text{NO}_x$  and Br containing systems. The red curve is the spectrum of the standard  $\text{TBABr}_3$  which has the strong characteristic  $\text{Br}_3^-$  peak located at 269 nm. The

purple curve is the spectrum of Br<sub>2</sub> dissolved in acetonitrile. Br<sub>2</sub> has a known maximum absorption near 420 nm in gas phase. When Br<sub>2</sub> dissolves in acetonitrile, the broad peak remains around 400 nm and two more peaks appear. The peak under 200 nm is assigned to Br<sup>-</sup> and the 269 nm peak is assigned to Br<sub>3</sub><sup>-</sup>. These two species were formed by a small amount of disproportionation of Br<sub>2</sub> in the presence of trace amount of H<sub>2</sub>O in CH<sub>3</sub>CN (eqs. 1-2). The small amount of Br<sub>3</sub><sup>-</sup> exhibits a strong peak because of its very high extinction coefficient<sup>6,7</sup> ( $\epsilon = 3.8 \times 10^4 \text{ M}^{-1} \text{ cm}^{-1}$ , which is 200 times larger than that of Br<sub>2</sub>) in solution. Both of the NO<sub>x</sub>/Br systems prepared from TBANO<sub>2</sub> + TBABr (blue curve) and NOBF<sub>4</sub> + TBABr (green curve) give the same peak at 269 nm, which indicates the formation of Br<sub>3</sub><sup>-</sup> in these systems.



$$K_2 = 9 \times 10^6 \text{ M}^{-1} \quad \text{in acetonitrile}^8$$

Previous work performed by Lengyel, Nagy and Bazsa<sup>9</sup> also support the generation of Br<sub>2</sub>/Br<sub>3</sub><sup>-</sup> in the NO<sub>x</sub>/Br system. They studied the oxidation of bromide by nitric acid in water, eqs. 2-3:



$$K_{\text{exp}} = 1.6 \times 10^{-6} \text{ M}^{-4}$$



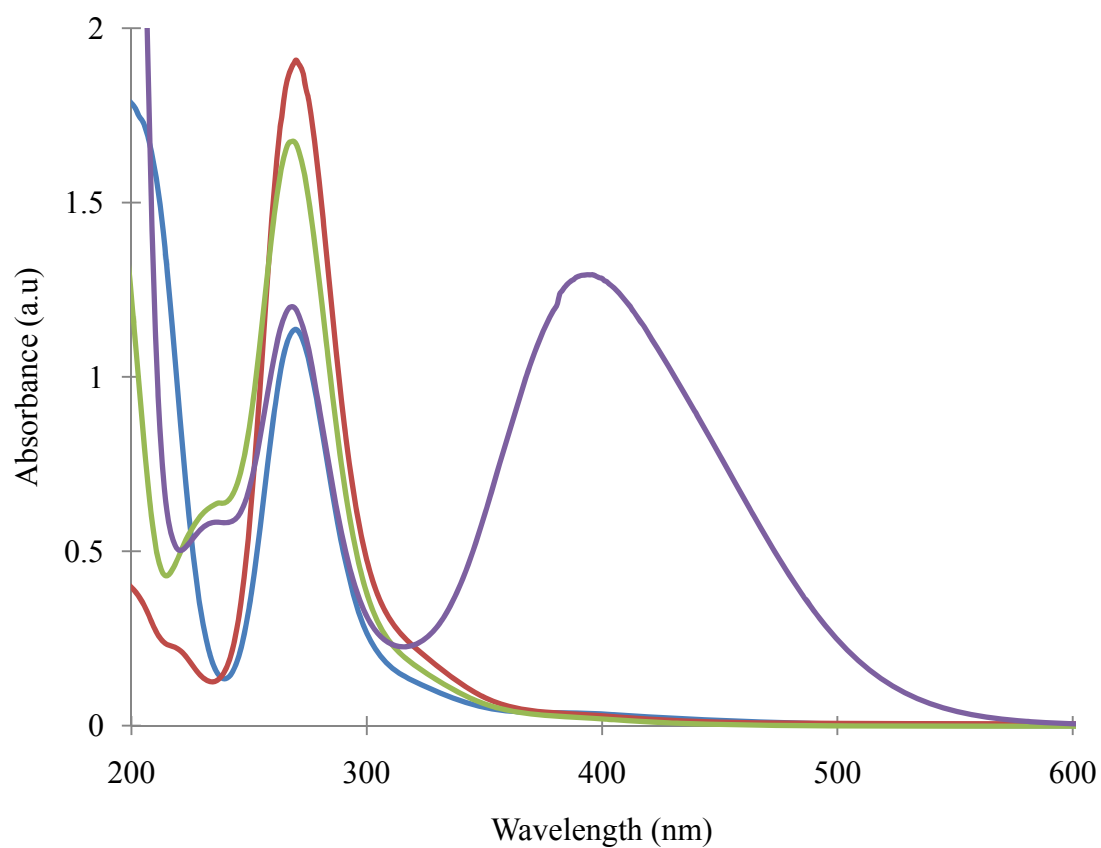


**Figure 3-1.** The absorption spectra of different NO<sub>x</sub>/Br systems in acetonitrile. From up to down at peak 269 nm: red — TBABr<sub>3</sub>; green — TBABr/NOBF<sub>6</sub>; purple —, Br<sub>2</sub>; blue — TBABr/TBANO<sub>2</sub>.

They found that the reaction is autocatalytic. An induction period was observed and the length of induction period depends very strongly on the initial concentration of  $\text{NO}_2^-$  ( $\text{HNO}_2$  in acidic condition). Based on the reaction in eq. 3 proton should greatly enhance the tendency to form  $\text{Br}_2$  but  $\text{H}_2\text{O}$  could inhibit the formation of  $\text{Br}_2$ . The formation of  $\text{HNO}_2$  catalyzes the formation of  $\text{Br}_2$  which makes the reaction autocatalytic. As see in Figure 3-2 an induction period appears in the aerobic sulfoxidation catalyzed by the freshly prepared  $\text{TBANO}_3/\text{TBABr}$  system (no acid added). Also the water inhibition has been observed in our earlier work (see Chapter 2). The appearances of an induction period and water inhibition also suggest that the formation of  $\text{Br}_2/\text{Br}_3^-$  could be the first step of the catalytic reaction.

Previously, Okun and coworkers<sup>5</sup> in our group found a mono-iron-substituted POM system can efficiently catalyzed the aerobic sulfoxidation. No bromide seems involved in the system. However, carefully investigation finds that a huge excess of  $\text{TBABr}$  was used in their preparation of the precursor,  $\text{TBA}_{7-x}\text{Na}_x\text{PW}_{11}\text{O}_{39}$ . By applying the precursor without purification in their preparation, a considerable amount of  $\text{Br}^-$  was inevitably introduced into their final catalytic complex. In order to test the catalytic activity of the real bromide-free system,  $\text{TBANO}_3$  is used instead of  $\text{TBABr}$  in the preparation (see preparation 3). The kinetic data of sulfoxidation catalyzed by the modified system are shown in Figure 3-3.

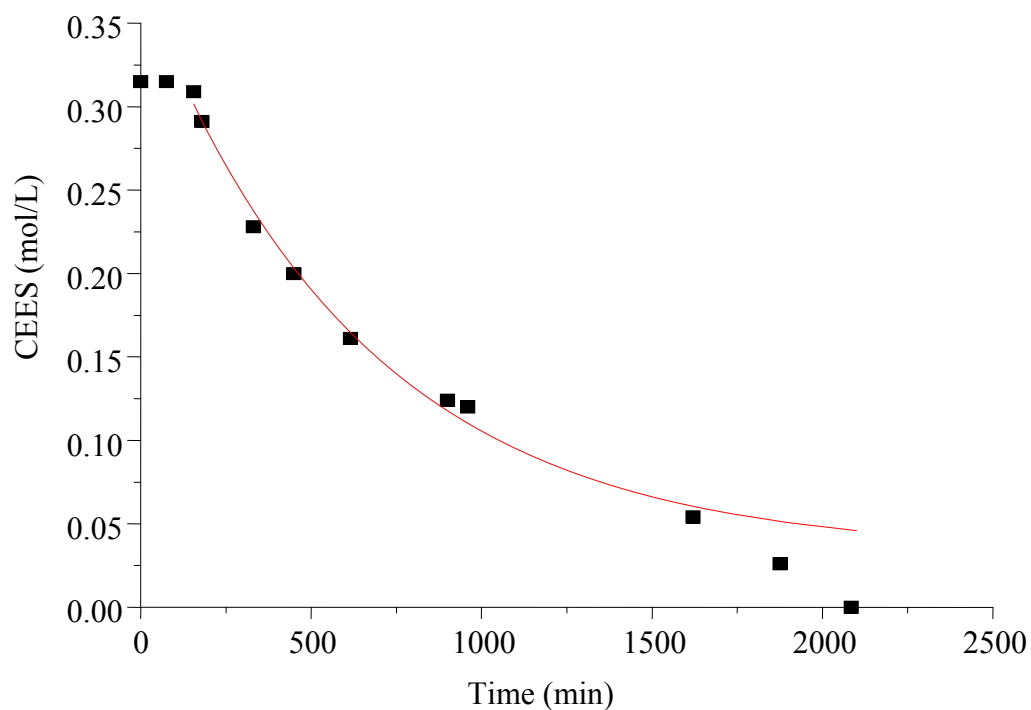


**Figure 3-2.** Time profile of catalytic CEES consumption in a freshly prepared TBABr/TBANO<sub>3</sub> system. Conditions: [CEES]<sub>0</sub> = 0.32 M, [TBANO<sub>3</sub>] = 0.016 M, [TBABr] = 0.016 M, CH<sub>3</sub>CN=2.3 mL, T = 70 °C. Solid square, ■: experimental data. Red line, —: exponential fit from 200 to 1600 min.

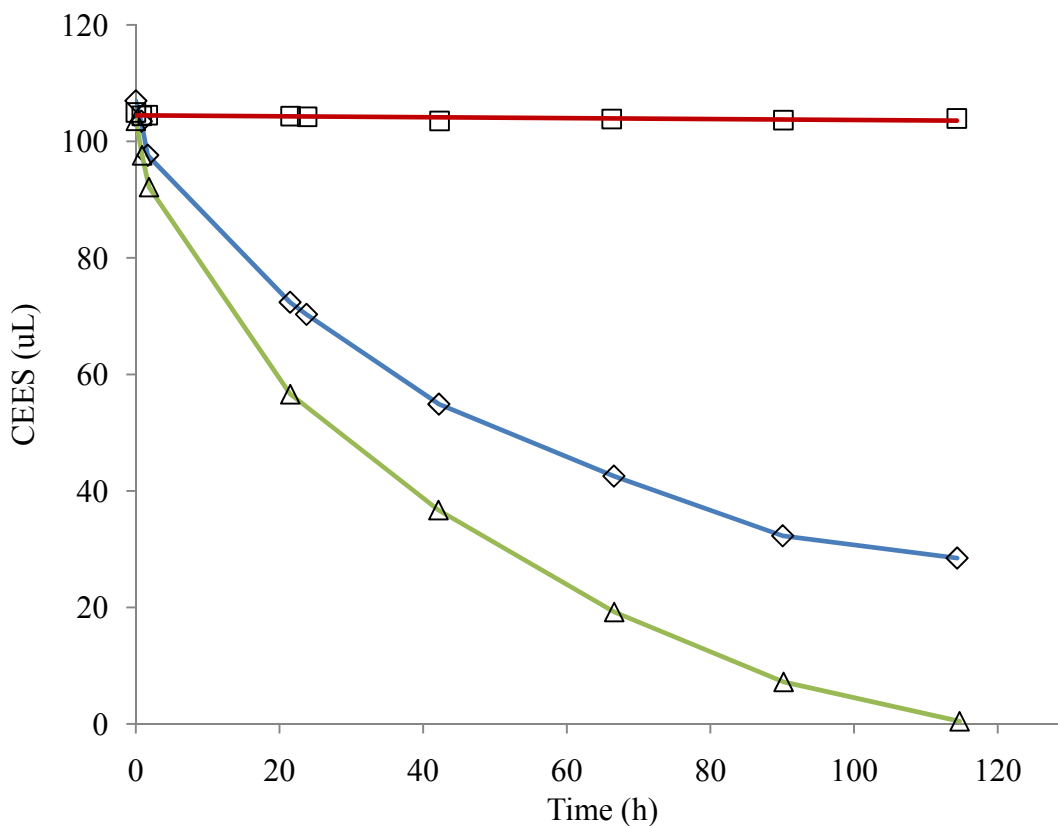


**Figure 3-3.** Kinetics of CEES oxidation by air catalyzed by bromide-free  $\text{TBA}_3\text{H}_2[\text{Fe}(\text{NO}_3)\text{PW}_{11}\text{O}_{39}]$  ( $\text{TBA}\{\text{FePW}_{11}\}$ ) ( $\square$ ),  $\text{TBA}\{\text{FePW}_{11}\} + \text{TBABr}$  ( $\diamond$ ) and  $\text{TBA}\{\text{FePW}_{11}\} + \text{TBABr} + \text{TBANO}_3$  ( $\triangle$ ) at  $25^\circ\text{C}$  (ambient conditions) in acetonitrile. Conditions:  $[\text{CEES}]_0 = 0.35 \text{ M}$  ( $105 \mu\text{L}$ ),  $\text{TBA}\{\text{FePW}_{11}\} = 0.016 \text{ M}$ ,  $[\text{TBABr}] = 0.016 \text{ M}$ ,  $[\text{TBANO}_3] = 0.016 \text{ M}$ ,  $\text{CH}_3\text{CN} = 2.3 \text{ mL}$ .

The catalytic data in Figure 3-3 clearly show that the bromide-free system obtained by the modified method exhibits no catalytic aerobic sulfoxidation activity. However, with the addition of TBABr the system becomes active. Adding TBANO<sub>3</sub> to the TBABr added system can further improve the activity. This collective evidence strongly suggests that formation of Br<sub>2</sub>/Br<sub>3</sub><sup>-</sup> could be the first step in catalytic aerobic sulfoxidation by the NO<sub>x</sub>/Br system and that TBABr<sub>3</sub> is the yellow active species.

#### *The mechanism of sulfoxidation catalyzed by NO<sub>x</sub>/Br system*

In Chapter 2, a nitrosonium intermediate was proposed to be involved in the reaction mechanism. However, isolation of the actively yellow solid<sup>3</sup> cast doubt on nitrosonium being the active intermediate. The experiments and results outlined above suggest that Br<sub>2</sub>, instead of nitrosonium or its derivatives, is likely to be the active oxidant in sulfoxidation. The NO<sub>x</sub>, still a crucial component, oxidizes Br<sup>-</sup> to Br<sub>2</sub> and after aerobic oxidation the oxidative form of NO<sub>x</sub> is regenerated.

Previously, Rossi, Martin and coworkers<sup>10-14</sup> had investigated selective sulfoxidation catalyzed by metallic nitrate and bromide salts. They had studied the catalytic system by electrochemical methods and suggested that the catalytic and selective oxidation of sulfide into sulfoxide takes place in the metallic center with nitrate/nitrite and bromide/bromine redox cycles as oxidant and mediator respectively. However, they paid no attention to the kinetics and barely did any kinetics and thermodynamics studies to prove their proposal. That may partially be because the presence of metals makes the kinetics of the catalyzed reactions

too complicated to be analyzed. Combining data from their investigations and those performed by our group, a mechanism similar to what they postulated for aerobic sulfoxidation catalyzed by our  $\text{NO}_x/\text{Br}$  system could also be viable. The proposed mechanism involving no metal center is shown in Figure 3-4.

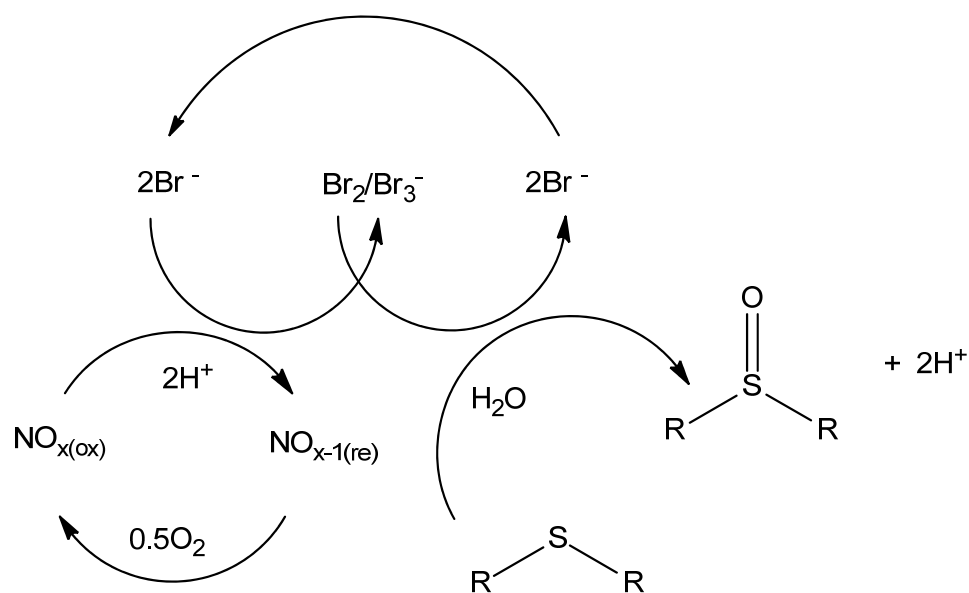
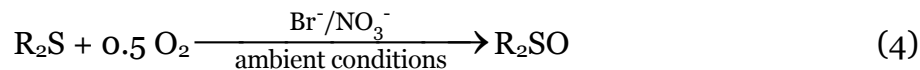


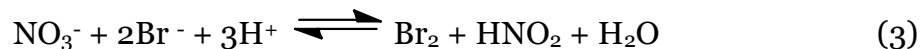
**Figure 3-4.** Proposed mechanism for the selective aerobic oxidation of sulfide to sulfoxide catalyzed by the  $\text{NO}_x/\text{Br}$  systems.

The mechanism of the overall reaction in eq. 4 can be written as follows:

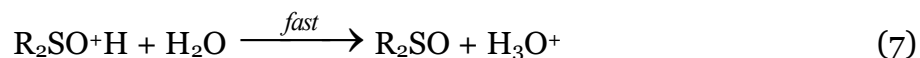
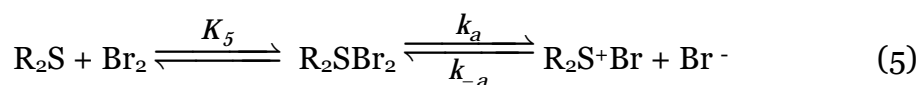
Net reaction:



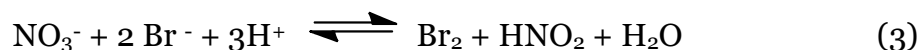
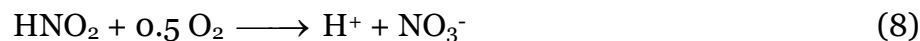
I) The formation of Br<sub>2</sub>



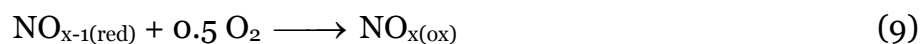
II) The sulfide oxidation by Br<sub>2</sub>



III) The regeneration of Br<sub>2</sub>

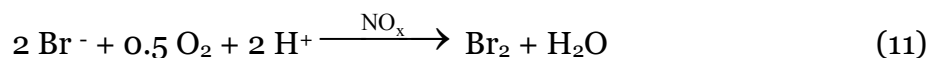


In the formation of Br<sub>2</sub> several different reduced forms of NO<sub>x</sub> (NO, NO<sub>2</sub>, NO<sub>2</sub><sup>-</sup> and BrNO) are produced based on the work of Bazsa and coworkers.<sup>9</sup> With the introduction of air, the oxidation of these reduced forms to oxidized forms is much faster than the reaction shown in eq. 8. Therefore, the formation of Br<sub>2</sub> and regeneration of oxidant could be better represented by eqs. 9 and 10:



where  $\text{NO}_{x(\text{ox})}$  and  $\text{NO}_{x-1(\text{red})}$  represent the oxidized and reduced forms of  $\text{NO}_x$ , respectively.

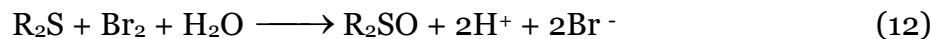
Or the regeneration of  $\text{Br}_2$  can be simply written as eq. 11:



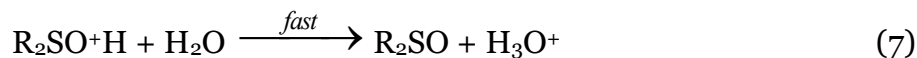
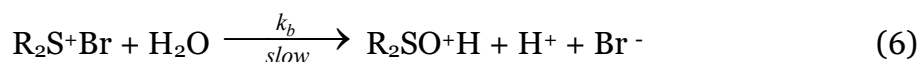
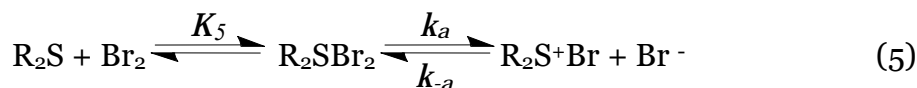
Keep in mind that in acetonitrile the  $K$  value of eq. 2 is much higher than that in water ( $9 \times 10^6 \text{ M}^{-1}$  v.s.  $17 \text{ M}^{-1}$ ). Therefore,  $\text{Br}_3^-$  is the main specie present in the  $\text{Br}_2/\text{Br}_3^-$  equilibrium under our catalytic conditions.

### *The sulfide oxidation by $\text{Br}_2$*

The oxidation of organic sulfides to sulfoxides with halogens (eq. 12) is well known.



The mechanism of the oxidation of thioethers by halogens has been intensively investigated and proposed to be that below: <sup>15-19</sup>



Mixing sulfide with bromine initially forms a sulfide-bromine complex. The sulfide in the complex is oxidized to a sulfonium cation by transfer of an electron from the sulfur center to a bromine atom. The resulting sulfonium-

bromine complex loses another electron to bromide upon attack by water. Hydrolysis of the sulfonium-bromine complex is assumed to be the rate-limiting step. Subsequent hydrolysis produces one mole of sulfoxide and two moles of hydrobromic acid (or H<sup>+</sup> and Br<sup>-</sup>) completing the overall reaction. According to the proposed mechanism, the kinetics of the sulfoxidation can be deduced by applying the steady state approximation. In the steady state approximation, the formation and consumption of the intermediate, R<sub>2</sub>S<sup>+</sup>Br, in equation (5) are equal. Therefore:

$$\frac{d[\text{R}_2\text{S}^+\text{Br}]}{dt} = k_a[\text{R}_2\text{SBr}_2] - k_{-a}[\text{R}_2\text{S}^+\text{Br}][\text{Br}^-] - k_b[\text{R}_2\text{S}^+\text{Br}][\text{H}_2\text{O}] = 0 \quad (13)$$

$$\Rightarrow [\text{R}_2\text{S}^+\text{Br}] = \frac{k_a[\text{R}_2\text{SBr}_2]}{k_{-a}[\text{Br}^-] + k_b[\text{H}_2\text{O}]} = K_5 \frac{k_a[\text{R}_2\text{S}][\text{Br}_2]}{k_{-a}[\text{Br}^-] + k_b[\text{H}_2\text{O}]} \quad (14)$$

$$-\frac{d[\text{R}_2\text{S}^+\text{Br}]}{dt} = k_b[\text{R}_2\text{S}^+\text{Br}][\text{H}_2\text{O}] = k_b K_5 \frac{k_a[\text{H}_2\text{O}]}{k_{-a}[\text{Br}^-] + k_b[\text{H}_2\text{O}]} [\text{R}_2\text{S}][\text{Br}_2] \quad (15)$$

Because the hydrolysis step (eq. 6) is the slowest step in the postulated mechanism, it is reasonable to assume  $k_b[\text{H}_2\text{O}] \ll k_{-a}[\text{Br}^-]$ . Then,

$$-\frac{d[\text{R}_2\text{S}]}{dt} = -\frac{d[\text{R}_2\text{S}^+\text{Br}]}{dt} \approx K_5 \frac{[\text{H}_2\text{O}][\text{Br}_2]}{[\text{Br}^-]} [\text{R}_2\text{S}] \quad (16)$$

$$\text{where } K_5 = k_b \times K_5 \times k_a / k_{-a}$$

Since Br<sub>3</sub><sup>-</sup> is the main form of the Br<sub>2</sub>/Br<sub>3</sub><sup>-</sup> equilibrium in our catalytic system, and also because Br<sub>3</sub><sup>-</sup> has a much higher absorption coefficient compared to Br<sub>2</sub> in acetonitrile solution, the absorption of Br<sub>3</sub><sup>-</sup> has been chosen for the kinetic studies. Therefore, considering eq. 2 we have:

$$-\frac{d[\text{Br}_3^-]}{dt} = -\frac{d[\text{R}_2\text{S}]}{dt} = K_s \frac{[\text{H}_2\text{O}]}{[\text{Br}^-]} [\text{R}_2\text{S}] \times \frac{[\text{Br}_3^-]}{K_2[\text{Br}^-]} = K_B \frac{[\text{H}_2\text{O}]}{[\text{Br}^-]^2} [\text{R}_2\text{S}][\text{Br}_3^-] \quad (17)$$

Where  $K_B = K_S / K_2$ .

In the catalytic system, all  $\text{Br}_2$  and  $\text{Br}_3^-$  are generated from the oxidation of bromide, then:

$$[\text{Br}^-] = [\text{Br}^-]_0 - 3[\text{Br}_3^-] - 2[\text{Br}_2]/(K_2[\text{Br}^-]) \quad (18)$$

In a typical catalytic system, the initial bromide concentration,  $[\text{Br}^-]_0$ , is 25 mM; the absorbance of a 50-folds diluted ongoing system is around 0.04 a.u at  $\lambda = 270$  nm, which translates to  $[\text{Br}_3^-] = 0.04 \times 50 / \epsilon \approx 0.05$  mM ( $\epsilon = 3.8 \times 10^4$   $\text{M}^{-1}\text{cm}^{-1}$ ); and  $[\text{Br}_2] = [\text{Br}_3^-]/(K_2[\text{Br}^-]) \approx 2.2 \times 10^{-7}$  mM, where  $K_2 = 9 \times 10^6$   $\text{M}^{-1}$  in acetonitrile.<sup>8</sup> The total amount of  $3[\text{Br}_3^-]$  and  $2[\text{Br}_2]$  is about 0.6% of  $[\text{Br}^-]_0$ . Therefore the concentration of bromide is nearly constant in the catalytic reaction and it can be written as  $[\text{Br}^-] \approx [\text{Br}^-]_0$ , or:

$$-\frac{d[\text{Br}_3^-]}{dt} = -\frac{d[\text{R}_2\text{S}]}{dt} = K_B \frac{[\text{H}_2\text{O}]}{[\text{Br}^-]_0^2} [\text{R}_2\text{S}][\text{Br}_3^-] \quad (19)$$

In the catalytic sulfoxidation reaction, the formation and consumption of  $\text{Br}_2$  are assumed as equal for a steady-state approximation. Therefore, the concentration of  $\text{Br}_2/\text{Br}_3^-$  would be stable in the reaction. In order to prove the postulation, a catalytic sulfoxidation system is setup and the concentration of  $\text{Br}_3^-$  is monitored vs. time.

Figure 3-5 is the kinetics of the consumption of CEES and the absorbance of  $\text{Br}_3^-$  at 269 nm of an aged  $\text{NO}_3^-/\text{Br}^-$  system catalyzing the aerobic oxidation of

CEES. In the aged system, the induction period is eliminated because the addition of acid facilitated formation of  $\text{Br}_2/\text{Br}_3^-$  prior to catalytic sulfoxidation. The UV-Vis absorption time profile shows that the concentration of  $\text{Br}_3^-$  drops dramatically in the first few minutes which is attributed to the fast reaction between  $\text{Br}_2$  and CEES before the steady state (which might be an establishment of steady-state conditions). The absorbance of  $\text{Br}_3^-$  then remains at a low level and nearly unchanged throughout the rest of the reaction (the absorbance values are near 0.5 a.u because the GC internal standard, 1,3-dichlorobenzene, has absorption peaks overlap with  $\text{Br}_3^-$ . In order to avoid such interference the bromocyclohexane, which has no absorption around 250 to 400 nm, was chosen as GC internal standard for the remainder of the experiments). The data for consumption of CEES after the induction period is well fit by an exponential function. According to eq. 19 the first-order decay of CEES suggests the concentration of bromide and tribromide are constant, which strongly supports steady-state approximation.

According to the postulated mechanism of catalytic reaction, the consumption and regeneration of  $\text{Br}_2/\text{Br}_3^-$  occur simultaneously; therefore, in order to obtain an equation that precisely describes the kinetics, both the formation and regeneration steps in the catalytic system must be considered.

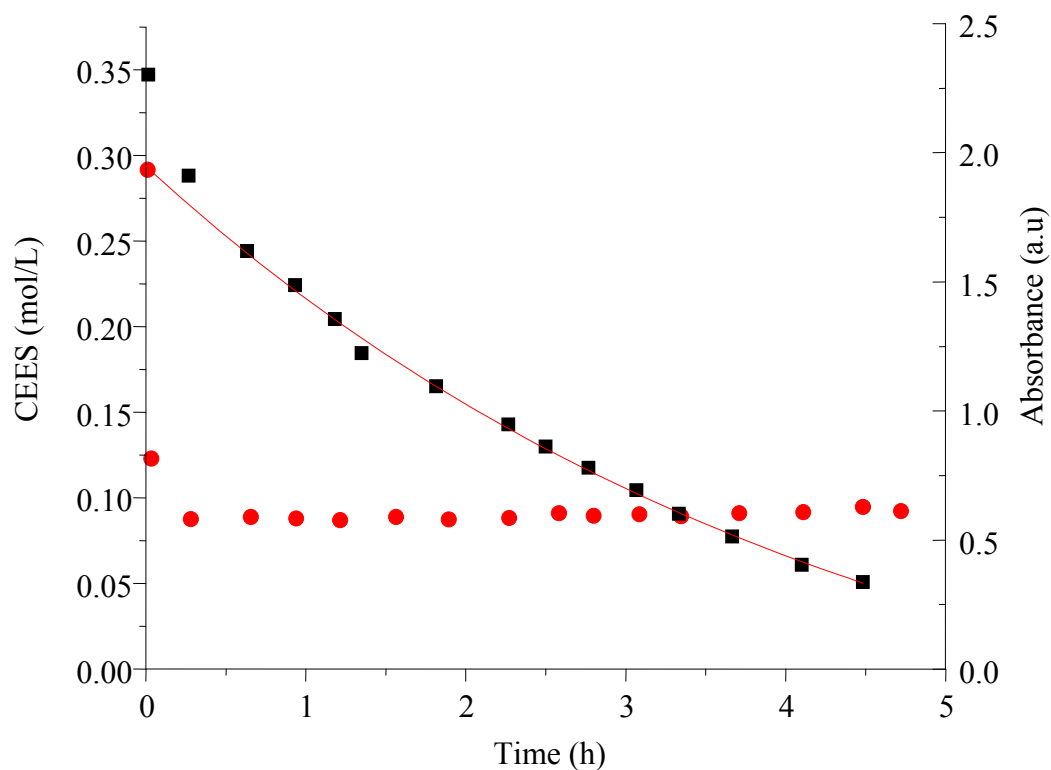


**Figure 3-5.** Kinetics of CEES consumption in an aged TBANO<sub>3</sub>/TBABr system catalyzed sulfoxidation (■); red curve (—): first order fit; (●): time profile of the absorbance at 269 nm of the reaction system (200 times diluted). Conditions: [CEES] = 0.35 M, [TBANO<sub>3</sub>] = 0.018 M, [TBABr] = 0.110 M, [TsOH] = 0.018 M, [1,3-dichlorobenzene] = 0.018 M, CH<sub>3</sub>CN=2.3 mL, T = 70 °C.

### *The regeneration of Br<sub>2</sub>/Br<sub>3</sub><sup>-</sup>*

In the steady-state approximation, the formation and consumption of Br<sub>2</sub>/Br<sub>3</sub><sup>-</sup> is dynamic. The kinetics of Br<sub>3</sub><sup>-</sup> consumption is obtained as in eq. 19. However, unlike the well known sulfide oxidation by halogens, the formation and regeneration of Br<sub>2</sub>/Br<sub>3</sub><sup>-</sup> are much more complicated. Without a detailed mechanism the kinetics of the regeneration of Br<sub>3</sub><sup>-</sup> cannot be concluded solely from eqs. 9-10. Therefore, here, the equation used to describe the regeneration kinetics is acquired from experiments. To measure the kinetics of the regeneration of Br<sub>2</sub>/Br<sub>3</sub><sup>-</sup> a 10 μL solution of an ongoing aerobic sulfoxidation reaction is transferred to a quartz cuvette which contains 2 mL of acetonitrile. The reaction between Br<sub>2</sub> and CEES, therefore, is nearly arrested as a consequence of the 50-fold dilution. The regeneration of Br<sub>2</sub>, if not inhibited by dilution, may be detected. Figure 3-6 is a typical Br<sub>3</sub><sup>-</sup> regeneration time profile measured by UV-Vis.

The non-linear regression of the experimental data gives kinetics of the regeneration in eq. 20 as shown in the table inserted in Figure 3-6. The coefficient of determination, R<sup>2</sup>, is 0.99978 which means a perfect fit.

$$[\text{Br}_3^-] = c_1 - c_2 \times \exp [-(c_3 \times t)] \quad (20)$$

where  $c_1 = y_0$ ,  $c_2 = -A_1$  and  $c_3 = 1/t_1$ , respectively.

Thus, the differential equation for the regeneration of Br<sub>3</sub><sup>-</sup> can be written in eq. 21:

$$-\frac{d[\text{Br}_3^-]}{dt} = R - r[\text{Br}_3^-] \quad (21)$$

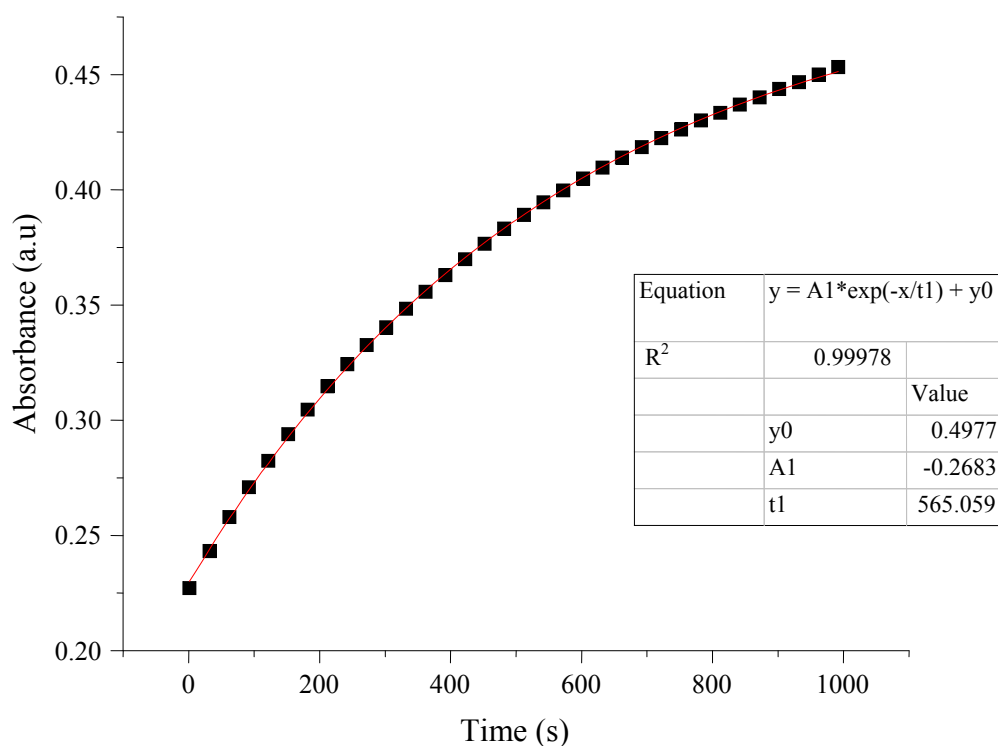


**Figure 3-6.** (■): time profile of the absorbance at 269 nm of the regeneration of  $\text{Br}_3^-$ . Red curve (—): fit with eq. 18. Conditions: a portion of 10  $\mu\text{L}$  solution from an ongoing catalytic sulfoxidation reaction was diluted 50-fold; conditions of the sulfoxidation reaction:  $[\text{CEES}]_0 = 108 \text{ mM}$ ,  $[\text{TBANO}_3] = 25 \text{ mM}$ ,  $[\text{TBABr}] = 25 \text{ mM}$ ,  $[\text{HClO}_4] = 5 \text{ mM}$ ,  $\text{CH}_3\text{CN} = 2.0 \text{ mL}$ ,  $T = 70 \text{ }^\circ\text{C}$ .

Although the mechanism of the formation and regeneration of  $\text{Br}_2/\text{Br}_3^-$  is complex and not yet quite clear, the experimental reaction rate law is simple. There are two terms in the right side of the differential eq. 21:  $R$  represents a zero-order (with respect to  $\text{Br}_3^-$ ) rate for the regeneration of  $\text{Br}_3^-$ ;  $r$  is an apparent first order rate constant, which might be dependent on  $\text{NO}_x$  and  $\text{O}_2$  concentrations. This experimental eq. 21 describes well the experimental kinetics for  $[\text{Br}_3^-]$  regeneration in Figure 3-6.

Knowing the kinetics of  $\text{Br}_2/\text{Br}_3^-$  regeneration, the detailed kinetics of CEES consumption can be deduced as follows. The concentration of water and bromide are nearly constant in the catalytic reaction, then eq. 19 can be written as follows:

$$-\frac{d[\text{Br}_3^-]}{dt} = -\frac{d[\text{R}_2\text{S}]}{dt} = K_B \frac{[\text{H}_2\text{O}]}{[\text{Br}^-]_0^2} [\text{R}_2\text{S}][\text{Br}_3^-] = K[\text{R}_2\text{S}][\text{Br}_3^-] \quad (22)$$

where  $K = K_B \times [\text{H}_2\text{O}] / [\text{Br}^-]_0^2$

Therefore in the steady-state approximation, the consumption and regeneration of  $\text{Br}_2$  is equal, i.e. (21)-(22) = 0; which is,

$$K[\text{R}_2\text{S}][\text{Br}_3^-] = R - r[\text{Br}_3^-] \quad (23)$$

then,

$$[\text{Br}_3^-] = \frac{R}{r + K[\text{R}_2\text{S}]} \quad (24)$$

Put (24) back into (22), we get,

$$-\frac{d[\text{R}_2\text{S}]}{dt} = K[\text{R}_2\text{S}] \frac{R}{r + K[\text{R}_2\text{S}]} \quad (25)$$

Based on eq. 25 two important conclusions can be deduced. First, when  $r \gg K[R_2S]$  the equation can be simplified to eq. 26. This equation indicates that when the reaction rate of bromine sulfoxidation is much slower than that of the regeneration of bromine, the CEES consumption should obey a first-order rate law.

$$-\frac{d[R_2S]}{dt} = \frac{RK}{r}[R_2S] \quad (26)$$

Second, if  $K[R_2S] \gg k_2I$ , the eq. 25 can be simplified to eq. 27. Obviously, this equation indicates that when the sulfoxidation becomes much faster, the overall kinetics will be controlled by a zero-order bromine/tribromide regeneration rate.

$$-\frac{d[R_2S]}{dt} = R \quad (27)$$

In aerobic oxidation catalyzed by the  $NO_x/Br$  system the hydrolysis step is usually slower which results in the pseudo-first order kinetics of CEES consumption. However,  $r$  is not always larger than  $K[R_2S]$ , therefore, exponential decay do not always fit the experimental data well. A precise fit can be obtained by solving the differential eq. 25. The results cannot be expressed as a simple function of  $[R_2S]$  versus time. Instead, they can be written as follows:

$$t = \frac{-1}{R} \left\{ \frac{r}{K} \ln \left( \frac{[R_2S]_t}{[R_2S]_0} \right) + [R_2S]_t - [R_2S]_0 \right\} \quad (28)$$

or

$$t = A + B \cdot \ln[R_2S]_t + C \cdot [R_2S]_t \quad (29)$$

where,

$$A = \{(r/K)\ln[R_2S]_0 + [R_2S]_0\}/R$$

$$B = -r/(KR), \quad C = -1/R$$

The eq. 29 is the precise kinetics expression for CEES consumption by aerobic sulfoxidation catalyzed by the NO<sub>x</sub>/Br system derived from the proposed mechanism. This equation provides the best non-linear fit to the experimental data acquired in the following paragraphs.

### *The effect of water on the catalytic system*

Water is an important factor which greatly affects the activity of the catalytic system. The work performed in Chapter 2 showed that large amount of H<sub>2</sub>O significantly inhibits the activity of the catalyst; however, eq. 19 in this Chapter points out that the addition of water should accelerate the rate-determining hydrolysis step.

Considering the formation/regeneration of Br<sub>2</sub>/Br<sub>3</sub><sup>-</sup>, this paradox becomes explicable. Although the addition of water speeds up the hydrolysis step, the work performed by Bazsa and coworkers<sup>9</sup> revealed that water inhibits the autocatalytic reaction (eq. 3). Therefore the more water added to an un-aged system, the longer the observed induction period. Also, the addition of water not only affects the formation of Br<sub>2</sub> but also regeneration of key intermediate oxidants. Based on the proposed mechanism, the water effect becomes very complex because water could affect nearly all the rate constants in eq. 28.

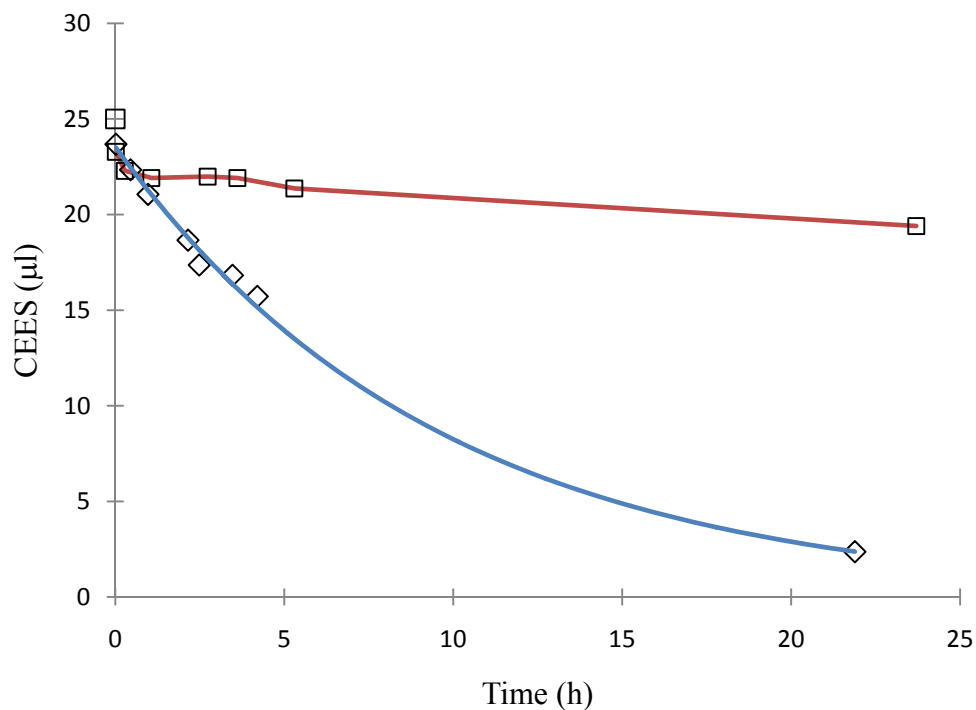


**Figure 3-7.** Kinetics of CEES oxidation by air in water-free (□) and water containing (◇)  $\text{NO}_x/\text{Br}$  systems at 70 °C in acetonitrile. Conditions for the water-free system:  $[\text{CEES}]_0 = 108 \text{ mM}$  (25  $\mu\text{L}$ ),  $[\text{TBANO}_3] = 25 \text{ mM}$ ,  $[\text{TBABr}] = 25 \text{ mM}$ ,  $[\text{H}_2\text{SO}_4] = 2.5 \text{ mM}$   $\text{CH}_3\text{CN} = 2.0 \text{ mL}$ ,  $T = 70^\circ\text{C}$ ; conditions for the water-containing system:  $[\text{CEES}]_0 = 108 \text{ mM}$  (25  $\mu\text{L}$ ),  $[\text{TBANO}_3] = 25 \text{ mM}$ ,  $[\text{TBABr}] = 25 \text{ mM}$ ,  $[\text{HClO}_4] = 5 \text{ mM}$ ,  $[\text{H}_2\text{O}] = 277 \text{ mM}$  (10  $\mu\text{L}$ ),  $\text{CH}_3\text{CN} = 2.0 \text{ mL}$ ,  $T = 70^\circ\text{C}$

To corroborate our proposed mechanism, it is important to investigate experimentally the effect of water on the kinetics of aerobic sulfoxidation catalyzed by the  $\text{NO}_x/\text{Br}$  system. The hydrolysis step in the mechanism, eq. 6, requires the presence of water for the net sulfoxidation process. Therefore the reaction in a water-free system was carried out. The preparation of a water-free  $\text{NO}_x/\text{Br}$  system is similar to that of the aged  $\text{NO}_x/\text{Br}$  catalyst except that fresh water-free acetonitrile (from Liotta's group) and concentrated  $\text{H}_2\text{SO}_4$  instead of  $\text{HClO}_4$  were used. The kinetic data in water-free system and water-containing system catalytic sulfoxidation are shown in Figure 3-7. Clearly, the consumption of CEES in water-free system is much slower than in the water-containing system. There is a rapid decrease in CEES concentration in the first 30 min in both systems due to reaction between the preformed  $\text{Br}_2$  and CEES. In the following hours the net CEES oxidation in the water-free system slowly decreases. According to the postulated mechanism in this case, the reaction should stop before the hydrolysis (eq. 5) because the intermediate,  $\text{R}_2\text{S}^+\text{Br}$ , is stable in the absence of water. Therefore, if all the  $\text{Br}^-$  in the water-free system is oxidized to  $\text{Br}_2$ , the maximum conversion of CEES is determined by the total amount of  $\text{Br}^-$ . In Figure 3-7, the kinetic data obtained at the 24 hrs in water-free system shows that 0.048 mmol of CEES is consumed, which is consistent with the amount of TBABr (0.05 mmol) used in the reaction. In addition, CEES consumption obeys an exponential law in the water-containing system.

As discussed before, the concentration of water affects nearly all rate equilibrium constants ( $K$ ,  $R$  and  $r$ ) in eq. 28:  $K$  is promotional to water concentration according to eq.22;  $R$  is the zero order rate of

formation/regeneration of  $\text{Br}_2$ , which is known to be inhibited by the addition of water; and  $r$  is the apparent rate constant for the reverse reaction in eq. 10, which likely includes an  $[\text{H}_2\text{O}]$  factor because water is present on the right side of the reaction. From eqs. 25-27, it is expected that the changes of  $K$  and  $r$  would result in different reaction kinetics. Therefore, varying the amount of water added into the system may provide insightful information. Figure 3-8 shows the kinetic data obtained with different amounts of water in catalytic  $\text{NO}_x/\text{Br}$  systems. The kinetic data and the non-linear fits perfectly match with each other and the figure clearly shows that the appearance of the kinetic data is strongly affected by the concentration of water. When 10  $\mu\text{L}$  of  $\text{H}_2\text{O}$  is added to the catalytic system, the consumption of CEES appears to be a typical first-order decay. Upon increasing the addition of  $\text{H}_2\text{O}$  to 50  $\mu\text{L}$  the CEES consumption kinetics become linear in the first few hours and then more like exponential at the end of the reaction. If 100  $\mu\text{L}$  of  $\text{H}_2\text{O}$  is added to the system, the kinetic curves appear to be almost linear. The A, B and C values obtained by a least-squares fit and the  $K$ ,  $R$  and  $r$  values obtained are listed in Table 3-1.

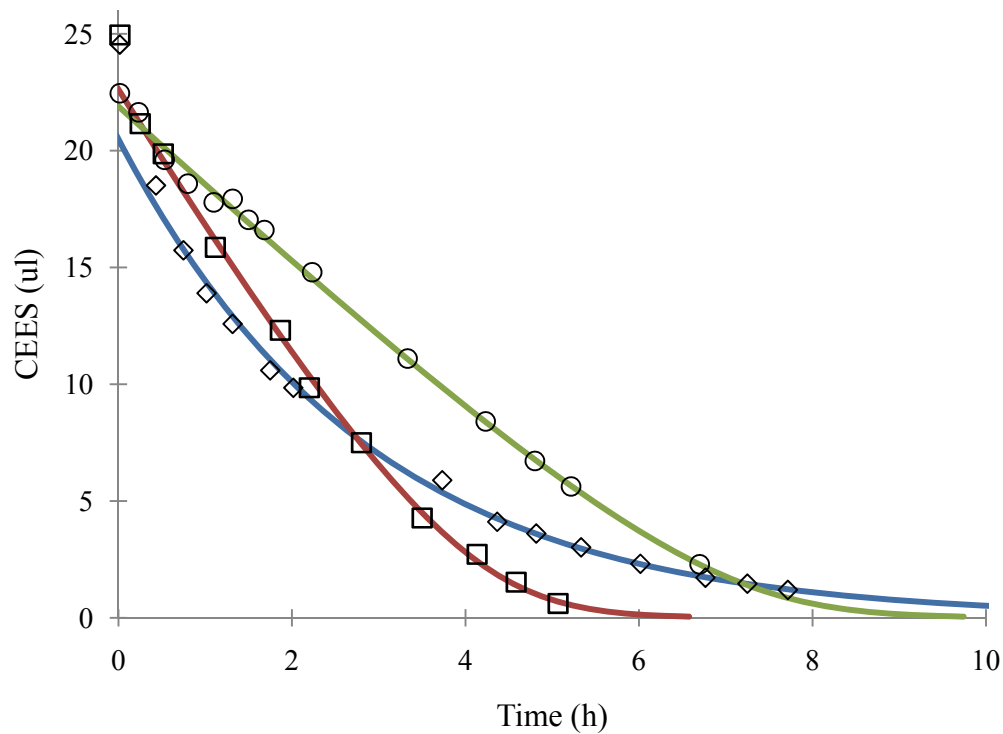


**Figure 3-8.** Kinetics of CEES consumption catalyzed by aged  $\text{NO}_x/\text{Br}$  system containing  $10 \mu\text{L}$  ( $277 \text{ mM}$ ) ( $\diamond$ ),  $50 \mu\text{L}$  ( $1.38 \text{ M}$ ) ( $\square$ ) and  $100 \mu\text{L}$  ( $2.77 \text{ M}$ ) ( $\circ$ ) of water under air at  $70^\circ\text{C}$  in acetonitrile. Conditions:  $[\text{CEES}]_0 = 108 \text{ mM}$  ( $25 \mu\text{L}$ ),  $[\text{TBANO}_3] = 25 \text{ mM}$ ,  $[\text{TBABr}] = 25 \text{ mM}$ ,  $[\text{HClO}_4] = 5 \text{ mM}$ ,  $\text{CH}_3\text{CN} = 2.0 \text{ mL}$ ,  $T = 70^\circ\text{C}$ . Color curves: least-squares fit based on eq. 29.

**Table 3-1.** The constants and the associated  $K$  values obtained by least-squares fit of aerobic CEES oxidation catalyzed by the  $\text{NO}_x/\text{Br}$  systems shown in Figure 3-8.

| $[\text{H}_2\text{O}]$ ( $\mu\text{L}$ ) | 10      | 50       | 100      |
|--|---------|----------|----------|
| A  | -6.8241 | 1.8930   | 4.2185   |
| B  | -2.6563 | -0.5419  | -0.6373  |
| C  | -3.2740 | -42.2900 | -78.1949 |
| $R$                                      | 0.3054  | 0.0237   | 0.0128   |
| $K/r^*$                                  | 1.2325  | 78.0402  | 122.6972 |

Unit for least squares fit: time = hour, concentration = mol/L; \* The individual values of  $K$  and  $r_A$  cannot be obtained according to the expression of A, B and C in eq. 29.

The table reveals that with the addition of water the  $R$  value decreases. The decreasing of  $R$  reflects the decreased rate of  $\text{Br}_2$  regeneration which again supports that the addition of water inhibits the catalytic reaction. The data in the table also reveal that the  $K/r$  increases with the addition of water. From eq. 26, an increase in  $K/r$  increases the overall reaction rate. The  $R$  and  $K/r$  changes observed here can be used to explain the water effects we observed in Chapter 2: the addition of small amount of water does not markedly change the activity of the solid-supported catalysts because the decrease of  $R$  is offset by the increase of  $K/r$ ; when a large amount of water is added to the catalyst there is considerable inhibition of the catalytic activity because the rate of decrease in  $R$  is faster than the rate of increase in  $K/r$  with increasing water concentration. Also the large changes of  $K/r$  from 10 to 50  $\mu\text{L}$  of  $\text{H}_2\text{O}$  added to the system indicates that  $[\text{H}_2\text{O}]$

may also be involved in the expression of  $r$  (in other words  $r$  is dependent on water concentration,  $r = f([\text{H}_2\text{O}])$ ).

All kinetic data in water-free and in water-containing systems match the proposed mechanism well. These data also strongly support the  $\text{Br}_2/\text{Br}_3^-$ -based mechanism for aerobic sulfoxidation catalyzed by  $\text{NO}_x/\text{Br}$ .

### **Conclusion**

A catalytic active yellow-colored solid has been isolated and identified as  $\text{TBABr}_3$  by UV-Vis spectrometry. A mechanism for the air-based (aerobic) sulfoxidation catalyzed by the  $\text{NO}_x/\text{Br}$  system based on the  $\text{Br}_2/\text{Br}_3^-$  as the active species has been proposed. The derived reaction rate law equations effectively describe the kinetics of the catalytic reaction thus supporting the postulated mechanism.

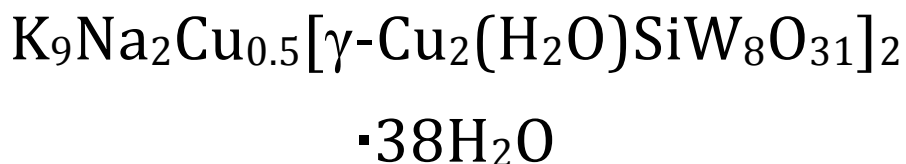
### **References**

- (1) Luo, Z.; Okun, N. M.; Hill, C. L. *P&G Research Report*; Emory University: Atlanta, 2007-2008.
- (2) Okun, N. M.; Luo, Z.; Hill, C. L. *P&G Research Report*; Emory University: Atlanta, 2006.
- (3) Hillesheim, D. A.; Young, P.; Geletii, Y. V., Unpublished Work.
- (4) Domaille, P. J., Vanadium (V) Substituted Dodecatungstophosphates. In *Inorganic Syntheses*, Ginsberg, A. P., Ed. John Wiley and Sons: New York, 1990; Vol. 27, pp 96-104.

- (5) Okun, N. M.; Tarr, J. C.; Hillesheim, D. A.; Zhang, L.; Hardcastle, K. I.; Hill, C. L., *J. Mol. Catal. A. Chem.* **2006**, *246*, 11-17.
- (6) Raphael, L., Bromine Compounds Chemistry and Applications. Price, D.; Iddon, B.; Wakefield, B. J., Eds. Elsevier: New York, 1988.
- (7) Domínguez, A.; Iglesias, E., *Langmuir* **1998**, *14*, 2677-2683.
- (8) Allen, G. D.; Buzzeo, M. C.; Villagra'n, C.; Hardacre, C.; Compton, R. G., *J. Electroanal. Chem.* **2005**, *575*, 311-320.
- (9) Lengyel, I.; Nagy, I.; Bazsa, G., *J. Phys. Chem.* **1989**, *93*, 2801-2807.
- (10) Suárez, A. R.; Baruzzi, A. M.; Rossi, L. I., *J. Org. Chem.* **1998**, *63*, 5689-5691.
- (11) Rossi, L. I.; Martin, S. E., *Appl. Catal. A* **2003**, *250*, 271-278.
- (12) Rossi, L. I.; Rossi, R. H. d., *Appl. Catal. A: Gen.* **2004**, *267*, 267-272.
- (13) Martín, S. E.; Rossi, L. I., *Tetrahedron Letters* **2001**, *42*, 7147-7151.
- (14) Rossi, L. I.; Suárez, Á. R., *Sulfur Lett.* **2002**, *25*, 123-127.
- (15) Higuchi, T.; Gensch, K.-H., *J. Am. Chem. Soc.* **1966**, *88*, 5486-5491.
- (16) Lardy, D. O. L. H. A., *Biochemistry* **1969**, *8*, 3395-3402.
- (17) Miotti, U.; Modena, G.; Sedeá, L., *J. Chem. Soc. (B)* **1970**, 802-804.
- (18) Choudhary, K.; Suri, D.; Kothari, S.; Banerji, K. K., *J. Phys. Org. Chem.* **2000**, *13*, 283-292.
- (19) Gensch, K.-H.; Pitman, I. H.; Higuchi, T., *J. Am. Chem. Soc.* **1968**, *90*, 2096-2104.

# *Chapter 4*

Multi-Copper Polyoxoanions. 1. Synthesis, Characterization, X-ray Crystal Structures, and magnetism of a new dimeric silicotungstate:



with Paul Kögerler, Rui Cao, Imroz Hakim, Craig L. Hill

(published partially in *Dalton Trans.* **2008** 54-58)

## Abstract

A new structurally distinct dimeric silicotungstate  $K_9Na_2Cu_{0.5}[\gamma-Cu_2(H_2O)SiW_8O_{31}]_2 \cdot 38H_2O$  (**1**) has been synthesized and characterized by infrared spectroscopy, elemental analysis and variable-temperature magnetic measurements. Blue needle-like crystals of **1** were obtained by reaction of  $K_8[\gamma-SiW_{10}O_{36}]$  with 2 equivalents of Cu(II) in a 0.5 M sodium acetate solution (pH 4.2) and subsequent addition of an equal volume of ethylene glycol. The structure of **1** was determined by single-crystal X-ray diffraction: final  $R_1 = 3.41\%$  based on 9709 independent reflections. The structure consists of two  $[\gamma-Cu_2(H_2O)SiW_8O_{31}]^{6-}$  Keggin-like units with the  $[Cu_2O(H_2O)(\mu_3-O)(\mu_2-O)]$  moiety of one unit bonded to the top of a  $[W_2O_6]$  moiety of the other unit. Magnetic susceptibility measurements indicate competing ferro- and antiferromagnetic intramolecular coupling between the four  $s = 1/2$  Cu(II) centers in the cluster anion.

## Introduction

Transition metal-substituted polyoxometalates (POMs) constitute a large class of highly tunable metal oxo clusters.<sup>1-3</sup> They continue to attract broad interest from basic studies such as electron transfer,<sup>4-6</sup> ion pairing<sup>6-11</sup> to potential applications in medicine<sup>12-18</sup> and redox catalysis.<sup>2, 19-26</sup> The incorporation of transition metals into lacunary (defect) POM precursors is generally simple and straightforward as these precursors effectively act as chelating ligand systems. The mechanisms, by which metal-substituted POMs are formed, however, are yet not well understood, and even subtle changes in the synthesis conditions may

result in different structures. Recently, much research has focused on di-vacant  $[\gamma\text{-SiW}_{10}\text{O}_{36}]^{8-}$  moiety because it can bind two transition metal groups adjacent to one another and might, as a consequence, reveal new features in the now well established field of POM-catalyzed homogeneous and heterogeneous catalytic oxidation.<sup>27-29</sup> In addition, recent research has established that this <sup>30</sup> moiety and its di-metal-substituted form readily, yielding diverse POM structures.<sup>31-42</sup>

Several research groups have recently investigated the reactions of the first-row transition metals with the potassium salt of  $[\gamma\text{-SiW}_{10}\text{O}_{36}]^{8-}$  and characterized the product complexes by single-crystal X-ray diffraction and other methods.<sup>29, 31-47</sup> Initially, Pope and coworkers<sup>31, 34, 43</sup> successfully obtained a series of in-pocket and out-of-pocket d-metal di-substituted  $[\gamma\text{-M}_2\text{SiW}_{10}\text{O}_{36}]^{n-}$  (M = V, Cr, Mn) compounds by reaction of  $\text{K}_8[\gamma\text{-SiW}_{10}\text{O}_{36}]$  with various metal cations in buffered aqueous solutions under ambient conditions. By using azido ligands, Mialane and coworkers<sup>39, 48</sup> obtained in-pocket di-Cu and di-Mn substituted complexes of formula,  $[\gamma\text{-M}_2\text{SiW}_{10}\text{O}_{36}]_2\text{L}_x^{n-}$ . Subsequently, Kortz and coworkers<sup>35</sup> reported a series of sandwich dimers,  $[\beta\text{-(M}_2\text{SiW}_9\text{O}_{34})_2]^{(2n+4)-}$  (M = Mn, Cr, Zn) by heating the precursor solutions to 90°C for 40 minutes. By changing the synthesis conditions, they obtained several other metal substituted silicotungstate derivatives.<sup>36, 37, 40, 41, 45, 49</sup> Interestingly, both Mialane<sup>39,50</sup> and Kortz <sup>37,45</sup> found that under certain preparation conditions, the  $[\gamma\text{-SiW}_{10}\text{O}_{36}]^{8-}$  decomposes to form a tetra-vacant  $\{\text{SiW}_8\text{O}_{31}\}$  fragment by losing a  $\{\text{W}_2\text{O}_5\}$  unit. Two or more of these  $\{\text{SiW}_8\text{O}_{31}\}$  fragments tend to incorporate multiple transition metal centers and these centers connect with each other forming multi-

metal-substituted polyoxoanions that frequently exhibit interesting magnetic properties.

Recently, Mizuno and coworkers reported that the diiron-substituted silicotungstate,  $[\gamma(1,2)\text{-SiW}_{10}\{\text{Fe}(\text{OH})_2\}_2\text{O}_{38}]^{6-}$ , is a catalyst for the  $\text{O}_2$ -based epoxidation of alkenes<sup>27, 28, 44</sup> and that the lacunary silicotungstate,  $[\gamma\text{-SiW}_{10}\text{O}_{36}]^{8-}$ , is a highly selective catalyst for the  $\text{H}_2\text{O}_2$ -based epoxidation of alkenes.<sup>27</sup> They proposed the former complex to be an in-pocket di-iron  $\gamma$ -Keggin derivative. Although this complex was thoroughly characterized by many techniques, no crystal structure was reported. Subsequent studies of this POM system by the Hill group<sup>29, 38</sup> resulted in X-ray structures of several iron substituted silicotungstates isolated from aqueous solution and realization that under these conditions the primary polyoxometalates present contain out-of-pocket  $[\gamma\text{-SiW}_{10}\{\text{Fe}_2(\text{H}_2\text{O})_2(\text{OH})_5\}\text{O}_{36}]^{7-}$  moieties.

In context with ongoing studies<sup>51-56</sup> of multi-metal-substituted POMs as catalysts for ambient-temperature, air-based oxidation of sulfides, aldehydes and alkenes, we report here the synthesis of a new di-copper substituted dimeric silicotungstate complex,  $\text{K}_9\text{Na}_2\text{Cu}_{0.5}[\gamma\text{-Cu}_2(\text{H}_2\text{O})\text{SiW}_8\text{O}_{31}]_2 \cdot 38\text{H}_2\text{O}$  (**1**) and characterization of this complex by many techniques.

## Experimental Section

*General Methods and Materials:*  $\text{K}_8[\gamma\text{-SiW}_{10}\text{O}_{36}] \cdot 12\text{H}_2\text{O}$  was prepared using the well-known procedure<sup>57</sup> and its purity was checked by infrared spectroscopy.  $\text{CuBr}_2$ , acetonitrile, ethylene glycol, sodium acetate and acetic acid were obtained from Aldrich and used without further purification. Elemental

analyses for K, Na, Cu, Si and W were performed by Galbraith Laboratories (Knoxville, Tennessee). The infrared spectrum (2% sample in KBr pellet) was recorded on a Nicolet™ 6700 FT-IR spectrometer from the ThermoElectron Corporation. The electronic absorption spectra were taken on an Agilent 8453 UV-vis spectrometer. The thermogravimetric data were collected on an ISI TGA 1000 instrument. Magnetic susceptibility measurements were performed at 0.1 to 5.0 Tesla for  $T = 1.8 - 290$  K using a Quantum Design MPMS-5S SQUID magnetometer. Experimental susceptibility data were corrected for diamagnetic and (significant) temperature-independent paramagnetic contributions that were determined from measurements on a range of diamagnetic  $\gamma$ -Keggin polyoxotungstate compounds ( $\chi_{\text{dia/TIP}}(\mathbf{1}) = -1.10 \times 10^{-3}$  emu/mol). Field-dependent magnetization studies at 1.8 K reveal the presence of a fraction of mononuclear Cu(II) (0.5 per mol), likely disordered over the crystal lattice.

*Synthesis of  $K_9Na_2Cu_{0.5}[Cu_2(H_2O)SiW_8O_{31}]_2 \cdot 38H_2O$  (1):* A 5-mL portion of acetonitrile solution containing 0.5 g (2.24 mmol) of  $CuBr_2$  was dissolved in 20 mL of di-ionized water. The pH of this solution became 2.7 in three minutes. After stirring the solution, 2.0 g (0.67 mmol) of  $K_8[\gamma-SiW_{10}O_{36}] \cdot 12H_2O$  was added, the solution was stirred for an additional 20 min, and the pH stabilized at 4.2. The undissolved residues were removed from the solution by a medium frit and the filtrate (20 mL) was collected. A 10-mL portion of filtrate was transferred to a 50 mL beaker and to this, 0.225 g of sodium acetate and 1.5 mL of glacial acetic acid (forming 0.5 M HOAc/NaOAc buffer solution, pH = 4.2) were added. After stirring the solution for 5 minutes, 10 mL of ethylene glycol (EG) was added. The solution was stirred for an additional 5 minutes and then

placed in a 30-mL beaker in a dark cabinet. Light blue, needle-like diffraction quality crystals of **1** grown from this 1:1 water: ethylene glycol mixed buffer solution after three days (0.26 g, yield 13.4%). IR (2% KBr pellet, 1200-400 cm<sup>-1</sup>): 1081 (w), 1037 (w), 998 (w), 950 (m), 876 (s, sh), 797 (w), 735 (s), 670 (w), and 517 (w). Anal. calcd. for **1**: Cu, 5.30; K, 6.54; Na, 0.85; Si, 1.04; W, 54.53. Found: Cu, 5.07; K, 6.27; Na, 0.81; Si, 0.97; W, 53.90. [MW = 5394.2 g/mol].

*X-ray Crystallography of 1:* A light-blue needle-like crystal of **1** with dimensions of 0.47 x 0.10 x 0.06 mm<sup>3</sup> was coated with Paratone N oil and mounted on a small fiber loop for index and intensity data collection. The data were collected under a nitrogen stream at 173 K on a Bruker D8 SMART APEX CCD single-crystal diffractometer using Mo K $\alpha$  (0.71073 Å) radiation. Data collection, indexing, and initial cell refinements were processed using the SMART<sup>58</sup> software. Frame integration and final cell refinements were carried out using the SAINT<sup>59</sup> software. The final cell parameters were determined from the least-squares refinement of 56705 reflections. From these unique reflections ( $2\theta_{\max} = 56.82^\circ$ ), 9709 reflections ( $R_{\text{int}} = 0.0741$ ) were considered to be observed. The structure was determined through direct methods (SHELXS97) for locating the tungsten atoms and difference Fourier maps (SHELXL97). The hydrogen atoms of the water molecules were not located in the difference Fourier maps. The final cycle of refinement resulted at  $R = 0.034$  and  $R_w = 0.048$  ( $I > 2\sigma(I)$ ) (Table 4-1). In the final difference map, the highest peak was at 3.687 e Å<sup>-3</sup> and the deepest hole was at -3.387 e Å<sup>-3</sup>.

**Table 4-1.** Crystallographic Data and Structure Refinement for **1**

|                                 | <b>1</b>  |
|---------------------------------|---|
| empirical formula               | Cu <sub>4.5</sub> H <sub>80</sub> K <sub>9</sub> Na <sub>2</sub> O <sub>102</sub> Si <sub>2</sub> W <sub>16</sub>           |
| formula weight                  | 5394.2 g mol <sup>-1</sup>  |
| space group                     | P2(1)/n   |
| unit cell                       | $a = 10.8173(9) \text{ \AA}$<br>$b = 19.5927(17) \text{ \AA}$<br>$c = 18.2517(16) \text{ \AA}$<br>$\beta = 90.165(2)^\circ$ |
| volume                          | 3868.3(6) Å <sup>3</sup>  |
| <i>Z</i>                        | 2   |
| density (calcd)                 | 4.039 g cm <sup>-3</sup>  |
| temperature                     | 173(2)K   |
| wavelength                      | 0.71073 Å   |
| abs. coeff                      | 25.116 mm <sup>-1</sup>   |
| GOF                             | 1.019   |
| final $R_1^a [I > 2\sigma(I)]$  | 0.0341  |
| final $wR_2^b [I > 2\sigma(I)]$ | 0.0482  |

$$^a R_1 = \Sigma ||F_o| - |F_c|| / \Sigma |F_o|; wR_2 = \Sigma [w(F_o^2 - F_c^2)^2] / \Sigma [w(F_o^2)^2]^{1/2}$$

## Results and Discussion

### *Synthesis*

The  $K^+/Na^+$  salt of **1** is prepared in a 1:1 water-ethylene glycol mixed buffer solution (pH 4.2). Crystalline light-blue needles of **1** were obtained after three days in *ca.* 13% yield. Attempts to improve the yield by increasing the crystallization time failed; only crystals of copper acetate were produced. If no ethylene glycol is added, a white-blue colored powder appears after several hours in a yield of more than 40%. The FT-IR of the aforementioned powder is very similar to that of **1**. The major difference between the two IR spectra is the absence of the peaks at 1081 and 1037  $cm^{-1}$  attributed to the C-O stretch of the ethylene glycol.

Previously, Kortz and co-workers<sup>35</sup> studied the reaction of Cu(II) with the  $K^+$  salt of  $[\gamma-SiW_{10}O_{36}]^{8-}$ . They mixed a slight excess  $CuCl_2$  with  $K_8[\gamma-SiW_{10}O_{36}]$  (3 equivalents of Cu(II) per equivalent of  $K_8[\gamma-SiW_{10}O_{36}]$ ) in pH = 4.8 buffer solution and heated the solution to 90 °C for 40 min. This procedure was similar to that used by Pope and co-workers<sup>34</sup> to synthesize di-chromium substituted derivative of  $[\gamma-SiW_{10}O_{36}]^{8-}$  (reaction conducted at pH = 4.8 in NaOAc/HOAc buffer solution followed by heating to 80 °C). However, their final Cu(II)-containing product did not retain the  $\{\gamma-SiW_{10}\}$  framework but isomerized to a typical sandwich-type dimer  $[Cu_2SiW_9O_{34}(H_2O)_2]_2^{12-}$  by formally losing one  $\{WO_6\}$  group per polyanion unit.

Previously, Mialane and co-workers<sup>39, 60</sup> showed that addition of azide may be an efficient way to generate interaction between metal centers in context with

formation of new POM structures. By adding 5.25 equivalents of  $\text{NaN}_3$  to a 2:1 mixture of  $\text{CuCl}_2$  and  $\text{K}_8[\gamma\text{-SiW}_{10}\text{O}_{36}]$ , and subsequent addition of cesium cation afforded the cesium salt of a di-copper substituted  $\gamma$ -silicotungstate dimer,  $[\gamma\text{-SiW}_{10}\text{O}_{36}\text{Cu}_2(\text{H}_2\text{O})(\text{N}_3)_2]_2^{12-}$ .<sup>39</sup> By increasing the concentration of  $\text{K}_8[\gamma\text{-SiW}_{10}\text{O}_{36}]$  and using  $\text{Cu}(\text{NO}_3)_2$  instead of  $\text{CuCl}_2$ , they obtained a copper-substituted trimer,  $[\{\text{SiW}_8\text{Cu}_3(\text{OH})(\text{H}_2\text{O})_2(\text{N}_3)\}_3(\text{N}_3)]^{19-}$ . Each subunit of the trimer contains a structural analogue of the  $[\gamma\text{-Cu}_2\text{SiW}_8\text{O}_{32}]^{8-}$  subunit of **1**. It is worth mentioning that by investigating the system of  $\text{Co}(\text{II})/(\gamma\text{-SiW}_{10}\text{O}_{36})^{8-}$ , Kortz and co-workers obtained a cobalt-substituted trimer<sup>45</sup>  $[\{\text{Co}_9\text{Cl}_2(\text{OH})_3(\text{H}_2\text{O})_9(\text{SiW}_8\text{O}_{31})_3\}]^{17-}$  which has a very similar framework to the copper-substituted trimer. Although some other cobalt-substituted polyoxometalates prepared by Kortz,<sup>37</sup> Mialane<sup>50</sup> and co-workers also contain  $\{\text{M}_2\text{SiW}_8\}$ , the actual structural unit in these product complexes is a  $\{\text{M}_3\text{SiW}_8\}$  unit in which the third metal center, M, is bound on the outside of the original  $\gamma\text{-}\{\text{M}_2\text{SiW}_8\}$ .

### Structures

The novel dimeric silicotungstate, **1**, crystallizes in the monoclinic space group,  $P2_1/n$ . The polyanion contains two equivalent  $[\gamma\text{-Cu}_2(\text{H}_2\text{O})\text{SiW}_8\text{O}_{31}]^{6-}$  subunits related by an inversion center ( $C_i$  symmetry; Figure 4-1). In contrast to the great majority of d-electron transition-metal substituted silicotungstates in which the new d-electron metal center fills the vacant position (lacuna) forming a saturated Keggin structure, two of the five-coordinated copper atoms in **1** exist as  $\{\text{Cu}_2\text{O}(\text{H}_2\text{O})(\mu_3\text{-O})(\mu_2\text{-O})\}$  units and replace a  $\{\text{W}_2\text{O}_6\}$  group instead of filling the

two vacancies in each subunit of the structure. Both of the  $[\gamma\text{-Cu}_2(\text{H}_2\text{O})\text{SiW}_8\text{O}_{31}]$  subunits maintain the lacunary Keggin framework of  $[\gamma\text{-SiW}_{10}\text{O}_{36}]^{8-}$  (Figure 4-2).

O11 is a  $\mu_3$ -oxo bridging W4 on one  $\{\text{SiW}_8\}$  unit and Cu1 and Cu2 on the other  $\{\text{SiW}_8\}$  unit. O12 is a  $\mu_2$ -oxo bridging W5 on one  $\{\text{SiW}_8\}$  unit and Cu2 on the other  $\{\text{SiW}_8\}$  unit. Alternatively O12 can be viewed as linking a  $\{\text{Cu}_2\text{O}(\text{H}_2\text{O})(\mu_3\text{-O})(\mu_2\text{-O})\}$  group and a  $\{\text{W}_2\text{O}_6\}$  group and thereby connecting two adjacent  $[\gamma\text{-Cu}_2(\text{H}_2\text{O})\text{SiW}_8\text{O}_{31}]^{6-}$  moieties. Cu1 and Cu2 in each half of the polyanion are five-coordinate and linked to define a di-pyramidal moiety. Six oxygens and two copper atoms in this di-pyramid lie in an approximate plane ( $d_{\text{Cu-O}} = 1.926(6) - 2.023(6) \text{ \AA}$ ). The significant Jahn-Teller distortion characteristic of d9 metal centers is manifested in part by longer Cu-terminal oxygen distances ( $d_{\text{Cu-O}} = 2.366(7) - 2.368(7) \text{ \AA}$ ). Jahn-Teller effects have been noted for Cu-containing POMs<sup>61</sup> and can exert considerable control in the self assembly of sandwich type POMs.<sup>62</sup> The distance between the two coppers is  $2.9651(16) \text{ \AA}$ . Bond valence sum (BVS) calculations<sup>63</sup> for Cu1 and Cu2 yield an average oxidation state of 1.984 and 2.013, respectively. To our knowledge, polyanion **1** represents an unprecedented dimeric POM structure.

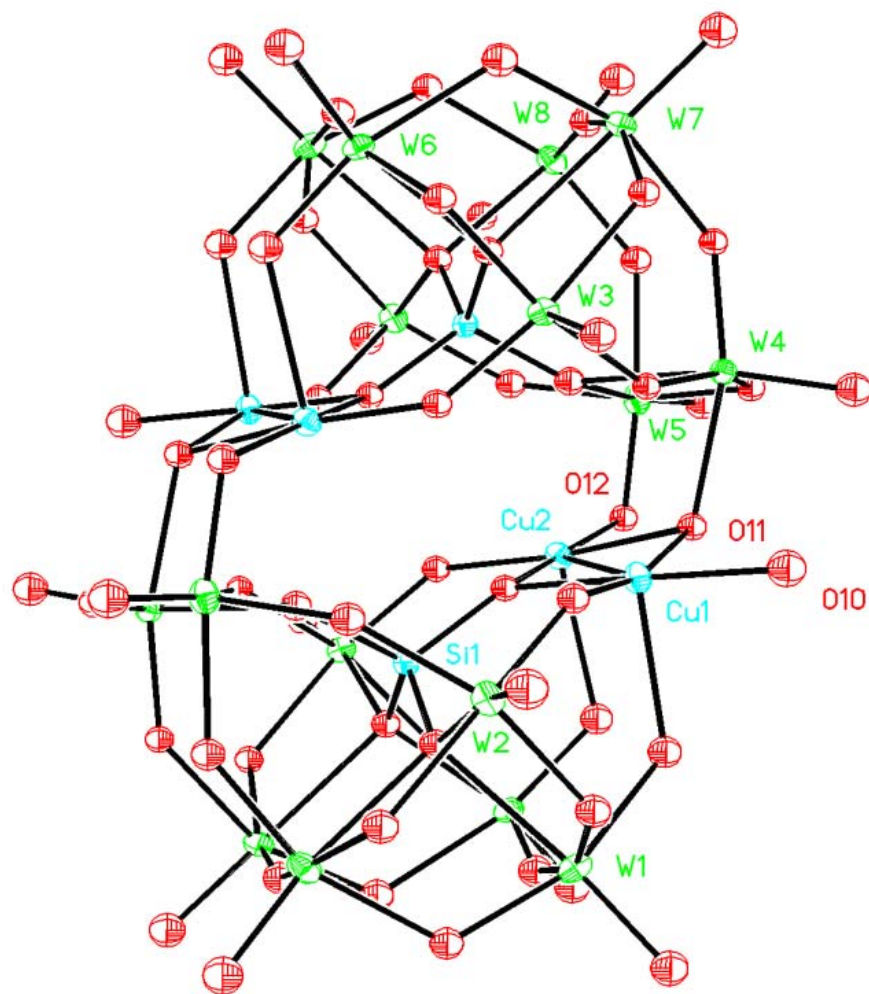


**Figure 4-1.** Ball and stick representation of  $[\gamma\text{-Cu}_2(\text{H}_2\text{O})\text{SiW}_8\text{O}_{31}]_2^{12-}$  (**1a**, the polyanion of **1**) showing 50% probability ellipsoids and selected atomic labels.

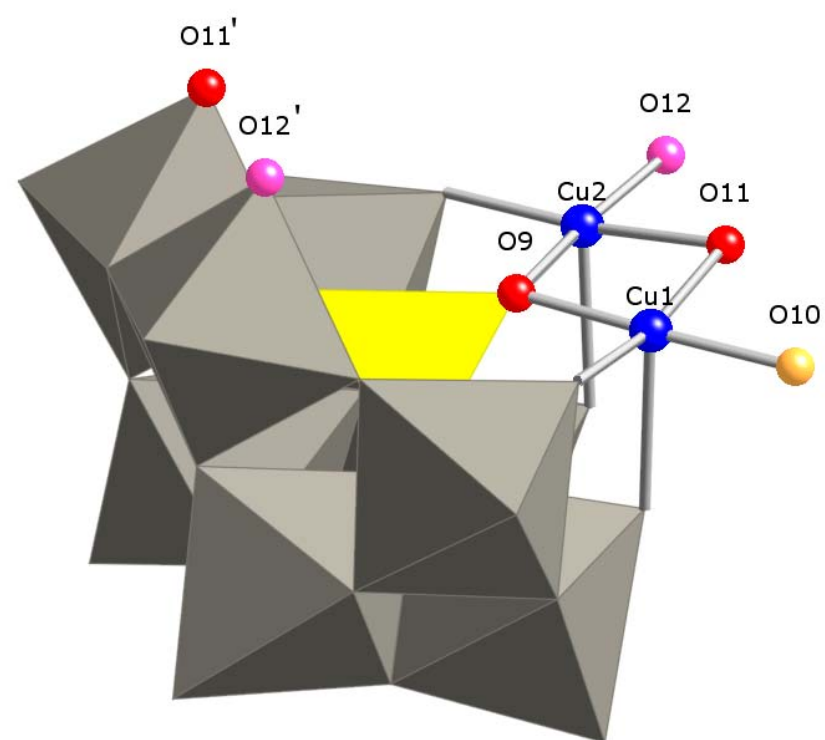


**Figure 4-2.** A combination polyhedral/ball-and-stick representation of the  $[\gamma\text{-Cu}_2(\text{H}_2\text{O})\text{SiW}_8\text{O}_{31}]^{6-}$  subunit of **1**.

## Magnetic properties

The temperature dependence of the low-field susceptibility data (Figure 4-3) reflects moderately strong ferromagnetic (FM) superexchange between the  $s = 1/2$  Cu(II) centers within the  $[\gamma\text{-Cu}_2(\text{H}_2\text{O})\text{SiW}_8\text{O}_{31}]^{6-}$  subunits and (weaker) antiferromagnetic (AFM) exchange between these subunits, causing a characteristic maximum in  $\chi T$  vs.  $T$  plots. Interestingly, similar competing AFM/FM intramolecular exchange has been observed for other Cu(II) and Co(II)-functionalized POMs.<sup>37, 39, 45, 48, 64</sup> The intra-subunit coupling ( $J_1$ ) is mediated via two  $\mu_3$ -oxo groups (O9 and O11), whereby the nearly planar  $\text{Cu}_2\text{O}_2$  motif coincides with the equatorial coordination plane of the Jahn-Teller-distorted Cu(II) centers, maximizing interactions between the single occupied Cu(3d)  $d_{x^2-y^2}$  orbitals (Cu1...Cu2: 2.9651(16) Å). Based on empirical correlation studies of oxo-bridged Cu(II) dimer compounds, the particular geometry of the  $\text{Cu}_2(\mu\text{-O})_2$  fragments, i.e. the angles and bond distances of the Cu-O-Cu bridges (Figure 4-4), are expected to cause FM intra-subunit exchange.<sup>65-68</sup> On the other hand, several exchange pathways of the type O-Si-O and O-W-O exist for the inter-subunit coupling ( $J_2$ ) over rather wide distances (Cu1...Cu1': 6.312 Å, Cu1...Cu2': 4.593 Å). Such scenarios have are known to cause weak AFM exchange as each pathway involves a coordination mode to one apical oxo position of the Jahn-Teller-distorted  $\text{CuO}_6$  environment (Figure 4-4), thereby minimizing overlap between the relevant magnetic Cu(3d) orbitals. To establish exact exchange parameters, a least-squares fitting procedure was adopted that linked the susceptibility to the isotropic Heisenberg-type model Hamiltonian:  $H$

$= -J_1[S(\text{Cu1})S(\text{Cu2}) + S(\text{Cu1}')S(\text{Cu2}')] - J_2[S(\text{Cu1})S(\text{Cu2}') + S(\text{Cu1})S(\text{Cu1}') + S(\text{Cu2})S(\text{Cu1}') + S(\text{Cu2})S(\text{Cu2}')].$

A uniform Jahn-Teller effect for all four Cu(II) sites was taken into account by using typical axial and equatorial  $g$  elements ( $g_z = 2.25$ ,  $g_{xy} = 2.02$ ); a fraction of uncoupled Cu(II) sites resulting in a paramagnetic background was treated as additional parameter (see Experimental section). The experimental data are well reproduced by an intra-subunit coupling parameter  $J_1/k_B = 53.2$  K and an inter-subunit coupling parameter  $J_2/k_B = -1.0$  K (Figure 4-3). These results therefore confirm the afore-mentioned expected trends and predict a singlet ( $S = 0$ ) ground state for **1**.

**Table 4-2.** Select bond distance (Å) and bond angles (°) for **1**

|             |          |            |            |
|-------------|----------|------------|------------|
| Cu1-O11     | 2.023(6) | Cu2-O9     | 1.926(6)   |
| Cu2-O11     | 2.035(6) | Cu1-Cu2    | 2.9651(16) |
| Cu1-O9      | 1.957(6) | Cu1-O10    | 1.972(7)   |
| Cu1-O11-Cu2 | 99.6(3)  | Cu1-O9-Cu2 | 93.9(3)    |

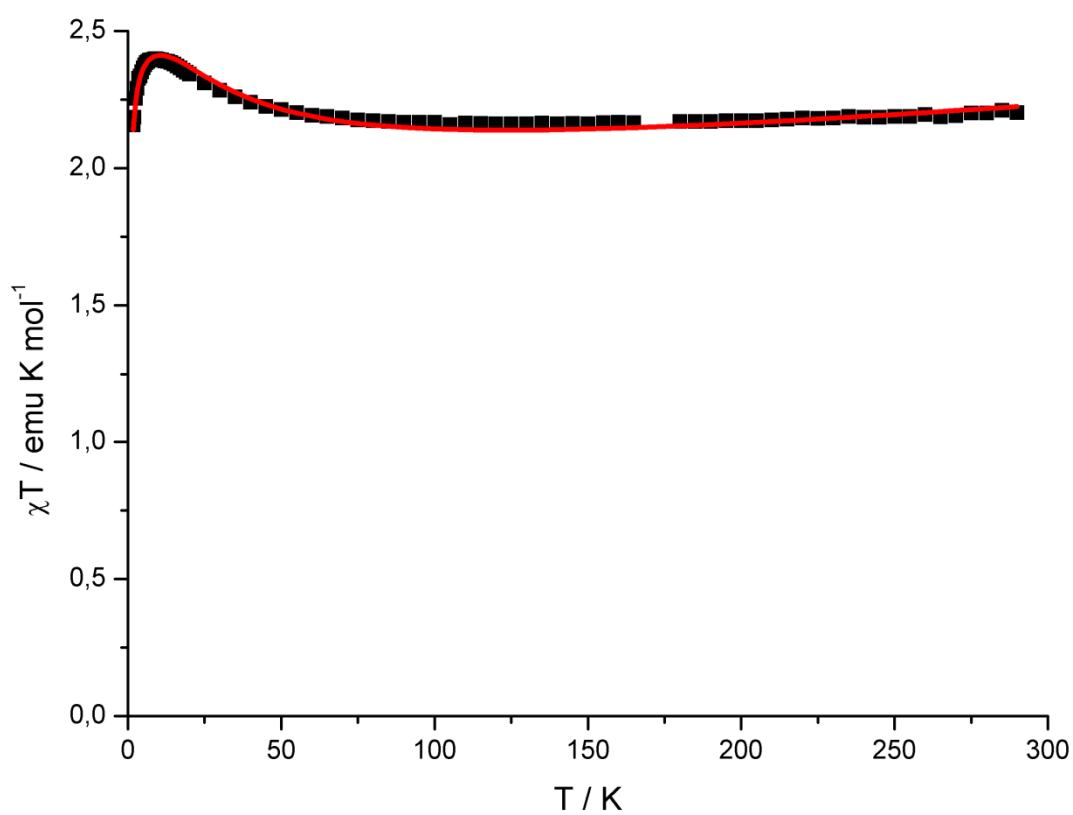


**Figure 4-3.** Temperature dependence of  $\chi T$  at 0.1 Tesla for **1** featuring a maximum at approx. 10 K due to competing FM/AFM exchange coupling. Black squares: experimental data; Solid line: best fit to model Hamiltonian (see text).

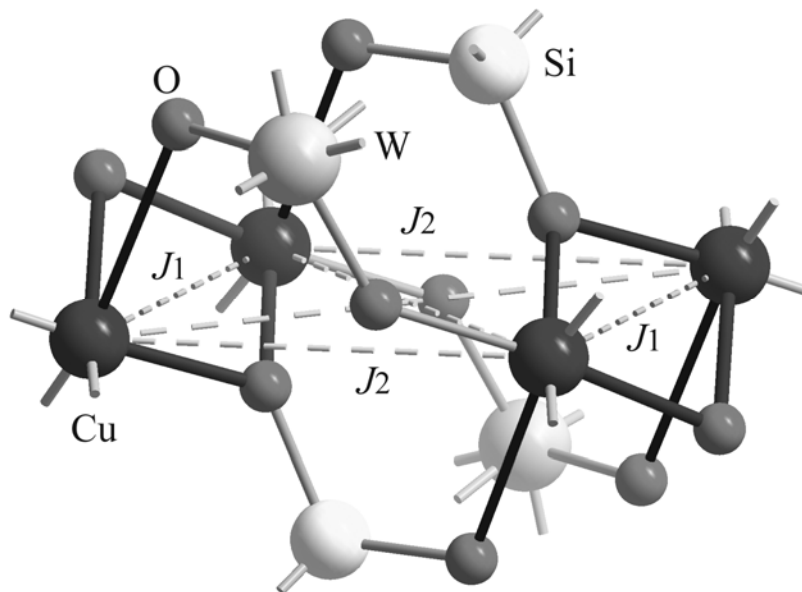


**Figure 4-4.** The central fragment of the  $\{\text{Cu}_4\text{W}_{16}\}$  cluster anion emphasizing the superexchange pathways between the  $s = 1/2$  Cu(II) centers (Cu: dark gray spheres, O: small gray spheres, Si: white spheres, W: light grey spheres). FM  $J_1$  exchange (represented by short dashed lines) is mediated by  $\mu$ -O bridges with Cu-O bond distances of 1.93 – 2.04 Å (dark grey bonds) and Cu-O-Cu bond angles of 93.9° and 99.6°. Weak AFM coupling ( $J_2$ , long dashed lines) between the FM coupled  $\text{Cu}_2$  dimers proceeds through O-Si-O and O-W-O groups (light grey bonds) that, in all cases, involves one Jahn-Teller elongated Cu-O bond (thin black).

## Acknowledgments

We thank TDA Research Corporation (W911NF-04-C-0136) and the U.S. Army Research Office (W911NF-05-1-0200) for funding this work.

## References

- (1) Pope, M. T., *Heteropoly and Isopoly Oxometalates*. Springer-Verlag: Berlin, 1983; p 180.
- (2) Hill, C. L.; Prosser-McCartha, C. M., *Coord. Chem. Rev.* **1995**, *143*, 407-455.
- (3) Hill, C. L., *Chem. Rev.* **1998**, *98*, 1-2.
- (4) Kozik, M.; Baker, L. C. W., *J. Am. Chem. Soc.* **1990**, *112*, 7604-7611.
- (5) Kozik, M.; Baker, L. C. W., Blue Electron Distributions in Diamagnetic Reduced Heteropolytungstates. Insights Concerning Conduction Pathways and Spin Coupling Patterns. <sup>183</sup>W NMR Chemical Shift Calculations. In *Polyoxometalates: From Platonic Solids to Anti-retroviral Activity*, Pope, M. T.; Müller, A., Eds. Kluwer Academic Publishers: Dordrecht, 1994; pp 191-202.
- (6) Weinstock, I. A., *Chem. Rev.* **1998**, *98*, 113-170.
- (7) Grigoriev, V. A.; Hill, C. L.; Weinstock, I. A., *J. Am. Chem. Soc.* **2000**, *122*, 3544-45.
- (8) Grigoriev, V. A.; Cheng, D.; Hill, C. L.; Weinstock, I. A., *J. Am. Chem. Soc.* **2001**, *123*, 5292-5307.
- (9) Kirby, J. F.; Baker, L. C. W., *Inorg. Chem.* **1998**, *37*, 5537-5543.
- (10) Metelski, P. D.; Swaddle, T. W., *Inorg. Chem.* **1999**, *38*, 301-307.
- (11) Czap, A.; Neuman, N. I.; Swaddle, T. W., *Inorg. Chem.* **2006**, *45*, 9518-9530.

- (12) Pope, M. T.; Müller, A., *Polyoxometalates: From Platonic Solids to Anti-retroviral Activity*. Kluwer Academic Publishers: Dordrecht, Netherlands, 1993.
- (13) Yamase, T.; Fujita, H.; Fukushima, K., *Inorg. Chimica Acta* **1988**, *151*, 15-18.
- (14) Hill, C.; Weeks, M.; Hartnup, M.; Sommadossi, J.-P.; Schinazi, R., *Ann. N. Y. Acad. Sci.* **1990**, *616*, 528-529.
- (15) Hill, C.; Weeks, M.; Schinazi, R. F., *Journal of Medicinal Chemistry* **1990**, *33*, 2767-2772.
- (16) Rhule, J. T.; Hill, C. L.; Judd, D. A.; Schinazi, R. F., *Chem. Rev.* **1998**, *98*, 327-357.
- (17) Rhule, J. T.; Hill, C. L.; Zheng, Z.; Schinazi, R. F., Polyoxometalates and Fullerenes as Anti-HIV Agents. In *Topics in Biological Inorganic Chemistry*, Clarke, M. J.; Sadler, P. J., Eds. Springer-Verlag: Heidelberg, 1999; Vol. 2: Metallopharmaceuticals, pp 117-137.
- (18) Yamase, T., Antitumoral and Antiviral Polyoxometalates (Inorganic Discrete Polymers of Metal Oxide). In *Polymeric Materials Encyclopedia*, Salamone, J. C., Ed. CRC Press: Boca Raton, 1996; pp 365-373.
- (19) Okuhara, T.; Mizuno, N.; Misono, M., *Advances in Catalysis* **1996**, *41*, 113-252.
- (20) Mizuno, N.; Misono, M., *Chem. Rev.* **1998**, *98*, 199-218.
- (21) Kozhevnikov, I. V., *Chem. Rev.* **1998**, *98*, 171-198.
- (22) Neumann, R., *Prog. Inorg. Chem.* **1998**, *47*, 317-370.
- (23) Katsoulis, D. E., *Chem. Rev.* **1998**, *98*, 359-388.
- (24) Coronado, E.; Gómez-García, C. J., *Chem. Rev.* **1998**, *98*, 273-296.
- (25) Klemperer, W. G.; Wall, C. G., *Chem. Rev.* **1998**, *98*, 297-306.

- (26) Müller, A.; Das, S. K.; Kuhlmann, C.; Bögge, H.; Schmidtman, M.; Diemann, E.; Krickemeyer, E.; Hormes, J.; Modrow, H.; Schindler, M., *ChemComm* **2001**, 655-656.
- (27) Kamata, K.; Yonehara, K.; Sumida, Y.; Yamaguchi, K.; Hikichi, S.; Mizuno, N., *Science* **2003**, *300*, 964-966.
- (28) Nishiyama, Y.; Nakagawa, Y.; Mizuno, N., *Angew. Chem. Int. Ed.* **2001**, *40*, 3639-3641.
- (29) Botar, B.; Geletii, Y. V.; Kögerler, P.; Musaev, D. G.; Morokuma, K.; Weinstock, I. A.; Hill, C. L., *J. Am. Chem. Soc* **2006**, *128*, 11268-11277.
- (30) Canny, J.; Tézé, A.; Thouvenot, R.; Hervé, G., *Inorg. Chem.* **1986**, *25*, 2114-2119.
- (31) Canny, J. T., R.; Tézé, A.; Hervé, G.; Leparulo-Loftus, M.; Pope, M. T., *Inorg. Chem.* **1991**, *30*, 976-981.
- (32) Xin, F.; Pope, M. T., *Inorg. Chem.* **1996**, *35*, 5693-5695.
- (33) Xin, F.; Pope, M. T.; Long, G. J.; Russo, U., *Inorg. Chem.* **1996**, *35*, 1207-1213.
- (34) Wassermann, K.; Lunk, H.-J.; Palm, R.; Fuchs, J.; Steinfeldt, N.; Stosser, R.; Pope, M. T., *Inorg. Chem.* **1996**, *35*, 3273-3279.
- (35) Kortz, U.; Isber, S.; Dickman, M. H.; Ravot, D., *Inorg. Chem.* **2000**, *39*, 2915-2922.
- (36) Kortz, U.; Matta, S., *Inorg. Chem.* **2001**, *40*, 815-817.
- (37) Bassil, B. S.; Kortz, U.; Tigan, A. S.; Clemente-Juan, J. M.; Keita, B.; Oliveira, P. d.; Nadjjo, L., *Inorg. Chem.* **2005**, *44*, 9360-9368.

- (38) Botar, B.; Geletii, Y. V.; Kögerler, P.; Musaev, D., G.; Morokuma, K.; Weinstock, I. A.; Hill, C. L., *J. Chem. Soc., Dalton Trans.* **2005**, *11*, 2017-2021.
- (39) Mialane, P.; Dolbecq, A.; Marrot, J.; Rivière, E.; Sécheresse, F., *Chemistry - A European Journal* **2005**, *11*, 1771-1778.
- (40) Bassil, B. S.; Dickman, M. H.; Kortz, U., *Inorg. Chem.* **2006**, *45*, 2394-2396.
- (41) Bassil, B. S.; Dickman, M. H.; Reicke, M.; Kortz, U.; Keita, B.; Nadjo, L., *J. Chem. Soc., Dalton Trans.* **2006**, 4253-4259.
- (42) Zhang, Z.; Li, Y.; Wang, E.; Wang, X.; Qin, C.; An, H., *Inorg. Chem.* **2006**, *45*, 4313-4315.
- (43) Zhang, X.; O'Connor, C. J.; Jameson, G. B.; Pope, M. T., *Inorg. Chem.* **1996**, *35*, 30-34.
- (44) Nozaki, C.; Kiyoto, K.; Minai, Y.; Misono, M.; Mizuno, M., *Inorg. Chem.* **1999**, *38*, 5724-5729.
- (45) Bassil, B. S.; Nellutla, S.; Kortz, U.; Stowe, A. C.; Tol, J. v.; Dalal, N. S.; Keita, B.; Nadjo, L., *Inorg. Chem.* **2005**, *44*, 2659-2665.
- (46) Goto, Y.; Kamata, K.; Yamaguchi, K.; Uehara, K.; Hikichi, S.; Mizuno, N., *Inorg. Chem.* **2006**, *45*, 2347-2356.
- (47) Sadakane, M.; Tsukuma, D.; Dickman, M. H.; Bassil, B.; Kortz, U.; Higashijima, M.; Ueda, W., *J. Chem. Soc., Dalton Trans.* **2006**, 4271-4276.
- (48) Mialane, P.; Duboc, C.; Marrot, J.; Rivière, E.; Dolbecq, A.; Sécheresse, F., *Chemistry - A European Journal* **2006**, *12*, 1950.
- (49) Kortz, U.; Jeannin, Y. P.; Tézé, A.; Hervé, G.; Isber, S., *Inorg. Chem.* **1999**, *38*, 3670-3675.

- (50) Lisnard, L.; Mialane, P.; Dolbecq, A.; Marrot, J.; Clemente-Juan, J. M.; Coronado, E.; Keita, B.; Oliveira, P. d.; Nadjo, L.; Sécheresse, F., *Chemistry - A European Journal* **2007**, *13*, 3525.
- (51) Anderson, T. M.; Hardcastle, K. I.; Okun, N.; Hill, C. L., *Inorg. Chem.* **2001**, *40*, 6418-6425.
- (52) Okun, N. M.; Anderson, T. M.; Hardcastle, K. I.; Hill, C. L., *Inorg. Chem.* **2003**, *42*, 6610-6612.
- (53) Okun, N. M.; Anderson, T. M.; Hill, C. L., *J. Am. Chem. Soc.* **2003**, *125*, 3194-3195.
- (54) Okun, N. M.; Anderson, T. M.; Hill, C. L., *J. Mol. Catal. A: Chem.* **2003**, *197*, 283-290.
- (55) Okun, N. M.; Ritorto, M. D.; Anderson, T. M.; Apkarian, R. P.; Hill, C. L., *Chem Mater.* **2004**, *16*, 2551-2558.
- (56) Okun, N. M.; Tarr, J. C.; Hillesheim, D. A.; Zhang, L.; Hardcastle, K. I.; Hill, C. L., *J. Mol. Catal. A: Chem.* **2006**, *246*, 11-17.
- (57) Tézé, A.; Hervé, G., In *Inorganic Syntheses*, Ginsberg, A. P., Ed. Joh Wiley and Sons: New York, 1990; Vol. 27, pp 88-89.
- (58) *SMART*, 5-55; Bruker AXS, Inc.: Madison, 2000.
- (59) *SAINT*, 6.02; Bruker AXS, Inc.: Madison, 1999.
- (60) Mialane, P.; Dolbecq, A.; Rivière, E.; Marrot, J.; Sécheresse, F., *Angew. Chem. Int. Ed.* **2004**, *43*, 2274-2277.
- (61) Finke, R. G.; Droege, M. W.; Domaille, P. J., *Inorg. Chem.* **1987**, *26*, 3886-3896.

- (62) Anderson, T. M.; Zhang, X.; Hardcastle, K. I.; Hill, C. L., *Inorg. Chem.* **2002**, *41*, 2477-2488.
- (63) Brown, I. D.; Altermatt, D., *Acta Cryst.* **1985**, *B41*, 244-247.
- (64) Kögerler, P.; Müller, A., *J. Appl. Phys.* **2003**, *93*, 7101-7103.
- (65) Chiari, B. H., J. H.; Piovesana, O.; Tarantelli, T.; Sanáis, P. F., *Inorg. Chem.* **1986**, *25*, 2408-213.
- (66) Melnik, M., *Coord. Chem. Rev.* **1982**, *42*, 259-293.
- (67) Kahn, O., *Angew. Chem., Int. Ed. Engl.* **1985**, *24*, 834-850.
- (68) Kato, M. M., Y. , *Coord. Chem. Rev.* **1988**, 45-83.

## *Chapter 5*

Multi-Copper Polyoxoanions. 2. Synthesis,  
Characterization, X-ray Crystal Structure  
and Magnetism of a One-dimensional  
Silicotungstate Array:  $\text{K}_3\text{H}_4\text{Cu}_{0.5}$



with Paul Kögerler, Rui Cao, and Craig L. Hill

(published partially in *Polyhedron* **2009**, *28*, 215-220)

## Abstract

A structurally distinct, multi-copper(II)-substituted silicotungstate  $\text{K}_3\text{H}_4\text{Cu}_{0.5}\{\text{Cu}[\text{Cu}_{7.5}\text{Si}_2\text{W}_{16}\text{O}_{60}(\text{H}_2\text{O})_4(\text{OH})_4]_2\}\cdot 9\text{H}_2\text{O}$  (**2**) has been synthesized and characterized by FT-IR, elemental analysis, variable-temperature magnetic measurements, electron spin resonance, and X-ray diffraction. Green crystalline plates of **2** were obtained by the reaction of  $\text{K}_8[\gamma\text{-SiW}_{10}\text{O}_{36}]\cdot 12\text{H}_2\text{O}$  with 8 equivalents of Cu(II) in a 50% ethylene glycol solution. The structure of **2** was determined by low-temperature single-crystal X-ray diffraction: monoclinic,  $C2/c$ ,  $Z = 4$ ,  $a = 27.268(8)$  Å,  $b = 22.895(6)$  Å,  $c = 33.304(9)$  Å,  $\beta = 111.070(9)^\circ$  and  $R_1 = 9.79\%$  based on 13924 independent reflections. A cationic copper center connects the terminal oxygen atoms of neighboring polyanions, resulting in a one-dimensional structure. Magnetic susceptibility measurements indicate weak ferromagnetic superexchange between the Jahn-Teller-distorted  $s = 1/2$  Cu(II) centers.

## Introduction

Polyoxometalates (POMs) substituted with one or more d-electron metal centers constitute a large class of electronically highly tunable and structurally robust multinuclear compounds<sup>1-3</sup> with applications in catalysis<sup>2, 4-11</sup> and potential applications in electroactive materials<sup>12-14</sup>, magnetism<sup>15-20</sup>, medicine (diagnostics or therapeutics)<sup>21-27</sup>, and other fields. The incorporation of transition metals into lacunary POM precursors is generally simple and straightforward; however, the exact mechanisms by which metal-substituted

POMs are formed are complex and not well understood. Most frequently, the d-electron metals fill the vacant positions of the lacunary POM forming a saturated (or plenary) structure. Complicating plenary structure reconstitution is the fact that multi-vacant (di-lacunary or tri-lacunary) POM precursors can isomerize under different synthetic conditions, leading to a range of metal-substituted structures. The di-vacant silicotungstate,  $[\gamma\text{-SiW}_{10}\text{O}_{36}]^{8-}$ , readily isomerizes to  $\alpha$  and  $\beta$  structures in aqueous solution<sup>28-30</sup>, and these processes result in the formation of a diverse set POM structures<sup>31-42</sup> upon reaction with transition metals.

Several research groups have investigated the reactions of  $[\gamma\text{-SiW}_{10}\text{O}_{36}]^{8-}$  with first-row transition metal salts<sup>31-48</sup>. Early work to prepare disubstituted  $\{\gamma\text{-M}_2\text{SiW}_{10}\}$  ( $M = \text{V}, \text{Cr}, \text{Mn}$ ), where the  $\gamma$ -isomer polyoxoanion structure is retained, was performed by Pope and co-workers<sup>32, 33, 44</sup>. These di-metal substituted structures contain the two d metals in adjacent positions as either “in-pocket” or “out-of-pocket” isomers. The in-pocket isomers contain bonds between the central heteroatom oxygens and the incorporated d-electron centers. In contrast, the out-of-pocket isomers do not contain this bond, and consequently the d-electron metals are displaced from the center of the polyanion and frequently multiply bonded to other adjacent polyanions or distinct structural units. Subsequently  $\{\gamma\text{-M}_x\text{SiW}_{10}\}$  structures were reported by the research groups of Mizuno<sup>43, 45, 46</sup>, Mialane<sup>39</sup>, Peng<sup>47</sup>, and others. By slightly changing the synthetic conditions, Kortz and co-workers<sup>36</sup> prepared a series of sandwich dimers,  $[\beta\text{-(M}_2\text{SiW}_9\text{O}_{34})_2]^{(2n+4)-}$  ( $M = \text{Mn}, \text{Cr}, \text{Zn}$ ). Further investigation of the

reactions of d-electron-metals with  $[\gamma\text{-SiW}_{10}\text{O}_{36}]^{8-}$  by this group afforded several other d-electron-metal-substituted silicotungstates<sup>37, 38, 40, 41, 48, 49</sup>. Meanwhile, Mialane and co-workers<sup>39, 50, 51</sup> reported several different metal-substituted silicotungstates with complicated structures by adding azide and/or other ligands to the reaction system. Peng, Wang and co-workers<sup>47</sup> described dimers,  $[\{\text{K}(\text{H}_2\text{O})\}_2\{(\mu_3\text{-H}_2\text{O})\text{M}(\text{H}_2\text{O})\}(\gamma\text{-Si}_2\text{W}_{20}\text{O}_{70})]^{8-}$  (M =  $\text{Mn}^{2+}$ ,  $\text{Co}^{2+}$ , and  $\text{Ni}^{2+}$ ), prepared in acidic aqueous solution, that retain the  $\{\gamma\text{-SiW}_{10}\}$  unit of the precursor.

Recently, we obtained a di-copper substituted dimeric silicotungstate complex,  $\text{K}_9\text{Na}_2\text{Cu}_{0.5}[\gamma\text{-Cu}_2(\text{H}_2\text{O})\text{SiW}_8\text{O}_{31}]_2 \cdot 38\text{H}_2\text{O}$  from the reaction of a copper(II) salt with  $\text{K}_8[\gamma\text{-SiW}_{10}\text{O}_{36}] \cdot 12\text{H}_2\text{O}$  in a acetate-buffered 50% ethylene glycol solution<sup>52</sup>. This copper substituted silicotungstate cluster contains two pseudo-planar  $\text{Cu}_2\text{O}_2$  motifs, and strong ferromagnetic superexchange between the  $S = 1/2$  Cu(II) centers was observed. Simultaneously, Peng and co-workers obtained a similar complex via a different synthetic approach<sup>56</sup>. We report here that reaction of  $[\gamma\text{-SiW}_{10}\text{O}_{36}]^{8-}$  and  $\text{Cu}(\text{NO}_3)_2$  in unbuffered aqueous solution followed by crystallization out of water:ethylene glycol (1:1) produces a one-dimensional polymeric structure comprising  $\{\text{Cu}_{16}\text{Si}_4\text{W}_{32}\}$  polyanions interlinked by additional individual Cu(II) centers,  $\text{K}_3\text{H}_4\text{Cu}_{0.5}\{\text{Cu}[\text{Cu}_{7.5}\text{Si}_2\text{W}_{16}\text{O}_{60}(\text{H}_2\text{O})_4(\text{OH})_4]_2\} \cdot 9\text{H}_2\text{O}$  (**2**). Magnetic susceptibility and ESR measurements of **2** show that this multi-copper substituted silicotungstate exhibits more complicated magnetic properties. As we were reporting our work, Su, Xu and co-workers<sup>53</sup> reported a similar multi-copper polyanion,  $\text{Na}_{16}[\text{Cu}_{14}(\text{OH})_4(\text{H}_2\text{O})_{16}]$

(SiW<sub>8</sub>O<sub>31</sub>)<sub>4</sub>·20.5H<sub>2</sub>O, but in this work the structure entails discrete polyanion units, and no magnetic data were reported. Herein, we describe the synthesis, structure, and magnetic properties of **2**.

## Experimental Section

### *General Methods and Materials*

K<sub>8</sub>[ $\gamma$ -SiW<sub>10</sub>O<sub>36</sub>]·12H<sub>2</sub>O was prepared according to literature procedure<sup>30</sup> and the purity was checked by infrared spectroscopy. Copper nitrate, acetonitrile and ethylene glycol were obtained from Aldrich and used without further purification. Elemental analyses for K, Cu, Si and W were performed by Galbraith Laboratories (Knoxville, Tennessee). The infrared spectrum (2 weight % sample in KBr pellet) was recorded on a Nicolet 6700 FT-IR spectrometer. Thermogravimetric data were collected on an ISI TGA 1000 instrument. ESR measurements were performed on a powder sample at 290 K using a Magnettech Miniscope MS-100 spectrometer and DPPH as an external standard. Magnetic susceptibility measurements were performed at 0.1 to 5.0 Tesla for  $T = 1.8 - 290$  K using a Quantum Design MPMS-5S SQUID magnetometer. Experimental susceptibility data were corrected for diamagnetic and (significant) temperature-independent paramagnetic contributions that were determined from measurements on a range of diamagnetic  $\gamma$ -Keggin polyoxotungstate compounds ( $\chi_{\text{dia/TIP}}(\mathbf{2}) = -1.10 \times 10^{-3}$  emu/mol). Field-dependent magnetization studies at 1.8 K reveal the presence of a fraction of mononuclear Cu(II) (0.5 per mol).

**Table 5-1.** Crystallographic Data and Structure Refinement for **2**

| <b>2</b>                            |   |
|-------------------------------------|---|
| empirical formula                   | $\text{Cu}_{16.5}\text{H}_{46}\text{K}_3\text{O}_{145}\text{Si}_4\text{W}_{32}$           |
| formula weight                      | 9527.6 g mol <sup>-1</sup>  |
| temperature                         | 173(2)K   |
| wavelength                          | 0.71073 Å   |
| crystal system                      | monoclinic  |
| space group                         | <i>C2/c</i> (#15)   |
| unit cell                           | $a = 27.268(8)$ Å<br>$b = 22.895(6)$ Å<br>$c = 33.304(9)$ Å<br>$\beta = 111.070(9)^\circ$ |
| volume                              | 19402(9) Å <sup>3</sup>   |
| <i>Z</i>                            | 4   |
| density (calcd)                     | 3.350 g cm <sup>-3</sup>  |
| abs. coeff                          | 20.778 mm <sup>-1</sup>   |
| GOF                                 | 1.034   |
| final $R_1^a$ [ $I > 2\sigma(I)$ ]  | 0.0979  |
| final $wR_2^b$ [ $I > 2\sigma(I)$ ] | 0.2524  |

$$^a R_1 = \Sigma ||F_o| - |F_c|| / \Sigma |F_o|; ^b wR_2 = \Sigma [w(F_o^2 - F_c^2)^2] / \Sigma [w(F_o^2)^2]^{1/2}$$

*Synthesis of  $K_3H_4Cu_{0.5}\{Cu[Cu_{7.5}Si_2W_{16}O_{60}(H_2O)_4(OH)_4]_2\}\cdot 9(H_2O)$  (**2**)*

A 5 mL aliquot of acetonitrile solution containing 0.5 g (2.66 mmol) of  $Cu(NO_3)_2$  was dissolved in 20 mL of deionized water. To this solution 1.0 g (0.33 mmol) of  $K_8[\gamma-SiW_{10}O_{36}]\cdot 12H_2O$  was added with stirring. After stirring for 20 minutes, the undissolved residues were removed from the solution by a medium frit and the filtrate (25 mL) was collected. A 5 mL portion of the filtrate was transferred to a 15 mL vial and 5 mL of ethylene glycol was added. The mixture was stirred for an additional 5 minutes and then placed into a dark cabinet. Green plate-like diffraction quality crystals of **2** grew from this 1:1 water: ethylene glycol mixed solution after two weeks (0.12 g, yield 14.4%). IR (2% KBr pellet, 1200-400  $cm^{-1}$ ): 1082 (w), 1039 (w), 990 (w, sh), 950 (m), 878 (s, sh), 787 (w), 736 (s), 696 (w), and 519 (w, sh), 491 (w). Elemental composition calcd. for  $K_3H_4Cu_{0.5}\{Cu[Cu_{7.5}Si_2W_{16}O_{60}(H_2O)_4(OH)_4]_2\}\cdot 9H_2O$ : Cu, 11.00; K, 1.23; Si, 1.18; W, 61.75; found: Cu, 11.9; K, 1.07; Si, 1.22; W, 58.2. [MW = 9527.6 g/mol].

*X-ray Crystallography of **2***

A green plate crystal of **2** with dimensions of 0.19 x 0.17 x 0.04  $mm^3$  coated in Paratone-N oil was mounted on a small fiber loop for index and intensity data collection. The data were collected at 30 K under a helium stream on a Bruker-AXS SMART 1000 CCD single-crystal diffractometer using Mo  $K_\alpha$  (0.71073 Å) radiation. Indexing, and initial cell refinements of the collected data were performed by the SMART<sup>54</sup> software. The frame integration and final cell refinements were carried out by using the SAINT<sup>55</sup> software. The final cell parameters were determined from the least-squares refinement of 79664

reflections. From these unique reflections ( $2\theta_{\max} = 46.52^\circ$ ), 13924 reflections ( $R_{\text{int}} = 0.2197$ ) were considered to be observed. The structure was determined through direct methods (SHELXS97) via locating the tungsten atoms and difference Fourier maps (SHELXL97). The hydrogen atoms of the water molecules were not located in the difference Fourier maps. The final cycle of refinement resulted at  $R = 0.0979$  and  $R_w = 0.1513$  ( $I > 2\sigma(I)$ ) (Table 5-1). In the final difference map, a residual electron density maximum of  $3.954 \text{ e } \text{\AA}^{-3}$  and a minimum of  $-3.304 \text{ e } \text{\AA}^{-3}$  were observed.

## Results and Discussion

### *Synthesis*

The potassium salt of **2** was prepared by mixing 8:1 mole ratio of  $\text{Cu}(\text{NO}_3)_2$  and  $\text{K}_8[\gamma\text{-SiW}_{10}\text{O}_{36}] \cdot 12\text{H}_2\text{O}$  in a 1:1 water-ethylene glycol solution. Green crystalline plates of **2** were obtained after weeks in *ca.* 14% yield. If the same synthetic procedure is followed but without the addition of ethylene glycol, small green needle-like crystals appear after several hours in significantly higher yield (c.a. 46%). The FT-IR spectrum of these needles are very similar to that of **2** except that there is an absence of two peaks at  $1082$  and  $1039 \text{ cm}^{-1}$ , which are attributed to the C-O stretch of ethylene glycol. Unfortunately, the needles diffracted X-rays poorly providing commensurately low quality datasets. Complex **2** was synthesized in an acidic environment ( $\text{pH} = 4.2$ ) without buffer and the blue needle-like crystals were obtained when HOAc/NaOAc buffer was used to maintain the same pH value. X-ray diffraction established that the blue

crystals are a dimeric silicotungstate which contains a  $\{\gamma\text{-Cu}_2(\text{H}_2\text{O})\text{SiW}_8\text{O}_{31}\}$  motif in each subunit. Both **2** and the dimeric POM contain the tetra-vacant  $\{\text{B-}\beta\text{-SiW}_8\text{O}_{31}\}$  fragment in their structures. The appearance of this  $\{\text{B-}\beta\text{-SiW}_8\text{O}_{31}\}$  fragment in both multi-copper-containing POM products may indicate that  $\text{Cu}^{2+}$  ions facilitate conversion of the di-vacant  $[\gamma\text{-SiW}_{10}\text{O}_{36}]^{8-}$  into  $\{\text{B-}\beta\text{-SiW}_8\text{O}_{31}\}$  *in situ* and/or stabilize the latter unit via coordination. It is reasonable that the excess acetate from the buffer and the polytungstate intermediates compete to coordinate to the hydrated  $\text{Cu}^{2+}$  ions, and this competition leads to the formation of the recently reported dimeric cluster<sup>52, 56</sup> which contains fewer copper centers per polyanion.

Kortz and co-workers<sup>38, 48</sup> recently reported several POM structures that contain the  $\{\text{B-}\beta\text{-SiW}_8\text{O}_{31}\}$  unit in their study of the  $\text{Co(II)}/[\gamma\text{-SiW}_{10}\text{O}_{36}]^{8-}$  system, where a large excess  $\text{CoCl}_2$  was reacted with  $[\gamma\text{-SiW}_{10}\text{O}_{36}]^{8-}$  in aqueous solution buffered at  $\text{pH} = 5.5$  and heated to  $50\text{ }^\circ\text{C}$  for 30 min. This procedure resulted in the cobalt-substituted silicotungstate trimer  $[\{\text{Co}_9\text{Cl}_2(\text{OH})_3(\text{H}_2\text{O})_9(\beta\text{-SiW}_8\text{O}_{31})_3\}]^{5-}$  of  $D_{3h}$  symmetry. Each subunit of this trimer contains a  $\{\text{B-}\beta\text{-SiW}_8\text{O}_{31}\}$  unit, which coordinates with three cobalt atoms and forms a  $\{\text{M}_3\text{SiW}_8\}$  motif. By changing the  $\text{pH}$  to 4.8 and the molar ratio of  $\text{Co}:[\gamma\text{-SiW}_{10}\text{O}_{36}]^{8-}$  to 2:1, another cobalt-substituted silicotungstate,  $[\{\text{Co}_3(\text{B-}\beta\text{-SiW}_9\text{O}_{33}(\text{OH}))(\text{B-}\beta\text{-SiW}_8\text{O}_{29}(\text{OH})_2\}_2]^{22-}$ , was obtained which also contains the  $\{\text{M}_3\text{SiW}_8\}$  motif<sup>38, 48</sup>.

Mialane and co-workers<sup>39, 51, 57</sup> have investigated the reaction of transition metals and  $[\gamma\text{-SiW}_{10}\text{O}_{36}]^{8-}$  in the presence of azide and documented several instances where azide interacts with metal centers, resulting in the formation of

new POM structures. They obtained a copper-substituted trimer,  $[\{\text{SiW}_8\text{O}_{31}\text{Cu}_3(\text{OH})(\text{H}_2\text{O})_2(\text{N}_3)\}_3(\text{N}_3)]^{19-}$ , that is structurally analogous to the Co-substituted trimer obtained by Kortz and co-workers when an excess of azide was used. Their study of the  $\text{Co}/[\gamma\text{-SiW}_{10}\text{O}_{36}]^{8-}$  system afforded several different cobalt-substituted silicotungstates, including the dimer polyanion  $[\{(\text{B-}\beta\text{-SiW}_9\text{O}_{33})(\text{OH})(\beta\text{-SiW}_8\text{O}_{29}(\text{OH})_2)\text{Co}_3(\text{H}_2\text{O})\}_2\text{Co}(\text{H}_2\text{O})_2]^{20-}$ . Each subunit of this dimer contains a  $\{\text{B-}\beta\text{-SiW}_8\text{O}_{31}\}$  and a  $\{\text{B-}\beta\text{-SiW}_9\text{O}_{34}\}$  motif connected by three cobalt atoms, and the  $\{\text{B-}\beta\text{-SiW}_8\text{O}_{31}\}$  motif in each subunit is linked to another by a six-coordinated cobalt center. The general polyanion framework of this Co-substituted POM is similar to our sixteen-copper-containing polyanion, **2**. Very recently, Zhang et al.<sup>53</sup> reported a 14-copper-containing silicotungstate by reaction of 12 mole equivalents of a copper salt with  $[\gamma\text{-SiW}_{10}\text{O}_{36}]^{8-}$  in a pH 5.5 boiling aqueous solution containing D-proline for 2 hours. This  $\text{Cu}_{14}$  silicotungstate is structurally analogous to **2** but contains less copper since the polyanions are not linked by Cu centres into a one-dimensional material as it is the case in **2** (*vide infra*).

### *Structural features*

The new polymeric multi-copper-substituted silicotungstate, **2**, crystallizes in the monoclinic space group,  $C2/c$ . The polyanion unit contains two equivalent  $[\text{Cu}_7\text{Si}_2\text{W}_{16}\text{O}_{60}(\text{H}_2\text{O})_4(\text{OH})_4]^{6-}$  subunits related by a four-coordinate copper located on the  $C_2$  axis ( $C_2$  local symmetry; Figure 5-1). The inversion center is not located at this copper, but lies in the center of the unit cell. Each subunit contains two multi-copper substituted  $\{\text{B-}\beta\text{-SiW}_8\text{O}_{31}\}$  motifs (Figure 5-2). The

two motifs connect to each other via three five-coordinate copper atoms: Cu2, Cu3 and Cu4. O30 is a  $\mu_3$ -oxo bridging Cu3, Cu4 and Si1; O35 is a  $\mu_4$ -oxo bridging Cu2, Cu3, Cu4 and Si2. In the  $\{\text{B-}\beta\text{-SiW}_8\text{O}_{31}\}$  motif containing Si1, two of the copper atoms, Cu3 and Cu4, exist as a  $\{\text{Cu}_2\text{O}_6\}$  unit which resides in the position of the conventional  $\{\text{W}_2\text{O}_6\}$  group, thus forming a  $\{\gamma\text{-Cu}_2\text{SiW}_8\text{O}_{31}\}$  unit that maintains the  $\gamma$  isomerism of the  $[\gamma\text{-SiW}_{10}\text{O}_{36}]^{8-}$  precursor. Alternatively, the  $\{\text{B-}\beta\text{-SiW}_8\text{O}_{31}\}$  motif with Si2 contains these three copper atoms, Cu2, Cu3 and Cu4, as a  $\{\text{Cu}_3\text{O}_5\}$  unit that defines a  $\beta$ -Keggin structure,  $\{\beta\text{-Cu}_3\text{SiW}_9\text{O}_{34}\}$ . The remaining lacunary (vacant) position of the  $\{\beta\text{-Cu}_3\text{SiW}_9\text{O}_{34}\}$  motif is filled by Cu6. Two more copper atoms, Cu5 and Cu7, are also five coordinate each forming a pyramidal unit linked to Cu6. The three copper atoms linked via four  $\mu_3$ -oxo groups form a nearly planar  $\text{Cu}_3\text{O}_4$  motif. The pyramidal units share the terminal O1 and O7 with the  $\{\gamma\text{-Cu}_2\text{SiW}_8\text{O}_{31}\}$  motif located on the other subunit, thus connecting the  $\beta$  and  $\gamma$  motifs in different subunits to form the large cluster. Cu1, the only four-coordinate copper in the structure which is located on the  $C_2$  axis, fills the lacunary position opposite to Cu3 and Cu4 on each  $\gamma$  motif. In each subunit, a copper atom, Cu8, is bonded to three oxygens on the outside (away from the central multi-copper region) of the  $\gamma$  motif. One more cationic copper, Cu9, connects to the terminal oxygen of W15 and W15' located on two neighboring molecules thereby linking the clusters to form the one-dimensional array (Figure 5-3).

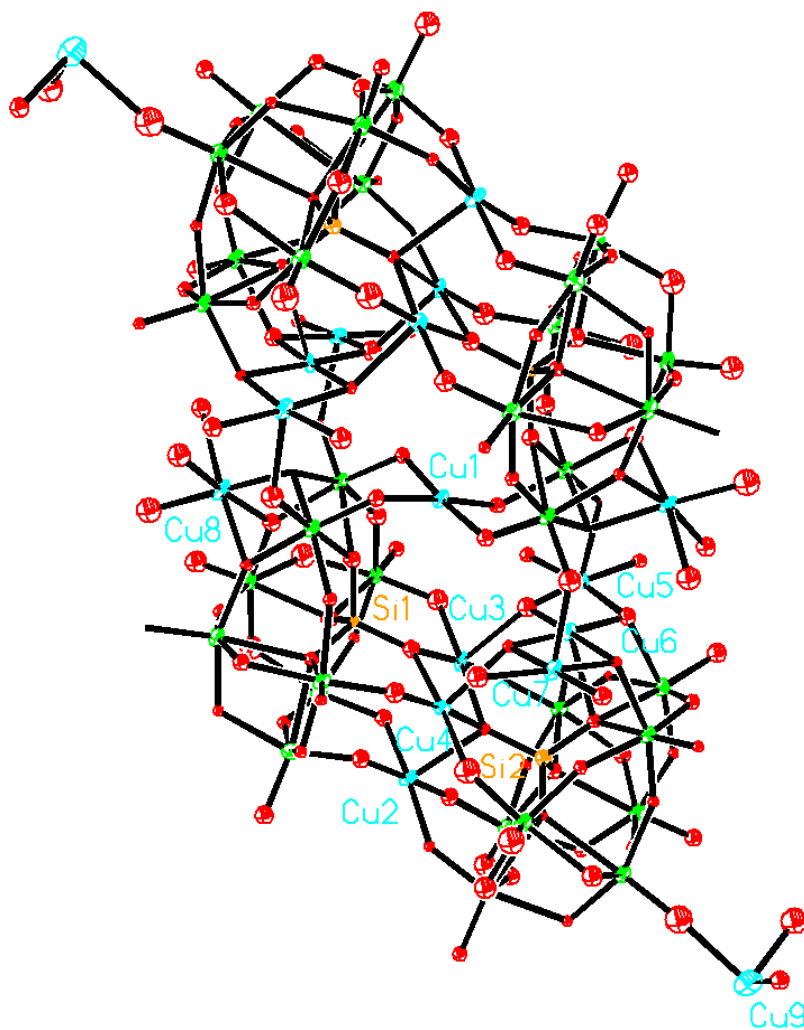


**Figure 5-1.** Ball and stick representation of  $[\text{Cu}\{\text{Cu}_{7.5}\text{Si}_2\text{W}_{16}\text{O}_{60}(\text{H}_2\text{O})_4(\text{OH})_4\}_2]^{8-}$  (**2a**, the polyanion of **2**) showing 50% probability ellipsoids and selected atomic labels. Cu: blue; O: red; Si: orange; W: green.

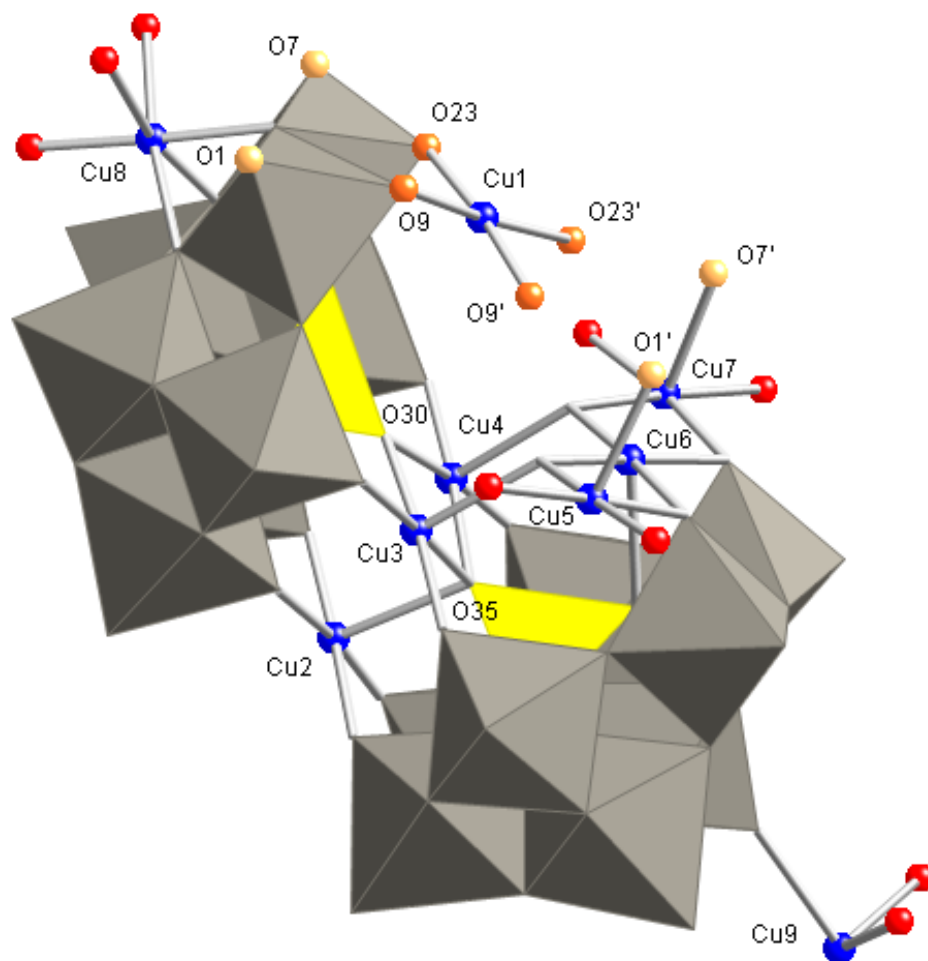


**Figure 5-2.** A combination polyhedral/ball-and-stick representation of the  $\{\text{Cu}_9\text{Si}_2\text{W}_{16}\text{O}_{60}(\text{H}_2\text{O})_4(\text{OH})_4\}$  subunit of **2**.

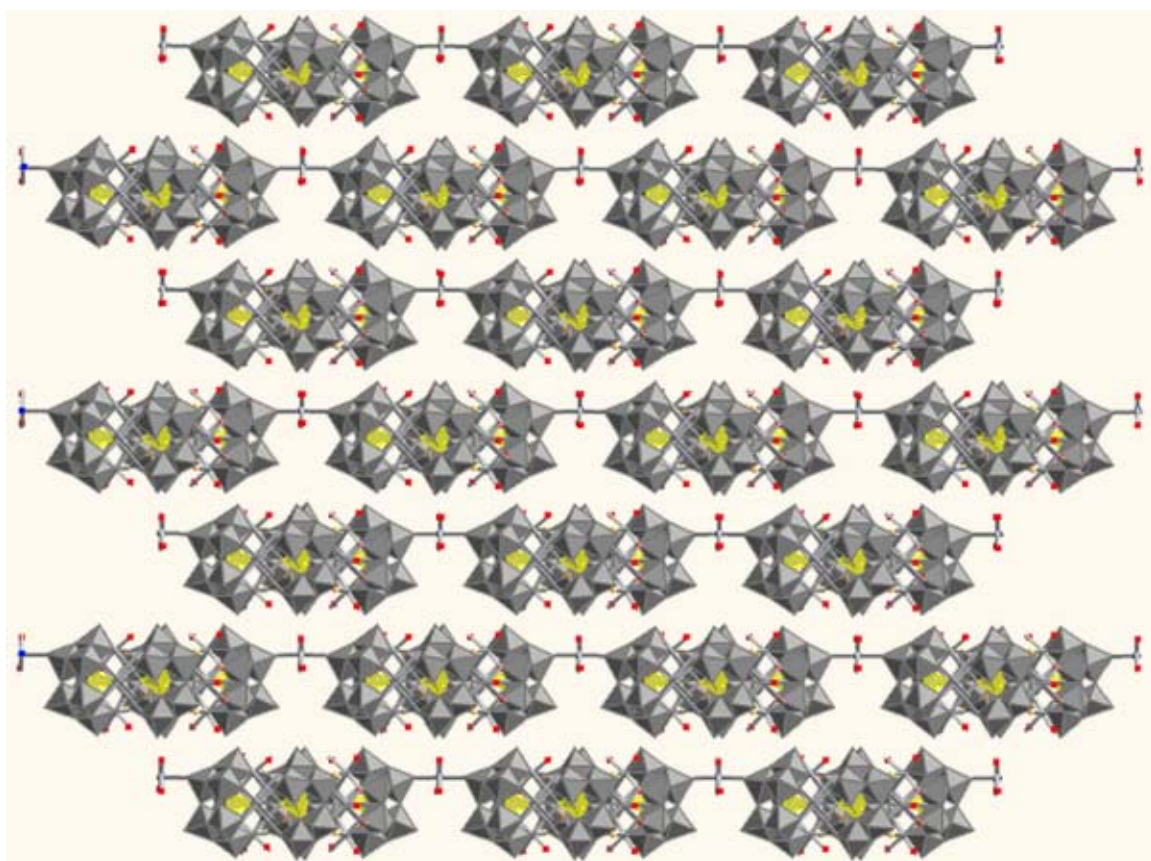


**Figure 5-3.** Structural view of the one-dimensional array of **2** from the *c* axis direction.

## Electron Spin Resonance

The X-band ESR spectrum of **2**, measured as a powder, displays an overlay of several different Cu(II) environments (Figure 5-4). However, the resulting convoluted response can be understood as an average of Jahn-Teller-distorted Cu(II) signals characterized by vertical and parallel  $g$  tensor components,  $g_{\perp} = (g_{xx} + g_{yy})/2$  and  $g_{\parallel} = g_{zz}$ , characteristic for Cu(II) centers in such distorted environments. From the average values  $g_{\perp} = 2.04$  and  $g_{\parallel} = 2.48$  an average isotropic value of  $g_{\text{iso}} = 2.19$  is derived. Note that limited solubility of **2** in polar and nonpolar solvents prevented recording of an ESR spectrum of **2** in solution of possibly significantly higher resolution.

### *Magnetic properties*

The low-field (0.1 Tesla) magnetism of compound **2** indicates dominating weak ferromagnetic intramolecular superexchange between the Jahn-Teller-distorted  $s = 1/2$  Cu(II) centers that are spaced apart less than 3 Å (Table 5-2). Note that ferromagnetic interactions of comparable strength are also observed in Cu(II)-substituted polyoxometalates such as  $\{\text{Mo}_{57}\text{Cu}_6\}$ -type clusters<sup>58</sup> in which the spin centers are bridged by O-Mo-O fragments and where the orthogonality of the magnetic Cu(3d) orbitals necessary for ferromagnetic exchange is achieved by rotation of their colinear local orbital coordinate frameworks by 60° around the local z axis, i.e. the elongated Jahn-Teller axis. Here, the coupling within a subunit (characterized by the exchange energy  $J_1$  between Cu3 and Cu4) is mediated via a  $\mu_3$ -oxo group (O30) and a  $\mu_4$ -oxo group (O35), whereby the Cu(II) centers form a nearly planar  $\text{Cu}_2\text{O}_2$  motif with oxo groups in the equatorial

coordination plane. The geometry of the  $\text{Cu}_2(\mu\text{-O})_2$  fragments are expected to cause ferromagnetic intra-subunit exchange based on the empirical correlation studies of oxo-bridged Cu(II) dimer compounds<sup>59-62</sup>. We expect that both of these effects, the rotation of the coordinate systems and the Cu-O-Cu bond angles in the subunits, are the primary source for the observed ferromagnetic coupling. However, additional weaker antiferromagnetic coupling is likely to be present, too. The high nuclearity and the large number of intramolecular exchange contacts in **2** precludes, however, the unambiguous determination of coupling constants  $J_n$  based on the susceptibility data, even if only a simple isotropic Heisenberg-type model Hamiltonian is employed.

The high-temperature limit of  $\chi T$  of 7.6 emuK/mol (at 290 K) corresponds to the spin-only moment of 17 spin-1/2 centers with ESR-derived  $g_{\text{iso}} = 2.19$ . Below ca. 100 K,  $\chi T$  rises continually, and even at 1.8 K (15.3 emuK/mol) the  $\chi T$  vs. T graph does not show any signs of approaching a maximum (Figure 5-4). This steep increase is, however, quenched at higher fields. At 5.0 Tesla,  $\chi T$  reaches a maximum at ca. 12 K.

Field-dependent magnetization measurements at 1.8 K (Figure 5-5) point to a singlet ground state for the cluster anion and the additional presence of uncoupled Cu(II) cations in the lattice. A fit to a Brillouin function  $B(s = 1/2)$  yields a best fit for 0.5 Cu(II) per formula unit and  $g_{\text{iso}} = 2.25$ . The difference to the ESR-derived value is due to the different coordination environments of the uncoupled Cu(II) centers in the lattice and of the Cu(II) centers incorporated into the POM structure. We are currently working to characterize this system using

large-scale simulation techniques (Quantum Monte Carlo simulations) and will present a more detailed description of the magnetism of **2** in forthcoming work.

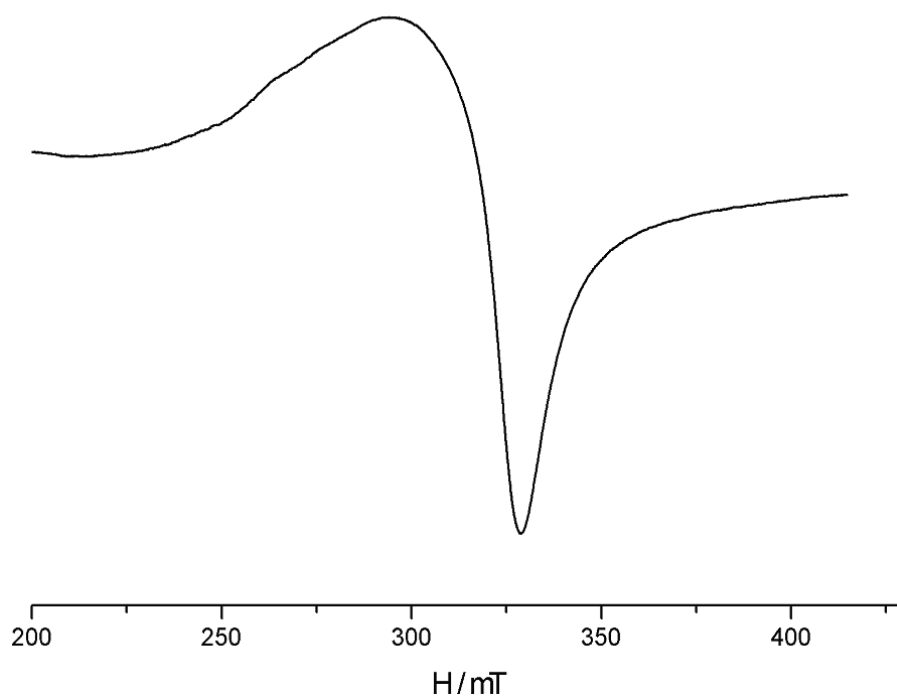


**Figure 5-4.** X-band ESR spectrum of compound **2**, measured as a microcrystalline powder at 290 K.

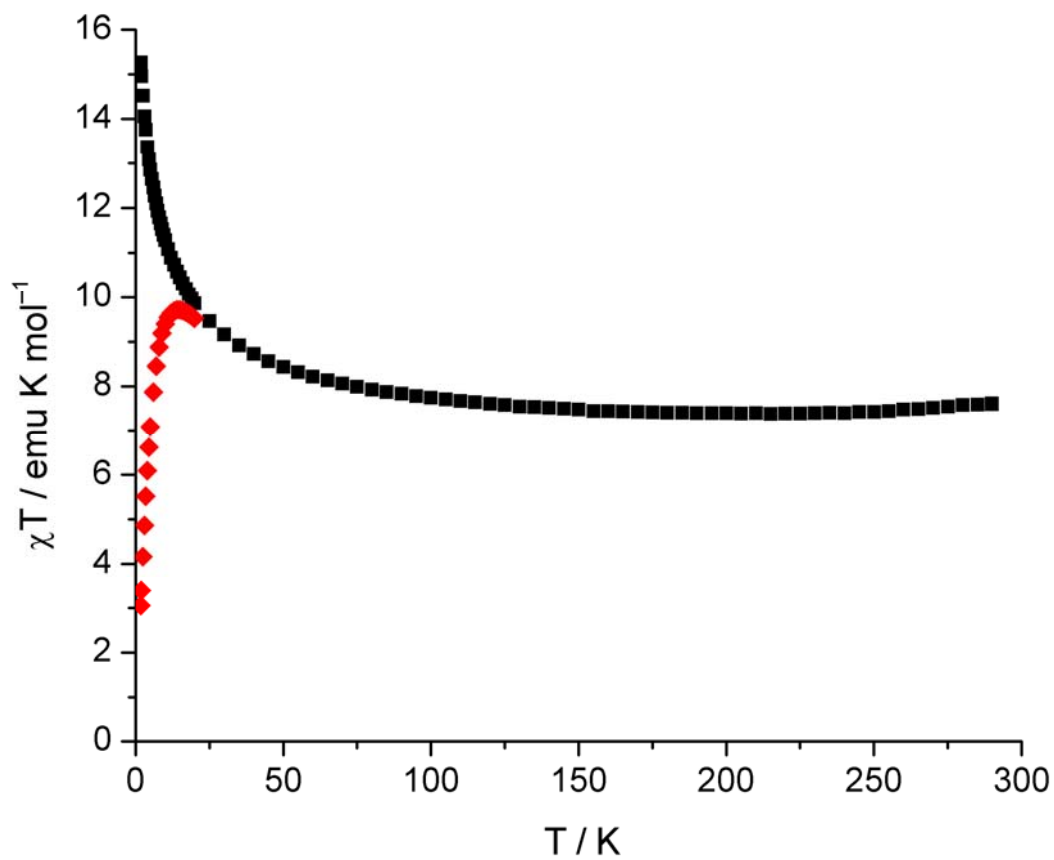


**Figure 5-5.** Temperature dependence of  $\chi T$  of **2** at 0.1 Tesla (black squares) and at 5.0 Tesla (red carets, the data follows the 0.1 Tesla curve for higher temperatures).

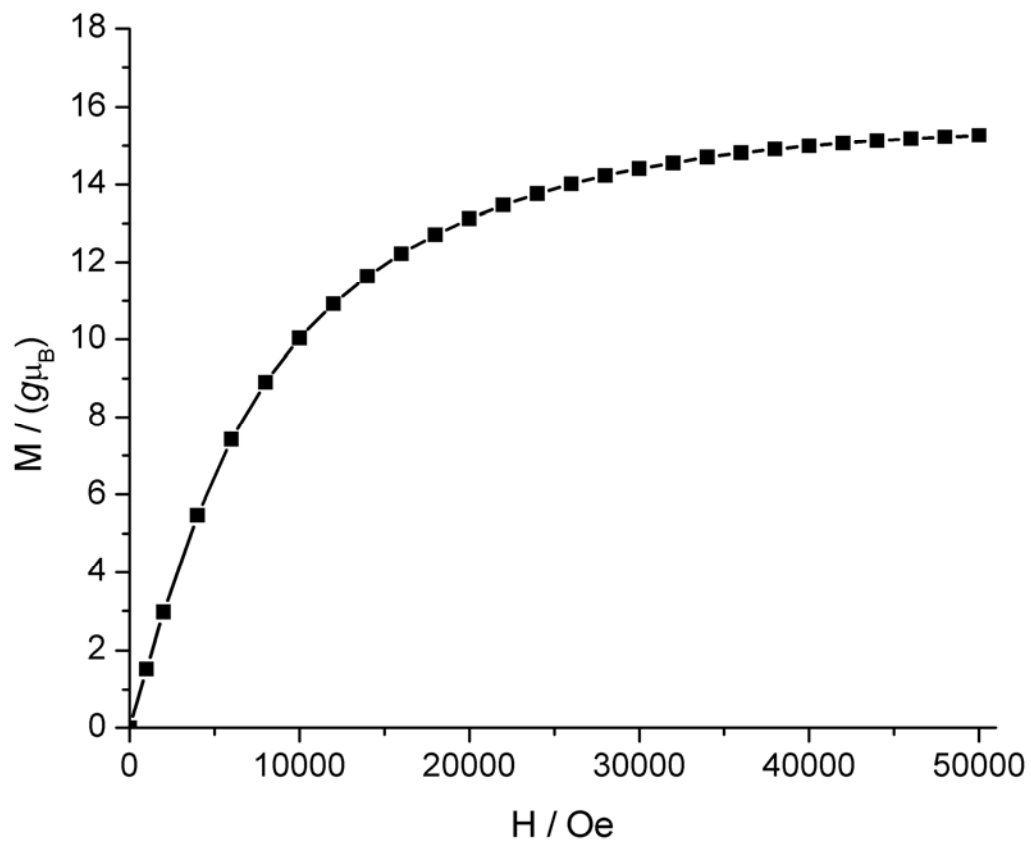


**Figure 5-6.** Field dependence of the magnetization,  $M$ , of **2** at 1.8

**Table 5-2.** Select bond distances (Å) and bond angles (°) for **2**

|         |          |             |           |
|---------|----------|-------------|-----------|
| Cu3-Cu4 | 2.930(6) | Cu6-O37     | 1.92(2)   |
| Cu5-Cu6 | 2.954(6) | Cu6-O38     | 1.85(3)   |
| Cu6-Cu7 | 2.927(6) | Cu3-O30-Cu4 | 95.9(12)  |
| Cu1-O9  | 1.90(3)  | Cu3-O35-Cu4 | 92.5(10)  |
| Cu3-O30 | 1.95(3)  | Cu5-O37-Cu6 | 101.9(15) |
| Cu3-O35 | 2.05(2)  | Cu5-O50-Cu6 | 97.1(13)  |
| Cu4-O30 | 2.00(3)  | Cu6-O38-Cu7 | 97.4(12)  |
| Cu4-O35 | 2.01(2)  | Cu6-O9-Cu7  | 94.9(11)  |

### Acknowledgments

We thank TDA Research Corporation (W911NF-04-C-0136), the U.S. Army Research Office (W911NF-05-1-0200), and the National Science Foundation (CHE-0553581) for funding this work and Dr. Joseph Reibenspies at Texas A & M University for collection of the low temperature X-ray dataset.

### References

- (1) Pope, M. T., *Heteropoly and Isopoly Oxometalates*. Springer-Verlag: Berlin, 1983; p 180.
- (2) Hill, C. L.; Prosser-McCartha, C. M., *Coord. Chem. Rev.* **1995**, *143*, 407-455.
- (3) Hill, C. L., *Chem. Rev.* **1998**, *98*, 1-2.
- (4) Coronado, E.; Gómez-García, C. J., *Chem. Rev.* **1998**, *98*, 273-296.
- (5) Kozhevnikov, I. V., *Chem. Rev.* **1998**, *98*, 171-198.

- (6) Okuhara, T.; Mizuno, N.; Misono, M., *Advances in Catalysis* **1996**, *41*, 113-252.
- (7) Mizuno, N.; Misono, M., *Chem. Rev.* **1998**, *98*, 199-218.
- (8) Neumann, R., *Prog. Inorg. Chem.* **1998**, *47*, 317-370.
- (9) Katsoulis, D. E., *Chem. Rev.* **1998**, *98*, 359-388.
- (10) Klemperer, W. G.; Wall, C. G., *Chem. Rev.* **1998**, *98*, 297-306.
- (11) Müller, A.; Das, S. K.; Kuhlmann, C.; Bögge, H.; Schmidtman, M.; Diemann, E.; Krickemeyer, E.; Hormes, J.; Modrow, H.; Schindler, M., *ChemComm* **2001**, 655-656.
- (12) Kozik, M.; Baker, L. C. W., *J. Am. Chem. Soc.* **1990**, *112*, 7604-7611.
- (13) Kozik, M.; Baker, L. C. W., Blue Electron Distributions in Diamagnetic Reduced Heteropolytungstates. Insights Concerning Conduction Pathways and Spin Coupling Patterns. <sup>183</sup>W NMR Chemical Shift Calculations. In *Polyoxometalates: From Platonic Solids to Anti-retroviral Activity*, Pope, M. T.; Müller, A., Eds. Kluwer Academic Publishers: Dordrecht, 1994; pp 191-202.
- (14) Weinstock, I. A., *Chem. Rev.* **1998**, *98*, 113-170.
- (15) Mbomekalle, I. M.; Keita, B.; Nadjò, L.; Berthet, P.; Hardcastle, K. I.; Hill, C. L.; Anderson, T. M., *Inorg. Chem.* **2003**, *42*, 1163-1169.
- (16) Okun, N. M.; Anderson, T. M.; Hill, C. L., *J. Am. Chem. Soc.* **2003**, *125*, 3194-3195.
- (17) Gómez-García, C. J.; Casañ-Pastor, N.; Coronado, E.; Baker, L. C. W.; Pourroy, G., *J. Appl. Physics* **1990**, *67*, 5995-5997.
- (18) Casañ-Pastor, N.; Bas-Serra, J.; Coronado, E.; Pourroy, G.; Baker, L. C. W., *J. Am. Chem. Soc.* **1992**, *114*, 10380-10383.

- (19) Galan-Mascaros, J. R.; Gomez-Garcia, C. J.; Borrás-Almenar, J. J.; Coronado, E., *Advanced Materials* **1994**, *6*, 221-223.
- (20) Clemente-Juan, J. M.; Coronado, E., *Chem. Rev.* **1999**, *193-195*, 361-394.
- (21) Pope, M. T.; Müller, A., *Polyoxometalates: From Platonic Solids to Anti-retroviral Activity*. Kluwer Academic Publishers: Dordrecht, Netherlands, 1993.
- (22) Yamase, T.; Fujita, H.; Fukushima, K., *Inorg. Chimica Acta* **1988**, *151*, 15-18.
- (23) Hill, C.; Weeks, M.; Hartnup, M.; Sommadossi, J.-P.; Schinazi, R., *Ann. N. Y. Acad. Sci.* **1990**, *616*, 528-529.
- (24) Hill, C. L.; Weeks, M. S.; Schinazi, R. F., *J. Med. Chem.* **1990**, *33*, 2767-2772.
- (25) Rhule, J. T.; Hill, C. L.; Judd, D. A.; Schinazi, R. F., *Chem. Rev.* **1998**, *98*, 327-357.
- (26) Rhule, J. T.; Hill, C. L.; Zheng, Z.; Schinazi, R. F., Polyoxometalates and Fullerenes as Anti-HIV Agents. In *Topics in Biological Inorganic Chemistry*, Clarke, M. J.; Sadler, P. J., Eds. Springer-Verlag: Heidelberg, 1999; Vol. 2: Metallopharmaceuticals, pp 117-137.
- (27) Yamase, T., Antitumoral and Antiviral Polyoxometalates (Inorganic Discrete Polymers of Metal Oxide). In *Polymeric Materials Encyclopedia*, Salamone, J. C., Ed. CRC Press: Boca Raton, 1996; pp 365-373.
- (28) Tézé, A.; Canny, J.; Gurban, L.; Thouvenot, R.; Hervé, G., *Inorg. Chem.* **1996**, *35*, 1001-1005.
- (29) Canny, J.; Tézé, A.; Thouvenot, R.; Hervé, G., *Inorg. Chem.* **1986**, *25*, 2114-2119.

- (30) Tézé, A.; Hervé, G.,  $\alpha$ -,  $\beta$ -, and  $\gamma$ -Dodecatungstosilicic Acids: Isomers and related Lacunary Compounds. In *Inorg. Syn.*, Ginsberg, A. P., Ed. John Wiley and Sons: New York, 1990; Vol. 27, pp 85-96.
- (31) Botar, B.; Geletii, Y. V.; Kögerler, P.; Musaev, D., G.; Morokuma, K.; Weinstock, I. A.; Hill, C. L., *J. Chem. Soc., Dalton Trans.* **2005**, *11*, 2017-2021.
- (32) Wassermann, K.; Lunk, H.-J.; Palm, R.; Fuchs, J.; Steinfeldt, N.; Stosser, R.; Pope, M. T., *Inorg. Chem.* **1996**, *35*, 3273-3279.
- (33) Canny, J.; Thouvenot, R.; Tézé, A.; Hervé, G.; Leparulo-Loftus, M.; Pope, M. T., *Inorg. Chem.* **1991**, *30*, 976-981.
- (34) Xin, F.; Pope, M. T., *Inorg. Chem.* **1996**, *35*, 5693-5695.
- (35) Xin, F.; Pope, M. T.; Long, G. J.; Russo, U., *Inorg. Chem.* **1996**, *35*, 1207-1213.
- (36) Kortz, U.; Isber, S.; Dickman, M. H.; Ravot, D., *Inorg. Chem.* **2000**, *39*, 2915-2922.
- (37) Kortz, U.; Matta, S., *Inorg. Chem.* **2001**, *40*, 815-817.
- (38) Bassil, B. S.; Kortz, U.; Tigan, A. S.; Clemente-Juan, J. M.; Keita, B.; Oliveira, P. d.; Nadjo, L., *Inorg. Chem.* **2005**, *44*, 9360-9368.
- (39) Mialane, P.; Dolbecq, A.; Marrot, J.; Rivière, E.; Sécheresse, F., *Chemistry - A European Journal* **2005**, *11*, 1771-1778.
- (40) Bassil, B. S.; Dickman, M. H.; Kortz, U., *Inorg. Chem.* **2006**, *45*, 2394-2396.
- (41) Bassil, B. S.; Dickman, M. H.; Reicke, M.; Kortz, U.; Keita, B.; Nadjo, L., *J. Chem. Soc., Dalton Trans.* **2006**, 4253-4259.

- (42) Zhang, Z.; Li, Y.; Wang, E.; Wang, X.; Qin, C.; An, H., *Inorg. Chem.* **2006**, *45*, 4313-4315.
- (43) Goto, Y.; Kamata, K.; Yamaguchi, K.; Uehara, K.; Hikichi, S.; Mizuno, N., *Inorg. Chem.* **2006**, *45*, 2347-2356.
- (44) Zhang, X.; O'Connor, C. J.; Jameson, G. B.; Pope, M. T., *Inorg. Chem.* **1996**, *35*, 30-34.
- (45) Nozaki, C.; Kiyoto, K.; Minai, Y.; Misono, M.; Mizuno, M., *Inorg. Chem.* **1999**, *38*, 5724-5729.
- (46) Yamaguchi, S.; Kikukawa, Y.; Tsuchida, K.; Nakagawa, Y.; Uehara, K.; Yamaguchi, K.; Mizuno, N., *Inorg. Chem.* **2007**, *46*, 8502-8504.
- (47) Liu, H.; Peng, J.; Su, Z.; Chen, Y.; Dong, B.; Tian, A.; Han, Z.; Wang, E., *Eur. J. Inorg. Chem.* **2006**, *2006*, 4827-4833.
- (48) Bassil, B. S.; Nellutla, S.; Kortz, U.; Stowe, A. C.; Tol, J. v.; Dalal, N. S.; Keita, B.; Nadjo, L., *Inorg. Chem.* **2005**, *44*, 2659-2665.
- (49) Kortz, U.; Jeannin, Y. P.; Tézé, A.; Hervé, G.; Isber, S., *Inorg. Chem.* **1999**, *38*, 3670-3675.
- (50) Mialane, P.; Dolbecq, A.; Marrot, J.; Rivière, E.; Sécheresse, F., *Angew. Chem. Int. Ed.* **2003**, *42*, 3523-3526.
- (51) Lisnard, L.; Mialane, P.; Dolbecq, A.; Marrot, J.; Clemente-Juan, J. M.; Coronado, E.; Keita, B.; Oliveira, P. d.; Nadjo, L.; Sécheresse, F., *Chem., Eur. J.* **2007**, *13*, 3525.
- (52) Luo, Z.; Kögerler, P.; Cao, R.; Hakim, I.; Hill, C. L., *J. Chem. Soc., Dalton Trans.* **2008**, *2008*, 54-58.
- (53) Zhang, Z.; Qi, Y.; Qin, C.; Li, Y.; Wang, E.; Wang, X.; Su, Z.; Xu, L., *Inorg. Chem.* **2007**, *46*, 8162-8169.

- (54) *SMART*, 5-55; Bruker AXS, Inc.: Madison, 2000.
- (55) *SAINTE*, 6.02; Bruker AXS, Inc.: Madison, 1999.
- (56) Liu, H.; Gomez-Garcia, C. J.; Peng, J.; Feng, Y.; Su, Z.; Sha, J.; Wang, L., *Inorg. Chem.* **2007**, *46*, 10041.
- (57) Mialane, P.; Duboc, C.; Marrot, J.; Rivière, E.; Dolbecq, A.; Sécheresse, F., *Chem., Eur. J.* **2006**, *12*, 1950.
- (58) P. Kögerler; Müller, A., *J. Appl. Phys.* **2003**, *93*, 7101-7102.
- (59) Chiari, B. H., J. H.; Piovesana, O.; Tarantelli, T.; Sanáís, P. F., *Inorg. Chem.* **1986**, *25*, 2408-213.
- (60) Kahn, O., *Angew. Chem., Int. Ed. Engl.* **1985**, *24*, 834-850.
- (61) Kato, M.; Muto, Y., *Coord. Chem. Rev.* **1988**, *92*, 45-83.
- (62) Melnik, M., *Coord. Chem. Rev.* **1982**, *42*, 259-293.

## *Chapter 6*

Multi-Copper Polyoxoanions. 3. Synthesis, structure, magnetism and catalytic properties of a polyoxometalate with coordinatively unsaturated d-electron-transition metal centers

with Paul Kögerler, Rui Cao, and Craig L. Hill

(published partially in *Inorg. Chem.* ASAP, DOI: 10.1021/ic9007729)

## Abstract

A series of tetrabutylammonium salts of transition-metal substituted Wells-Dawson polyoxometalates have been synthesized by phase transfer techniques and characterized by infrared spectroscopy, elemental analysis and variable-temperature magnetic measurements. X-ray quality crystals were obtained by a diffusion method using different organic solvents. The X-ray crystal structure of  $[(n\text{-C}_4\text{H}_9)_4\text{N}]_{11}\text{H}_5[\text{Cu}_4(\text{P}_2\text{W}_{15}\text{O}_{56})_2]$  (**3**) (monoclinic,  $P_{2(1)/n}$ ,  $Z = 2$ ,  $a = 19.7269(6)$  Å,  $b = 17.6602(5)$  Å,  $c = 44.2525(11)$  Å,  $\beta = 91.182(2)^\circ$ ;  $R_1 = 8.35\%$  based on 31282 independent reflections) reveals the presence of two unusual coordinatively unsaturated Cu(II) centers. In the absence of nitrate, **3** does not catalyze the aerobic oxidation of organic substrates in organic solvents.

## Introduction

The development of new materials to catalyze the selective aerobic oxidation of sulfur-based compounds under ambient conditions (1 atm air/O<sub>2</sub> and 25 °C) is of both intellectual and practical interest.<sup>1-6</sup> In the recent years, several different catalytic systems based on polyoxometalates (POMs) have been investigated. Okun *et al.*<sup>7-12</sup> reported several bulk and cationic-silica-supported POMs that catalyze the selective aerobic oxidation of 2-chloroethyl ethyl sulfide (CEES, a mustard gas simulant) to 2-chloroethyl ethyl sulfoxide (CEESO) under ambient conditions. The most recent work<sup>11, 12</sup> showed that tetrabutylammonium (TBA) salts of an iron(III)-substituted POM,  $\text{TBA}_3[\text{H}_2\text{Fe}[\text{H}(\text{ONO}_2)_2]\text{PW}_{11}\text{O}_{39}] \cdot (\text{HNO}_3)$  and related Cu(II)-substituted derivatives are extremely fast and selective catalysts for aerobic (air-based) sulfoxidation. These studies indicate

that the catalytic turnover frequency reflects a significant synergy between the d-electron-metal-substituted POM unit and nitrate. Unfortunately, the exact nature of this nitrate-POM interaction, despite considerable effort to clarify this issue experimentally, remains unclear for two reasons: (1) the X-ray structural determinations of these mono-substituted  $\alpha$ -Keggin polyanions reveal that the substituted position (most frequently copper and iron in these highly active catalysts) is always 12-fold disordered precluding identification of the terminal ligand, and (2) the paramagnetism of these highly active catalysts makes observation of the terminal ligands on the d-electron-metal centers impossible.

In context with ongoing studies of metal-substituted POMs as catalysts for ambient-temperature, air-based oxidation of sulfides, tri-vacant  $\text{Na}_{12}[\alpha\text{-P}_2\text{W}_{15}\text{O}_{56}] \cdot 18\text{H}_2\text{O}$  was chosen as the precursor to prevent disorder in the X-ray structures of the Cu- and Fe-substituted derivatives. We report here the synthesis of Cu<sub>4</sub>-, Co<sub>4</sub>-, Mn<sub>4</sub>-, Fe<sub>4</sub>-substituted derivatives of  $[\text{P}_2\text{W}_{15}\text{O}_{56}]^{12-}$  as their tetra-*n*-butylammonium (TBA) or tetra-*n*-heptylammonium (THpA) salts using a phase transfer method that simulates the environment of the organic-solvent-soluble POM component of the highly active Cu- and Fe-substituted POM aerobic oxidation catalysts. The organic-soluble POMs were characterized by a range of techniques including magnetochemical analysis of the Cu(II)-based polyanion. We further report the provocative finding that the Cu(II) centers in the polyanion of **3**, namely **3a**, are coordinatively unsaturated. The coexistence of unsaturated and saturated Cu(II) centers is reminiscent of the polyanion,  $\{\text{Cu}_4(\text{GeW}_9\text{O}_{34})_2\}$ , recently reported by Yamase and coworkers.<sup>13</sup>

## Experimental Section

### *General methods and materials*

$\text{Na}_{12}[\alpha\text{-P}_2\text{W}_{15}\text{O}_{56}]\cdot 18\text{H}_2\text{O}$  and  $\text{Na}_{14}\text{Cu}[\text{Cu}_4(\text{H}_2\text{O})_2(\alpha\text{-P}_2\text{W}_{15}\text{O}_{56})_2]\cdot 53\text{H}_2\text{O}$  were prepared by literature methods,<sup>14, 15</sup> and their purities were checked by FT-IR. All the starting reagents,  $\text{Cr}(\text{NO}_3)_3\cdot 9\text{H}_2\text{O}$ ,  $\text{Mn}(\text{NO}_3)_2$ ,  $\text{Fe}(\text{NO}_3)_3\cdot 9\text{H}_2\text{O}$ ,  $\text{Co}(\text{NO}_3)_2$ ,  $\text{Cu}(\text{NO}_3)_2\cdot 2.5\text{H}_2\text{O}$ ,  $\text{AgNO}_3$ ,  $\text{CuBr}_2$ ,  $(n\text{-C}_4\text{H}_9)_4\text{NBr}$  (TBABr),  $(n\text{-C}_4\text{H}_9)_4\text{NNO}_3$  (TBANO<sub>3</sub>),  $(n\text{-C}_7\text{H}_{15})_4\text{NBr}$  (THpABr), acetonitrile, dichloromethane, chloroform, carbon tetrachloride, 1,2-dichloroethane, tetrahydrofuran, toluene, hexane, decane, octadecene, 1,3-dichlorobenzene and 2-chlorethyl ethyl sulfide (CEES) were purchased from Aldrich and used without further purification. Gas chromatography (GC) was performed on a Hewlett-Packard 5890 gas chromatograph equipped with a 5% phenyl methyl silicone capillary column, flame ionization detector, and a Hewlett-Packard 3390A series integrator using  $\text{N}_2$  as the carrier gas. Elemental analyses for K, Na, Cu, Si and W were performed by Galbraith Laboratories (Knoxville, Tennessee). The infrared spectrum (2% sample in KBr pellet) was recorded on a Nicolet™ 6700 FT-IR spectrometer from ThermoElectron Corporation. The thermogravimetric data were collected on an ISI TGA 1000 instrument. Potentiometric titrations of the organic-solvent-soluble POMs in acetonitrile solution with 1.0 M methanolic  $(n\text{-C}_4\text{H}_9)_4\text{NOH}$  to assess protonation states were carried out using a Model 240 Corning pH meter equipped with a combination micro glass electrode at room temperature. Magnetic susceptibility measurements were performed at applied fields of 0.1 to 5.0 Tesla for the temperature range  $T = 1.8 - 290$  K using a Quantum Design MPMS-5XL SQUID magnetometer.

### *General method to synthesize the organic-soluble POM compounds*

Phase transfer was used to produce the organic-solvent-soluble transition-metal substituted POMs. The synthetic route to these compounds involves a metathetical exchange by adding and mixing a stoichiometric amount of TBA salt in organic solution to an aqueous solution of the potassium or sodium salt of the POMs with stringent control of the solution pH.<sup>16</sup> At the appropriate pH, the desired TBA<sup>+</sup>/H<sup>+</sup> counterion combination associates and transfers the polyanions to the organic phase. The yield of the TBA salt is quite dependent on the pH. Optimizing the pH throughout the reaction can also minimize possible degradation or hydrolysis of the POMs.

### *Synthesis of [(n-C<sub>4</sub>H<sub>9</sub>)<sub>4</sub>N]<sub>11</sub>H<sub>5</sub>[Cu<sub>4</sub>(P<sub>2</sub>W<sub>15</sub>O<sub>56</sub>)<sub>2</sub>] (3).*

Na<sub>14</sub>Cu[Cu<sub>4</sub>(H<sub>2</sub>O)<sub>2</sub>(α-P<sub>2</sub>W<sub>15</sub>O<sub>56</sub>)<sub>2</sub>]·53H<sub>2</sub>O (0.60 g, 0.066 mmol) was dissolved in 10 mL of deionized water. TBANO<sub>3</sub> (0.32g, 1.06 mmol) was dissolved in 10 mL of CH<sub>2</sub>Cl<sub>2</sub>. These two solutions were mixed together with vigorous stirring. To this mixture a solution of 4 M HNO<sub>3</sub> was added dropwise under stirring until the solution became turbid. The final pH was 4.6. Upon standing, the solution separated into a cloudy, white aqueous layer and a clear green organic layer. The solution was then transferred to a separatory funnel and the bottom layer (organic layer) was collected. The organic layer was transferred into a round-bottom flask and concentrated to a solid gel using a rotary evaporator. This green gel (0.90 g) was dissolved in a minimum amount of CH<sub>3</sub>CN and an excess quantity (ca. 50 mL) of deionized water was then added. The light-green precipitate that formed was collected, dried under vacuum,

redissolved in a minimum amount of  $\text{CH}_2\text{Cl}_2$ , and anhydrous diethyl ether (ca. 100 mL) was added to afford a light-green powder (0.61 g, 88% yield). Crystals of this TBA salt were obtained by gas phase (vapor) diffusion. Initially the light-green powder of **3** (20 mg) was dissolved in 2 mL of  $\text{ClCH}_2\text{CH}_2\text{Cl}$  in a 5 mL vial. This small vial was then moved into a 15 mL vial containing 5 mL of  $\text{CHCl}_3$ . The 15 mL vial was capped and placed in a dark cabinet. Green, block-like crystals were obtained after one week. X-ray quality single crystals were obtained by recrystallization using the same gas phase diffusion method. The number of TBA cations, determined by the TGA measurement (Figure 6-1), was ca. 5.5 per P atom. The TGA measurement also indicates the presence of solvent molecules ( $\text{ClCH}_2\text{CH}_2\text{Cl}$  and  $\text{CHCl}_3$ ) in the freshly prepared **3**. However, the solvent molecules quickly evaporated under air, which caused cracks in the crystal of **3**. No Cl was found in the elemental analysis of the cracked crystals. Potentiometric titration of **3** indicated about five protons in the formulation (Figure 6-2). IR (2% KBr pellet, 1200-400  $\text{cm}^{-1}$ ): 1090 (s), 1060 (w, sh), 952 (s), 916(w), 850 (w), 806 (s), 761 (s), 594 (w) and 525 (w). Anal. Calcd for  $\text{C}_{176}\text{Cu}_4\text{H}_{401}\text{N}_{11}\text{O}_{112}\text{P}_4\text{W}_{30}$ ,  $[(\text{n-C}_4\text{H}_9)_4\text{N}]_{11}\text{H}_5[\text{Cu}_4(\text{P}_2\text{W}_{15}\text{O}_{56})_2]$ : Cu, 2.45; P, 1.20; W, 53.25; C, 20.41; H, 3.90; N, 1.49. Found: Cu, 2.42; P, 1.1; W 50.2; C, 20.61; H, 3.75; N, 1.39. [MW = 10357.705 g/mol].

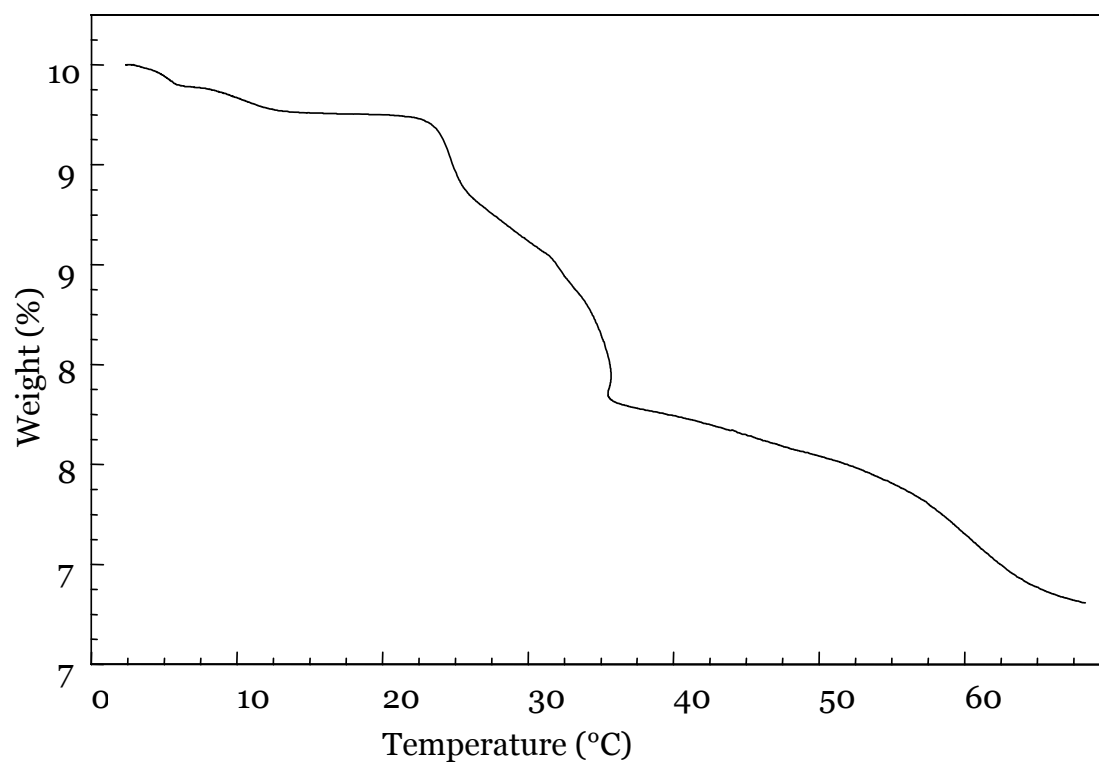


**Figure 6-1.** Thermogravimetric analysis (TGA) of fresh crystallized **3**.

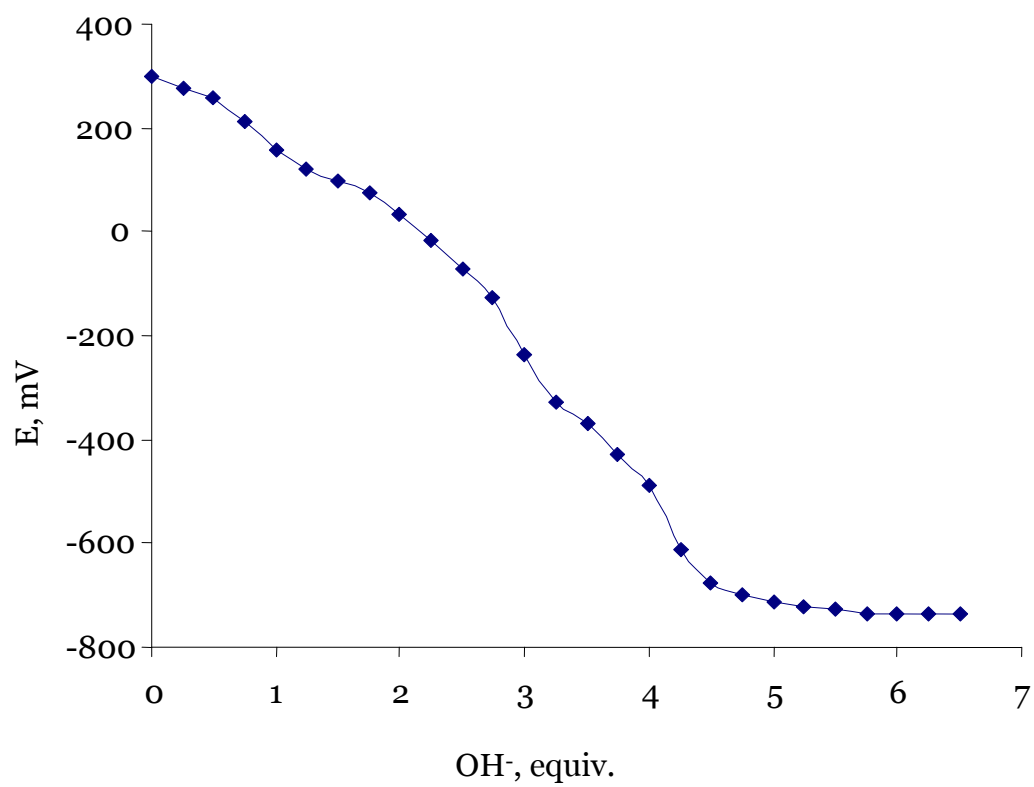


**Figure 6-2.** Potentiometric titration of the **3** by using TBAOH (1 M in methanol)

*Synthesis of TBA<sub>x</sub>H<sub>16-x</sub>[M<sub>4</sub>(OH<sub>2</sub>)<sub>2</sub>(P<sub>2</sub>W<sub>15</sub>O<sub>56</sub>)<sub>2</sub>]<sub>2</sub>, M=Co (**4**), Mn (**5**)*

Syntheses of the TBA salts of cobalt- and manganese-substituted {P<sub>2</sub>W<sub>15</sub>} derivatives are similar to that of copper-substituted analogue, **3**, except that Na<sub>16</sub>[Co<sub>4</sub>(H<sub>2</sub>O)<sub>2</sub>(α-P<sub>2</sub>W<sub>15</sub>O<sub>56</sub>)<sub>2</sub>] or Na<sub>16</sub>[Mn<sub>4</sub>(H<sub>2</sub>O)<sub>2</sub>(α-P<sub>2</sub>W<sub>15</sub>O<sub>56</sub>)<sub>2</sub>] were used in the procedure. Prior to recrystallization, the TBA salt of the Co-substituted POM and the Mn-substituted POM were yellow-brown and brown, respectively. X-ray quality single crystals were obtained by vapor diffusion of CHCl<sub>3</sub> into a ClCH<sub>2</sub>CH<sub>2</sub>Cl solution of the POM.

*Synthesis of THpA<sub>x</sub>H<sub>44-x</sub>{[Fe<sub>4</sub>(OH<sub>2</sub>)(P<sub>2</sub>W<sub>15</sub>O<sub>56</sub>)<sub>2</sub>]<sub>2</sub>}{[Fe<sub>4</sub>(P<sub>2</sub>W<sub>15</sub>O<sub>56</sub>)<sub>2</sub>](H<sub>2</sub>O)<sub>2</sub>} (**6**)*

A procedure very similar to that used for the other salts was used to prepare the highly hydrophobic THpA salt of the structurally analogous Fe<sub>4</sub> complex, but toluene, and THpANO<sub>3</sub> were used for the liquid phase transfer process. Accordingly, the solvents for purification and crystal growing were changed. The sodium salt of iron(III)-substituted POM precursor, H<sub>3</sub>Na<sub>9</sub>[Fe<sub>4</sub>(H<sub>2</sub>O)<sub>2</sub>(P<sub>2</sub>W<sub>15</sub>O<sub>56</sub>)<sub>2</sub>].62H<sub>2</sub>O, (0.62 g, 0.069 mmol) was dissolved in 20 mL of deionized water. THpANO<sub>3</sub> (0.39g, 0.828 mmol) was dissolved in 25 mL of toluene. The solutions were then mixed and vigorously stirred for 30 min. No acid was added. Upon standing, a colorless aqueous layer and a yellow brown organic layer separately easily. The mixture was placed in a separatory funnel and the bottom (organic) layer was collected, transferred to a round-bottom flask and concentrated to a thick yellow brown oil using a rotary evaporator. The yellow brown product was redissolved a minimum amount of toluene. The resulting solution was treated with 25 mL of anhydrous diethyl ether, which

produced an oil-like precipitate. The precipitate was collected by centrifuge and air dried overnight. The dried product is a yellow brown solid gel (0.78g, yield 77%). X-ray quality single crystals of the THpA salt were obtained by liquid phase diffusion. The yellow brown solid gel of the THpA POM salt (20 mg) was dissolved in 2 mL of toluene in a 2 mL vial. The 2 mL vial was then placed in a 15 mL vial. To the 15 mL vial was added octadecene until the octadecene level was just above the small vial to allow for slow mixing. The 15 mL vial was then capped and placed in a dark cabinet. Yellow needle-like crystals were obtained on the inside wall of the small vial after three weeks.

### *Magnetochemical analysis*

The magnetic susceptibility of **3** was recorded in the temperature interval 2 – 300 K and applied fields ranged from 0.1 to 5.0 Tesla. All data were corrected for diamagnetic and temperature-independent paramagnetic (TIP) contributions (the latter are significant for polyoxotungstates) that were partly derived from tabulated values and partly from measurements on similar yet diamagnetic polyoxotungstate compounds ( $\chi_{\text{dia/TIP}}(\mathbf{3}) = -2.79 \times 10^{-5} \text{ cm}^3\text{mol}^{-1}$ ). All simulations were performed using an extended version of the program CONDON for fully isotropic Heisenberg-type exchange.<sup>17</sup> Compound **3**, measured as solid, is ESR silent at room temperature (X-band).

### *X-ray Crystallography*

The X-ray quality crystal of **3** was removed from the mother liquid and quickly coated with Paratone N oil. The coated crystal was mounted on a small fiber loop for index and intensity data collection. Because of the crystals were

prone to cracking quickly, extra care was needed when treating the organic-soluble crystals, especially the TBA salts obtained from chlorinated solvents. The X-ray diffraction data were collected under a nitrogen stream at 173 K on a Bruker D8 SMART APEX CCD single-crystal diffractometer using Mo K $\alpha$  (0.71073 Å) radiation. Data collection, indexing, and initial cell refinements were processed using the SMART<sup>18</sup> software. Frame integration and final cell refinements were carried out using the SAINT<sup>19</sup> software. The final cell parameters were determined from the least-squares refinement of total reflections. The structures were determined through direct methods (SHELXS97) for locating the tungsten atoms and difference Fourier maps (SHELXL97). The Squeeze method was used for crystals of **4**, **5** and **6** which contained large numbers of disordered counteractions. The hydrogen atoms of the water molecules were not located in the difference Fourier maps. The final results of the refinement are listed in Table 6-1.

**Table 6-1.** Crystal data for **3**·2ClCH<sub>2</sub>CH<sub>2</sub>Cl·2CHCl<sub>3</sub>

|   | <b>3</b>   |
|---|--|
| empirical formula   | C <sub>182</sub> Cl <sub>10</sub> Cu <sub>4</sub> H <sub>411</sub> N <sub>11</sub> O <sub>112</sub> P <sub>4</sub> W <sub>30</sub> |
| formula weight  | 10794.0 g mol <sup>-1</sup>  |
| space group   | <i>P</i> <sub>2(1)/n</sub>   |
| unit cell   | <i>a</i> = 19.7269(6) Å<br><i>b</i> = 17.6602(5) Å<br><i>c</i> = 44.2525(11) Å<br><i>β</i> = 91.182(2)°                            |
| volume  | 15413.5(7) Å <sup>3</sup>  |
| <i>Z</i>  | 2  |
| temperature   | 173(2)K  |
| wavelength  | 0.71073 Å  |
| F(000)  | 9088   |
| θ range, deg  | 1.48 - 26.37   |
| abs corr  | semi-empirical   |
| no. of total reflcns  | 31282  |
| no. of restraints   | 0  |
| no. of parameters   | 814  |
| abs. coeff  | 11.588 mm <sup>-1</sup>  |
| GOF   | 1.006  |
| final R <sub>1</sub> <sup>a</sup> [ <i>I</i> > 2σ( <i>I</i> )]  | 0.0835   |
| final wR <sub>2</sub> <sup>b</sup> [ <i>I</i> > 2σ( <i>I</i> )] | 0.1904   |

$$^a R_1 = \Sigma ||F_o| - |F_c|| / \Sigma |F_o|; ^b wR_2 = \Sigma [w(F_o^2 - F_c^2)^2] / \Sigma [w(F_o^2)^2]^{1/2}$$

## Results and Discussion

### *Synthesis*

The TBA salt of the copper-substituted phosphotungstate, **3**, was prepared by an improved phase transfer method. In contrast to the general procedure in which a stoichiometric amount of TBABr is added to the aqueous solution of the polyoxometalate directly before the addition of organic solvent, we mixed a solution containing a stoichiometric amount of TBA salt in an organic solvent with an aqueous solution of the sodium salt of the polyoxometalate. The sequence change in the initial step helps avoid the formation of insoluble material induced by direct addition of TBA to the aqueous POM solution. The sequence change also results in a convenient route to optimize the amount of acid needed in the phase transfer process. Initially, with the addition of acid into the mixture, white floccules form and disappear instantly with the vigorous stirring. After a certain amount of acid is added, one “extra” drop of acid results in a large amount of precipitate that does not redissolve indicating that the optimal conditions have been reached. Absorption spectra showed the concentration of POM in the organic layer reaches a maximum value at pH 4.6. The solution of the crude, phase-transferred product was collected and concentrated. One drawback of this phase transfer method is the considerable amount of excess TBA cation present in the crude product and the less than quantitative transfer of the POM into the organic phase. However, the excess of TBA is also inevitable in the general literature method, and in either case the crude product must be purified before the final analysis. In the present study, the crude product was purified by repeated dissolving in a minimum amount of acetonitrile and then precipitation by addition of excess water. The purified product was transferred to an

anhydrous environment by dissolving it in a minimum amount of  $\text{CH}_2\text{Cl}_2$  and then precipitating with a large amount of anhydrous diethyl ether before growing crystals. Similar methods were applied to the preparation of the TBA salts of cobalt- or manganese-substituted POMs and the THpA salt of iron-substituted POM.

Previously, Pope and co-workers<sup>20-23</sup> thoroughly studied the preparation of transition-metal substituted POMs in anhydrous nonpolar solvents. They reported that the THpA cation can associate with the metal-substituted POMs resulting in phase transfer of the polyanions from aqueous solution to highly nonpolar organic solvents such as toluene. These investigators prepared a series of THpA salts of  $\text{MXW}_{11}\text{O}_{39}$ ,  $\text{MX}_2\text{W}_{17}\text{O}_{61}$  and  $\text{M}_4(\text{XW}_9)_2$  ( $\text{M} = \text{Mn}, \text{Ni}, \text{Cu}, \text{Co}$ ;  $\text{X} = \text{P}, \text{Si}, \text{Ge}$ ) in nonpolar solvents (benzene and toluene) by this phase transfer method. A considerable amount of water (20-30 mol of water / mol of POM) was found in the transferred organic layer. Further, they argued, reasonably, that the low activity of water in highly nonpolar solutions favors dissociation of the water molecule coordinated to the d-electron transition metal center substituted in the POM unit. This group provided evidence from visible and EPR spectra for the existence of unsaturated positions on the substituted d-electron-metals in the POMs. However, no X-ray crystal structures were presented.

Previously, Finke and co-workers<sup>16</sup> investigated the transfer of  $\alpha_2$ - $\text{P}_2\text{W}_{17}\text{O}_{61}(\text{M}^{n+}\cdot\text{OH}_2)^{n-10}$  ( $\text{M} = \text{Mn}^{3+}, \text{Fe}^{3+}, \text{Co}^{2+}, \text{Ni}^{2+}, \text{Cu}^{2+}$ ) from aqueous solution to less polar organic solvents like  $\text{CH}_2\text{Cl}_2$  by using TBABr. Two structurally distinct phosphorus atoms in this POM make NMR characterization possible

even with the existence of proximal paramagnetic transition metal centers. Their studies of this system afforded isomerically pure TBA salts of the monosubstituted Wells-Dawson POMs as confirmed by  $^{31}\text{P}$  NMR. Elemental analysis indicated that the TBA salts of their above mono-substituted Wells-Dawson POMs each contain exactly one extra equivalent of TBABr. This bromide was proposed to replace the terminal aqua ligand on the d-electron transition-metal in the polyanion. These investigators verified the existence of the bromide ligand by absorption spectra and measured the ligand-association equilibrium constants. Again, no X-ray structures of these hydrophobic salts were reported.

The TBA salts of POMs play an important role in studying the catalytic properties of POMs in organic solvents. However, not many<sup>24-32</sup> tetraalkylammonium POM structures, especially of the Well-Dawson type, have been reported which reflects the challenges in growing diffraction-quality crystals of many classes of these polyanion salts. The formation of gels, the rapid cracking of efflorescent crystals after removal from the mother liquid, and the disorder of counter-cations are some of the factors that render acquisition of X-ray quality crystals of the TBA salts problematical. We used both liquid and gas phase diffusion methods to grow crystals of the TBA salts in this work. Crystalline light-green blocks of **3** were obtained by gas-phase diffusion. Selecting the right solvents for gas phase diffusion is crucial to obtain suitable crystals. When  $\text{CH}_2\text{Cl}_2$  was used as the principal solvent for the TBA salts, all the crystals (obtained by diffusing THF or  $\text{Et}_2\text{O}$  into the  $\text{CH}_2\text{Cl}_2$ -based mother liquid) cracked in few minutes after removal from the mother liquid, ruining them for crystallographic study. The fast cracking of the TBAPOM crystals is mainly

attributed to the presence of low boiling solvents and consequent very rapid evaporation. Several different organic solvents with higher boiling points were tested. The results showed that the crystals obtained by diffusing  $\text{CHCl}_3$  into a  $\text{ClCH}_2\text{CH}_2\text{Cl}$  solution of **3** are stable for at least fifteen minutes, which is sufficient for crystal selection and mounting on the diffractometer.

The THpA salt of POM is even harder to crystallize than the TBA salt. Both  $\text{THpANO}_3$  and the THpA POM salt, **6**, dissolve only in quite nonpolar solvents like toluene and the resulting POM solutions are immiscible with most of the polar solvents, which prevent further purification. Wide spectrum tests of different solvents found that small amounts of floccules were formed when long-chain aliphatic hydrocarbons were added into the toluene solution of the THpA POM salt. Based on these findings, liquid phase diffusion was used to grow crystals instead of gas phase diffusion. The toluene solution of the THpA POM 2 (mL) in a 2 mL vial was placed into a 15 mL vial. To the 15 mL vial was added long-chain aliphatic hydrocarbons (decane or octadecene). The added volume of hydrocarbon was slowly increased until it topped the small vial. After one month a large portion of the THpA salt reformed an oil-like gel on the bottom of the small vial; however, needle-like X-ray quality single crystals were obtained on the inside wall of the small vial.

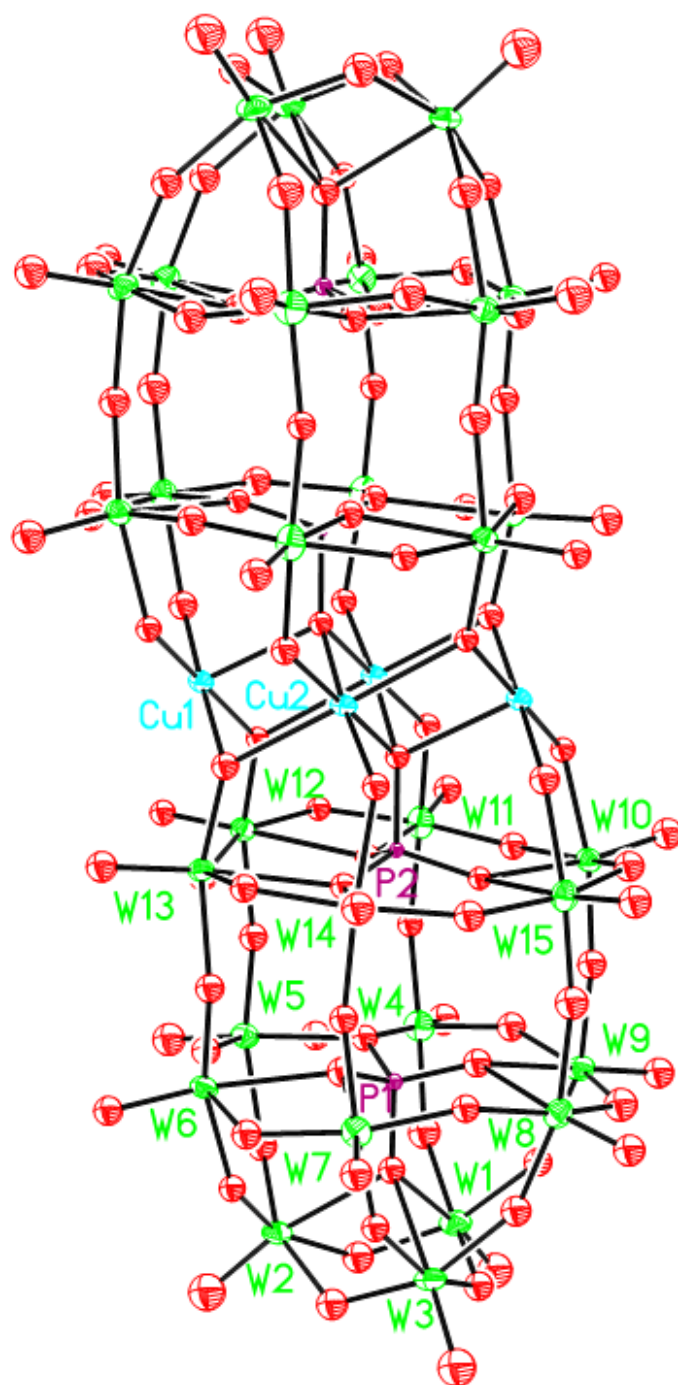


**Figure 6-3.** Ball-and-stick representation of  $[\text{Cu}_4(\text{P}_2\text{W}_{15}\text{O}_{56})_2]^{16-}$  (polyanion 3a of compound 3) showing 50% probability ellipsoids and selected atomic labels.

### *Structural features*

The TBA salt of a copper-substituted Wells-Dawson sandwich type POM,  $[(n\text{-C}_4\text{H}_9)_4\text{N}]_{11}\text{H}_5[\text{Cu}_4(\text{P}_2\text{W}_{15}\text{O}_{56})_2]$ , **3**, crystallizes in the monoclinic space group,  $P2(1)/n$  and shows well-separated polyanions (**3a**), TBA cations and solvent molecules ( $\text{ClCH}_2\text{CH}_2\text{Cl}$  and  $\text{CHCl}_3$ ). Ten of eleven TBA counterions refine clearly and a fragment of one additional TBA is also found. The numbers of TBA counterions exactly match that found by both elemental analysis and thermogravimetric analysis. The polyanion, **3a**, which is a conventional Wells-Dawson sandwich structure with central  $\beta$  junctions,<sup>33-56</sup> contains two equivalent  $[\text{Cu}_2\text{P}_2\text{W}_{15}\text{O}_{56}]^{8-}$  subunits related by an inversion center ( $C_i$  symmetry; Figure 6-3). The four Cu atoms in **3a** and the inversion center define a plane. Cu1 and Cu2 have different coordination environments. Cu2 is six-coordinate center internal to the structure and bonds to three oxygen atoms (O52, O53, O56 or O50A, O51A, O56A) in each  $[\text{P}_2\text{W}_{15}\text{O}_{56}]^{10-}$  unit. Significantly, and distinct from the sodium salt analogue synthesized in aqueous solution, the terminal aqua group is absent on the two Cu(II) centers that reside in the outside positions of the central  $\text{Cu}_4$  belt. Cu1 bonds to two oxygen atoms (O51 and O52) of  $[\text{P}_2\text{W}_{15}\text{O}_{56}]^{10-}$  on one side of the  $\text{Cu}_4$  plane and three oxygen atoms (O54A, O55A, and O56A) of  $[\text{P}_2\text{W}_{15}\text{O}_{56}]^{10-}$  on the other side. BVS calculation<sup>57</sup> of the bridging oxygen atoms (Table 6-2) reveals that four protons reside on O53, O53A, O55 and O55A and the remaining proton is disordered between O54 and O54A. Selected bond distances and bond angles are listed in Table 6-3. The absence of any diffraction peak proximal to these external Cu centers confirms they are indeed five-coordinate and coordinately unsaturated. Evidence from decades of

investigation (synthesis, spectroscopy, X-ray diffraction and other studies) of d-electron-transition-metal-substituted POMs (TMSPs) indicates that the d-electron centers always bear terminal ligands with the exception of the toluene extracted systems reported by Pope and co-workers (Katsoulis et al)<sup>20-23</sup>. We now supply a X-ray crystallographic confirmation of coordinatively unsaturated d-electron centers in POMs present in nonpolar environments. Note that a POM with partially unsaturated (5-coordinate) Cu(II) centers was very recently obtained from an aqueous reaction solution and reported by Yamase and coworkers.<sup>13</sup>

Previously, organic-solvent-soluble POM salts (especially TBA salts) were used during development of the catalytic aerobic oxidation systems by the Hill group. Nitrate salts of the d-electron transition metal were used most frequently as reactants in preparations of these POM catalysts. We propose that nitrate could bond to the d-electron-metal in the POM and that this unit is likely involved in catalytic turnover.<sup>11, 12</sup> In the phase transfer step of preparing **3**, considerable nitrate is present in the organic phase, and bonding between nitrate and Cu atoms is not unexpected. However, the X-ray structure of **3** clearly reveals that the external Cu(II) centers in the “belt” of the sandwich have no terminal ligands. The strong Jahn-Teller effect exhibited by d<sup>9</sup> Cu(II) centers certainly explains, in part, the coordinatively unsaturated Cu centers in **3**. We prepared, purified and characterized the structurally analogous Co(II)- and Mn(II)-substituted complexes by X-ray crystallography (S1, see appendix) and the external Co and Mn centers in both complexes bear terminal ligands. Interestingly, the nitrate group does not coordinate to any of these complexes.

The d<sup>7</sup> Co(II) centers exhibit Jahn-Teller distortion but far less than d<sup>9</sup> Cu(II), and high-spin d<sup>5</sup> Mn(II) exhibits no Jahn-Teller distortion.

**Table 6-2.** Bond valence sum of selected bridge atom of **3**

|     |       |     |       |
|-----|-------|-----|-------|
| O50 | 1.410 | O53 | 1.282 |
| O51 | 1.845 | O54 | 1.337 |
| O52 | 1.990 | O55 | 1.185 |

**Table 6-3.** Select bond distance (Å) and bond angles (°) for **3**

|          |           |              |           |
|----------|-----------|--------------|-----------|
| Cu1-Cu1A | 5.532(16) | Cu1-O51-Cu2A | 94.6(6)   |
| Cu2-Cu2A | 3.069(18) | Cu1-O52-Cu2  | 93.7(6)   |
| Cu1-Cu2  | 3.155(15) | Cu2-O56-Cu2A | 98.5(6)   |
| Cu1-O51  | 1.945(14) | Cu1-O52      | 1.942(15) |
| Cu1-O54A | 1.942(15) | Cu1-O55A     | 1.938(15) |
| Cu1-O56A | 2.356(15) | Cu2-O50A     | 1.930(15) |
| Cu2-O51A | 2.352(14) | Cu2-O52      | 2.365(16) |
| Cu2-O53  | 1.919(15) | Cu2-O56      | 2.036(14) |
| Cu2-O56A | 2.015(14) | O50-W11      | 1.955(15) |
| O51-W12  | 1.851(14) | O52-W13      | 1.808(15) |
| O53-W14  | 2.019(14) | O54-W15      | 1.979(15) |
| O55-W10  | 2.055(14) | O56-P2       | 1.631(15) |
| Cu1-Cu1A | 5.532(16) | Cu1-O51-Cu2A | 94.6(6)   |
| Cu2-Cu2A | 3.069(18) | Cu1-O52-Cu2  | 93.7(6)   |
| Cu1-Cu2  | 3.155(15) | Cu2-O56-Cu2A | 98.5(6)   |

### *Sulfoxidation of thioethers by air catalyzed by 3*

Initially, Okun and coworkers<sup>11, 12</sup> proposed that the mono-iron-substituted POM,  $\text{TBA}_3\text{H}_2\{\text{Fe}[\text{H}(\text{NO}_3)_2]\text{PW}_{11}\text{O}_{39}\}$ , is coordinated with a nitrate ligand which makes the POM active in the catalytic aerobic sulfoxidation and other organic oxidation reactions. However, as noted above, the substituted  $\alpha$ -Keggin structure precluded use of both X-ray crystallography (positionally disordered structures are invariably produced) and NMR for structural confirmation. Extensive studies with Cu- and Fe-substituted  $\{\gamma\text{-SiW}_{10}\}$  derivatives<sup>58-76</sup> conducted in media similar to those used in the catalytic aerobic oxidation studies also failed to provide insight into the structures of the highly reactive Cu/FePOM- $\text{NO}_x$  aerobic oxidation catalysts. Instead, multi-copper-substituted silicopolytungstates were obtained and characterized.<sup>77, 78</sup> The latter Cu-substituted POMs were sufficiently insoluble that investigation of their homogenous catalytic sulfoxidation chemistry in organic solvents was not possible.

In order to investigate the catalytic activity of **3**, analogues of the “hot catalyst” (see Chapter 3) were prepared by mixing **3** and  $\text{TBAFeBr}_4$ . The catalytic activities of CEES oxidation of different combinations of the POM catalyst are recorded as in Table 6-4. From Table 6-4 it is clear that the mixture of pure **3** with  $\text{TBAFeBr}_4$ , **I**, has no activity in catalyzing the sulfoxidation. This is a consequence of nitrate being absent in the system. According to the mechanism proposed in Chapter 3, without  $\text{NO}_x$  the system cannot form the direct oxidant,  $\text{Br}_2$ , which makes the mixture totally inactive. The systems contained transition metal and  $\text{NO}_x/\text{Br}$ , **III** and **IV**, are both active.

Interestingly, the one contained only one transition metal is more active than the one contained both iron and copper. With the addition of nitrate group, the mixture of **3** and TBABr<sub>4</sub>, **II**, shows the best activity in catalyzing the sulfoxidation. This result indicates that the TMSPs can facilitate sulfoxidation catalyzed by the NO<sub>x</sub>/Br systems. As such the former can be viewed as co-catalysts. Based on our proposed mechanism for catalytic aerobic sulfoxidation (Chapter 3), the TMSPs are likely important in the elementary processes involving formation and regeneration of bromine.

### *Magnetic properties*

The observed magnetism of **3** indicates medium antiferromagnetic intramolecular exchange between the four Jahn-Teller-distorted  $s = 1/2$  Cu(II) centers. The exchange, mediated by bridging oxo groups, primarily proceeds through the ligands binding to the equatorial coordination sites of the Cu centers since their magnetic orbitals are primarily of  $3d_{x^2-y^2}$  character. Therefore, the exchange pathways in **3** can be grouped into three classes (Figure 6-4): (1) significant exchange via two  $\mu_3$ -O centers (O56/O56A) bridging Cu2 and Cu2A (Cu...Cu: 3.07 Å; Cu-O-Cu: 98.5°); (2) weak exchange via  $\mu_3$ -O centers (O51, O52, O56 and symmetry equivalents) that interlink all four Cu centers in the Cu<sub>4</sub> ring and assume both axial and equatorial coordination sites (Cu...Cu: 3.16 Å); and (3) very weak exchange between the distal Cu centers (Cu1/Cu1A) mediated by -O-W-O-P-O- pathways (Cu...Cu: 5.53 Å). Using an isotropic Heisenberg-type exchange, Hamiltonian  $\mathbf{H} = -J_1\mathbf{S}_2 \cdot \mathbf{S}_{2A} - J_2(\mathbf{S}_1 \cdot \mathbf{S}_2 + \mathbf{S}_1 \cdot \mathbf{S}_{2A} + \mathbf{S}_{1A} \cdot \mathbf{S}_2 + \mathbf{S}_{1A} \cdot \mathbf{S}_{2A}) - J_3\mathbf{S}_1 \cdot \mathbf{S}_{1A}$  augmented by a Zeeman operator, both the low-field susceptibility and the field-dependence of the susceptibility at 2.0 K are best described for  $J_1 = -$

$10.05 \text{ cm}^{-1}$ ,  $J_2 = -2.08 \text{ cm}^{-1}$ ,  $J_3 = -0.41 \text{ cm}^{-1}$ , and  $g = 2.23$  (Figure 6-5), in line with the expected coupling strengths. This concurrent fitting approach avoids overparametrization issues, contrary for example to a least squares fit to the temperature dependence of the molar susceptibility,  $\chi_m$ , for only a single applied field  $B_0$ . The increased  $g$  factor is common for Cu(II) complexes and results from an admixture of higher terms with orbital momenta to the  ${}^2E_g$  ground state for Cu(II) in cubic and tetragonally distorted ligand fields. We compare the recently published  $[\text{Cu}_4(\text{GeW}_9\text{O}_{34})_2]^{12-}$  polyanion<sup>13</sup> that features a similar pattern of an elongated  $\text{Cu}_4$  rhombus with two ‘external’ 5-coordinate Cu(II) centers (Cu...Cu: 3.11 Å) and two ‘internal’ 6-coordinate Cu(II) centers (equivalent to Cu2/Cu2A; Cu...Cu: 5.36 Å). Note that the connectivity of the  $\text{Cu}_4\text{O}_{14}$  core in both **3** and  $[\text{Cu}_4(\text{GeW}_9\text{O}_{34})_2]^{12-}$  are identical, However, due to the geometric differences in bond lengths and angles the coupling parameters  $J_{1-3}$  for **3** differ markedly from the reported values for  $[\text{Cu}_4(\text{GeW}_9\text{O}_{34})_2]^{12-}$  ( $J_1 = -49.6 \text{ cm}^{-1}$ ,  $J_2 = -12.1 \text{ cm}^{-1}$ ,  $J_3 = +0.02 \text{ cm}^{-1}$  for the spin Hamilton adopted above). Note that for both  $[\text{Cu}_4(\text{GeW}_9\text{O}_{34})_2]^{12-}$  as well as its derivative containing two additional terminal  $\text{H}_2\text{O}$  ligands (completing the octahedral coordination environments of all four Cu centers) relatively high  $g$  factors are found (2.18 and 2.24, respectively) that compare well with the  $g$  value for **3**.

**Table 6-4.** Aerobic oxidation of 2-chloroethyl ethyl sulfide (CEES) in acetonitrile catalyzed by analogues or components of the “hot catalyst” .

| Catalyst combinations  | [catalyst](mg) | [POM]<br>(mmol) | [NO <sub>3</sub> ]<br>(mmol) | %<br>conv. |
|--|----------------|-----------------|------------------------------|------------|
| <b>3</b> /TBAFeBr <sub>4</sub> <sup>a</sup>                          | 100            | 0.0046          | 0                            | 0          |
| <b>3</b> /TBAFeBr <sub>4</sub> /TBANO <sub>3</sub> <sup>b</sup>      | 121            | 0.0046          | 0.069                        | 84         |
| TBAFeBr <sub>4</sub> /Cu(NO <sub>3</sub> ) <sub>2</sub> <sup>c</sup> | 57             | 0               | 0.069                        | 47         |
| TBAFeBr <sub>4</sub> /TBANO <sub>3</sub> <sup>d</sup>                | 71             | 0               | 0.069                        | 72         |

General conditions: 50 mg (0.081 mmol) of TBAFeBr<sub>4</sub> (0.324 mmol of Br<sup>-</sup>) was used in each sample, 0.875 mmol (0.35 M) of CEES, catalyst (quantity given in column 2, estimated amount of POM given in column 3), 1 atm of air, 0.876 mmol (0.35 M) of 1,3-dichlorobenzene (internal standard) were stirred in 2.5 mL of acetonitrile at 25 °C for 16.5 h in the 20-mL vial; <sup>a</sup> 50 mg of each; <sup>b</sup> 50 mg of **3**, 21 mg of TBANO<sub>3</sub>; <sup>c</sup> 6.5 mg of Cu(NO<sub>3</sub>)<sub>2</sub>; <sup>d</sup> 21 mg of TBANO<sub>3</sub>.

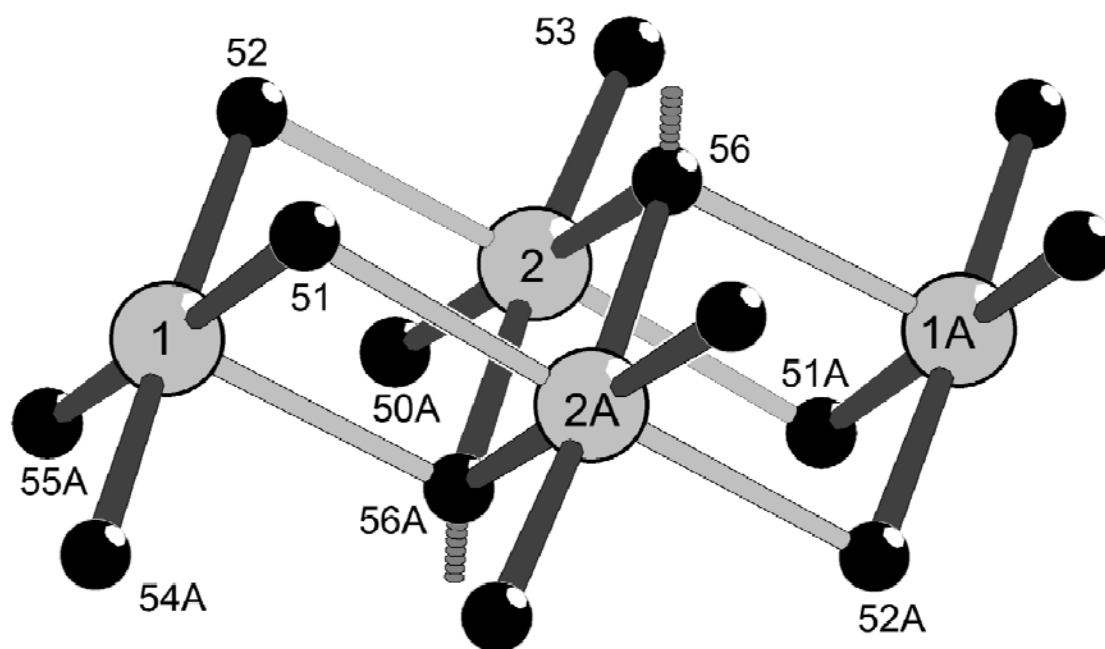


**Figure 6-4.** Coordination environments of the central  $\text{Cu(II)}_4$  group in **3** with atom numbers of positions primarily involved in magnetic exchange (Cu: large grey circles, O: small black circles). Bonds to equatorial ligand positions are highlighted in dark grey. Dotted bond lines indicate bonds to the two proximal P centers of the  $\{\text{P}_2\text{W}_{15}\}$  groups.

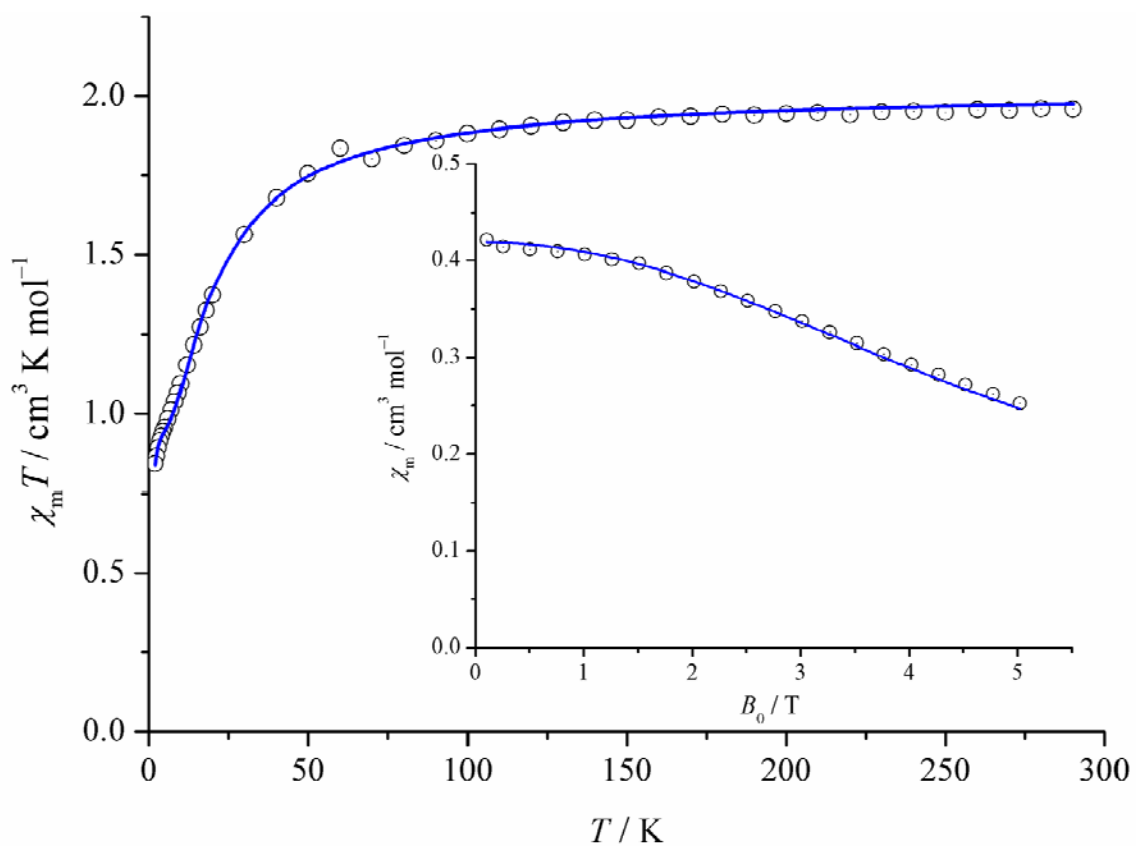


**Figure 6-5.** Temperature dependence of  $\chi_m T$  for **3** at 0.1 Tesla ( $2.0 \text{ K} < T < 300 \text{ K}$ ). Inset:  $\chi_m$  of **3** as a function of the applied field  $B_0$  at 2.0 K, illustrating saturation effects. Experimental data: open circles, least squares fit to the employed model (see text): blue line.

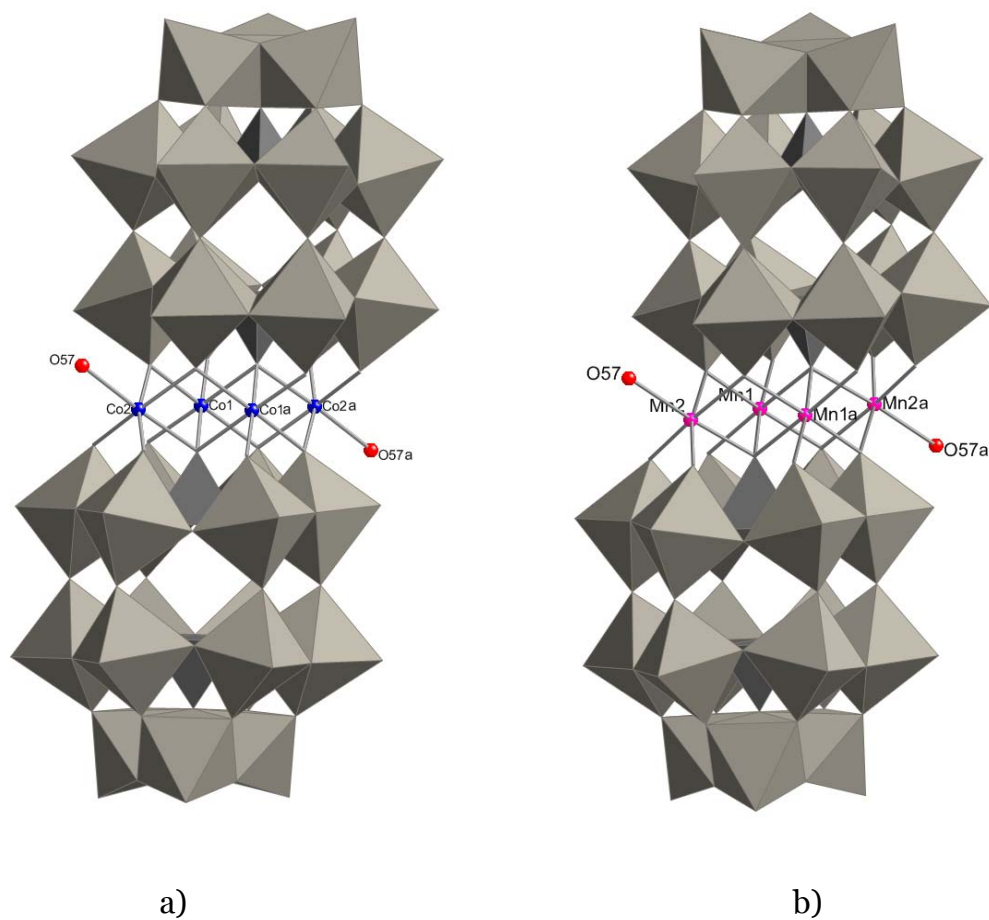
## Conclusions

Four organic-solvent-soluble d-electron-transition metal-substituted derivatives of the tri-vacant POM,  $[\alpha\text{-P}_2\text{W}_{15}\text{O}_{56}]^{12-}$ , have been prepared by phase transfer methods. By using  $\text{Na}_{12}[\alpha\text{-P}_2\text{W}_{15}\text{O}_{56}]\cdot 18\text{H}_2\text{O}$  as a precursor and gas or liquid phase diffusion techniques, the  $\text{Cu}_4$ ,  $\text{Co}_4$ ,  $\text{Mn}_4$  and  $\text{Fe}_4$  complexes have all yielded disorder-free X-ray crystal structures. All the polyanions in these hydrophobic POM salts exhibit the conventional Wells-Dawson sandwich structure. Interestingly the external Cu(II) centers in the central “belt” of the  $\text{Cu}_4$ -substituted compound,  $[(n\text{-C}_4\text{H}_9)_4\text{N}]_{11}\text{H}_5[\text{Cu}_4(\text{P}_2\text{W}_{15}\text{O}_{56})_2]$ , **3**, are coordinatively unsaturated. In contrast, the external Co, Mn and Fe centers in the structurally analogous  $\text{Co}_4^-$ ,  $\text{Mn}_4^-$  and  $\text{Fe}_4^-$ -substituted complexes do have terminal aqua ligands. The temperature-dependent magnetism of **3** indicates medium-strength antiferromagnetic intramolecular exchange between the four Jahn-Teller-distorted  $s = 1/2$  Cu(II) centers mediated by bridging oxo groups, the exchange proceeds primarily through the ligands binding to the equatorial coordination sites of the Cu centers. Significantly, there is no evidence from crystallographic or solution studies that nitrate binds competitively with the acetonitrile solvent molecules to the external Cu(II) centers in **3**. The nitrate-free crystals of **3** dissolved in acetonitrile, the principal solvent used in published studies of aerobic organic oxidations catalyzed by Cu(II)- or Fe(III)-POM/nitrate systems, show no catalytic activity implicating a central role for nitrate or related  $\text{NO}_x$  ligands, at least in the most active such catalysts to date, which like **3**, contain Cu(II) as the only d-electron-metal center.

## Acknowledgements

We thank DTRA and TDA Research Corporation (HDTRA1-08-C-0032) for support of this work.

## Appendix



**S1.** Combined polyhedral / ball-and-stick representations of the X-ray structures of (a)  $\text{TBA}_x\text{H}_{16-x}[\text{Co}_4(\text{H}_2\text{O})_2(\text{P}_2\text{W}_{15}\text{O}_{56})_2]$ , and (b)  $\text{TBA}_x\text{H}_{16-x}[\text{Mn}_4(\text{H}_2\text{O})_2(\text{P}_2\text{W}_{15}\text{O}_{56})_2]$

## References

- (1) Srivastava, R. S.; Milani, B.; Alessio, E.; Mestroni, G., *Inorg. Chimica Acta* **1992**, *191*, 15-17
- (2) Bosch, E.; Kochi, J. K., *J. Org. Chem.* **1995**, *60*, 3172-3183
- (3) Xu, L.; Boring, E.; Hill, C., *J. Catal.* **2000**, *195*, 394-405
- (4) Boring, E.; Geletii, Y. V.; Hill, C. L., *J. Am. Chem. Soc.* **2001**, *123*, 1625-1635
- (5) Martín, S. E.; Rossi, L. I., *Tetrahedron Letters* **2001**, *42*, 7147-7151
- (6) Rossi, L. I.; Martin, S. E., *Appl. Catal. A* **2003**, *250*, 271-278
- (7) Okun, N. M.; Anderson, T. M.; Hill, C. L., *J. Am. Chem. Soc.* **2003**, *125*, 3194-3195
- (8) Okun, N. M.; Anderson, T. M.; Hardcastle, K. I.; Hill, C. L., *Inorg. Chem.* **2003**, *42*, 6610-6612
- (9) Okun, N. M.; Anderson, T. M.; Hill, C. L., *J. Mol. Catal. A: Chem.* **2003**, *197*, 283-290
- (10) Okun, N. M.; Ritorto, M. D.; Anderson, T. M.; Apkarian, R. P.; Hill, C. L., *Chem Mater.* **2004**, *16*, 2551-2558
- (11) Okun, N. M.; Tarr, J. C.; Hillesheim, D. A.; Zhang, L.; Hardcastle, K. I.; Hill, C. L., *J. Mol. Catal. A: Chem.* **2006**, *246*, 11-17
- (12) Hill, C. L.; Okun, N. M.; Hillesheim, D. A.; Geletii, Y. V., Catalysts for Aerobic Decontamination of Chemical Warfare Agents Under Ambient Conditions. In *ACS Symposium Series*, Reynolds, J. G.; Lawson, G. E.; Koester, C. J., Eds. American Chemical Society: Washington, D.C., 2007; Vol. 980, pp 198-209.
- (13) Yamase, T.; Abe, H.; Ishikawa, E.; Nojiri, K.; Oshima, Y., *Inorg. Chem.* **2009**, *48*, 138-148

- (14) Domaille, P. J., Vanadium (V) Substituted Dodecatungstophosphates. In *Inorganic Syntheses*, Ginsberg, A. P., Ed. John Wiley and Sons: New York, 1990; Vol. 27, pp 96-104.
- (15) Randall, W. J.; Droege, M. W.; Mizuno, N.; Nomiya, K.; Weakley, T. J. R.; Finke, R. G., Metal Complexes of the Lacunary Heteropolytungstates [B-alpha-PW<sub>9</sub>O<sub>34</sub>]<sup>9-</sup> and [alpha-P<sub>2</sub>W<sub>15</sub>O<sub>56</sub>]<sup>12-</sup>. In *Inorg. Syn.*, Cowley, A. H., Ed. John Wiley & Sons, Inc.: New York, 1997; Vol. 31, pp 167-185.
- (16) Lyon, D. K.; Miller, W. K.; Novet, T.; Domaille, P. J.; Evitt, E.; Johnson, D. C.; Finke, R. G., *J. Am. Chem. Soc.* **1991**, *113*, 7209-7221
- (17) Schilder, H.; Lueken, H., *J. Magn. Magn. Mater.* **2004**, *281*, 17-26
- (18) Bruker AXS, I. *SMART*, ver. 5.55, Analytical X-ray Systems: Madison, WI, 2000.
- (19) Bruker AXS, I. *SAINT*, ver. 6.02, Analytical X-ray Systems: Madison, WI, 1999.
- (20) Harmalker, S. P.; Pope, M. T., *Inorganic Biochemistry* **1986**, *28*, 85-95
- (21) Katsoulis, D. E.; Tausch, V. S.; Pope, M. T., *Inorg. Chem.* **1987**, *26*, 215-216
- (22) Katsoulis, D. E.; Pope, M. T., *J. Am. Chem. Soc.* **1984**, *106*, 2737-2738
- (23) Katsoulis, D. E.; Pope, M. T., *J. Chem. Soc., Dalton Trans.* **1989**, 1483-1489
- (24) Radkov, E. V.; Young Jr, V. G.; Beer, R. H., *J. Am. Chem. Soc.* **1999**, *121*, 8953-8954
- (25) Zhang, X.; Chen, Q.; Duncan, D. C.; Lachicotte, R. J.; Hill, C. L., *Inorg. Chem.* **1997**, *36*, 4381-4386
- (26) Goto, Y.; Kamata, K.; Yamaguchi, K.; Uehara, K.; Hikichi, S.; Mizuno, N., *Inorg. Chem.* **2006**, *45*, 2347-2356

- (27) Niu, J.; Li, M.; Wang, J., *J. Organometallic Chem.* **2003**, *675*, 84-90
- (28) Huang, W.; Todaro, L.; Yap, G. P. A.; Beer, R.; Francesconi, L. C.; Polenova, T., *J. Am. Chem. Soc.* **2004**, *126*, 11564-11573
- (29) Kim, G. S.; Hagen, K. S.; Hill, C. L., *Inorg. Chem.* **1992**, *31*, 5316-24
- (30) Bar-Nahum, I.; Ettetdgui, J.; Konstantinovski, L.; Kogan, V.; Neumann, R., *Inorg. Chem.* **2007**, *46*, 5798-5804
- (31) Kholdeeva, O. A.; Maksimov, G. M.; Maksimovskaya, R. I.; Vanina, M. P.; Trubitsina, T. A.; Naumov, D. Y.; Kolesov, B. A.; Antonova, N. S.; Carbó, J. J.; Poblet, J. M., *Inorg. Chem.* **2006**, *45*, 7224-7234
- (32) Long, D.-L.; Streb, C.; Song, Y.-F.; Mitchell, S.; Cronin, L., *J. Am. Chem. Soc.* **2008**, *130*, 1830-1832
- (33) References 34-56 are representative papers address synthesis, isomerism and properties of Wells-Dawson sandwich POMs
- (34) Contant, R.; Ciabrini, J. P., *J. Inorg. Nucl. Chem.* **1981**, *43*, 1525-8
- (35) Finke, R. G.; Droege, M. W., *Inorg. Chem.* **1983**, *22*, 1006-1008
- (36) Finke, R. G.; Droege, M. W.; Domaille, P. J., *Inorg. Chem.* **1987**, *26*, 3886-3896
- (37) Gómez-García, C. J.; Coronado, E.; Borrassalmenar, J. J., *Inorg. Chem.* **1992**, *31*, 1667-1673
- (38) Gómez-García, C. J.; Borrás-Almenar, J. J.; Coronado, E.; Ouahab, L., *Inorg. Chem.* **1994**, *33*, 4016-4022
- (39) Coronado, E.; Gómez-García, C. J., *Chem. Rev.* **1998**, *98*, 273-296
- (40) Zhang, X.; Anderson, T. M.; Chen, Q.; Hill, C. L., *Inorg. Chem.* **2001**, *40*, 418-419

- (41) Anderson, T. M.; Hardcastle, K. I.; Okun, N.; Hill, C. L., *Inorg. Chem.* **2001**, *40*, 6418-6425
- (42) Ruhlmann, L.; Canny, J.; Contant, R.; Thouvenot, R., *Inorg. Chem.* **2002**, *41*, 3811-3819
- (43) Contant, R.; Herve, G., *Reviews in Inorganic Chemistry* **2002**, *22*, 63-111
- (44) Anderson, T. M.; Zhang, X.; Hardcastle, K. I.; Hill, C. L., *Inorg. Chem.* **2002**, *41*, 2477-2488
- (45) Ruhlmann, L.; Nadjo, L.; Canny, J.; Contant, R.; Thouvenot, R., *Eur. J. Inorg. Chem.* **2002**, 975-986
- (46) Mbomekalle, I. M.; Keita, B.; Nadjo, L.; Berthet, P.; Hardcastle, K. I.; Hill, C. L.; Anderson, T. M., *Inorg. Chem.* **2003**, *42*, 1163-1169
- (47) Mbomekalle, I. M.; Keita, B.; Nadjo, L.; Berthet, P.; Neiwert, W. A.; Hill, C. L.; Ritorto, M. D.; Anderson, T. M., *Dalton Trans.* **2003**, 2646-2650
- (48) Mbomekalle, I. M.; Keita, B.; Nadjo, L.; Neiwert, W. A.; Zhang, L.; Hardcastle, K. I.; Hill, C. L.; Anderson, T. M., *Eur. J. Inorg. Chem.* **2003**, 3924-3928
- (49) Keita, B.; Mbomekalle, I. M.; Lu, Y. W.; Nadjo, L.; Berthet, P.; Anderson, T. M.; Hill, C. L., *Eur. J. Inorg. Chem.* **2004**, 3462-3475
- (50) Keita, B.; Mbomekalle, I. M.; Nadjo, L.; Anderson, T. M.; Hill, C. L., *Inorg. Chem.* **2004**, *43*, 3257-3263
- (51) Mbomekalle, I. M.; Keita, B.; Nadjo, L.; Hardcastle, K. I.; Hill, C. L.; Anderson, T. M., *J. Chem. Soc. Dalton Trans.* **2004**, 4094-4095
- (52) Mbomekalle, I. M.; Cao, R.; Hardcastle, K. I.; Hill, C. L.; Ammam, M.; Keita, B.; Nadjo, L.; Anderson, T. M., *C. R. Chimie* **2005**, *8*, 1077-1086

- (53) Mbomekalle, I. M.; Lu, Y. W.; Keita, B.; Nadjó, L.; Neiwert, W. A.; Hardcastle, K. I.; Hill, C. L.; Anderson, T. M., *Eur. J. Inorg. Chem.* **2005**, 1547-1551
- (54) Anderson, T. M.; Fang, X.; Mbomekalle, I. M.; Keita, B.; Nadjó, L.; Hardcastle, K. I.; Farsidjani, A.; Hill, C. L., *J. Cluster Sci.* **2006**, *17*, 183-195
- (55) Fang, X.; Hill, C. L., *Angew. Chem. Int. Ed.* **2007**, *46*, 3877-3880
- (56) Zhang, X.; Chen, Q.; Duncan, D. C.; Campana, C.; Hill, C. L., *Inorg. Chem.* **1997**, *36*, 4208-4215
- (57) Brown, I. D.; Altermatt, D., *Acta Cryst.* **1985**, *B41*, 244-247
- (58) References 59-76 are representative papers that address synthesis, isomerism and properties of the products from reaction of d-electron-metals and { $\gamma$ -SiW<sub>10</sub>}
- (59) Canny, J. T., R.; Tézé, A.; Hervé, G.; Leparulo-Loftus, M.; Pope, M. T., *Inorg. Chem.* **1991**, *30*, 976-981
- (60) Wassermann, K.; Lunk, H.-J.; Palm, R.; Fuchs, J.; Steinfeldt, N.; Stosser, R.; Pope, M. T., *Inorg. Chem.* **1996**, *35*, 3273-3279
- (61) Xin, F.; Pope, M. T., *Inorg. Chem.* **1996**, *35*, 5693-5695
- (62) Xin, F.; Pope, M. T.; Long, G. J.; Russo, U., *Inorg. Chem.* **1996**, *35*, 1207-1213
- (63) Zhang, X.; O'Connor, C. J.; Jameson, G. B.; Pope, M. T., *Inorg. Chem.* **1996**, *35*, 30-34
- (64) Nozaki, C.; Kiyoto, K.; Minai, Y.; Misono, M.; Mizuno, M., *Inorg. Chem.* **1999**, *38*, 5724-5729
- (65) Kortz, U.; Isber, S.; Dickman, M. H.; Ravot, D., *Inorg. Chem.* **2000**, *39*, 2915-2922

- (66) Kortz, U.; Matta, S., *Inorg. Chem.* **2001**, *40*, 815-817
- (67) Bassil, B. S.; Kortz, U.; Tigan, A. S.; Clemente-Juan, J. M.; Keita, B.; Oliveira, P. d.; Nadjjo, L., *Inorg. Chem.* **2005**, *44*, 9360-9368
- (68) Bassil, B. S.; Nellutla, S.; Kortz, U.; Stowe, A. C.; Tol, J. v.; Dalal, N. S.; Keita, B.; Nadjjo, L., *Inorg. Chem.* **2005**, *44*, 2659-2665
- (69) Botar, B.; Geletii, Y. V.; Kögerler, P.; Musaev, D., G.; Morokuma, K.; Weinstock, I. A.; Hill, C. L., *J. Chem. Soc., Dalton Trans.* **2005**, *11*, 2017-2021
- (70) Mialane, P.; Dolbecq, A.; Marrot, J.; Rivière, E.; Sécheresse, F., *Chemistry - A European Journal* **2005**, *11*, 1771-1778
- (71) Bassil, B. S.; Dickman, M. H.; Kortz, U., *Inorg. Chem.* **2006**, *45*, 2394-2396
- (72) Bassil, B. S.; Dickman, M. H.; Reicke, M.; Kortz, U.; Keita, B.; Nadjjo, L., *J. Chem. Soc., Dalton Trans.* **2006**, 4253-4259
- (73) Botar, B.; Geletii, Y. V.; Kögerler, P.; Musaev, D. G.; Morokuma, K.; Weinstock, I. A.; Hill, C. L., *J. Am. Chem. Soc.* **2006**, *128*, 11268-11277
- (74) Goto, Y.; Kamata, K.; Yamaguchi, K.; Uehara, K.; Hikichi, S.; Mizuno, N., *Inorg. Chem.* **2006**, *45*, 2347-2356
- (75) Zhang, Z.; Li, Y.; Wang, E.; Wang, X.; Qin, C.; An, H., *Inorg. Chem.* **2006**, *45*, 4313-4315
- (76) Sadakane, M.; Tsukuma, D.; Dickman, M. H.; Bassil, B.; Kortz, U.; Higashijima, M.; Ueda, W., *J. Chem. Soc., Dalton Trans.* **2006**, 4271-4276
- (77) Luo, Z.; Kögerler, P.; Cao, R.; Hakim, I.; Hill, C. L., *Dalton Trans.* **2008**, 54-58
- (78) Luo, Z.; Kögerler, P.; Cao, R.; Hill, C. L., *Polyhedron* **2009**, *28*, 215-220